INSTITUT DE FRANCE
Académie des sciences

Comptes Rendus

Physique

Oguz Umut Salman, Roberta Baggio, Brigitte Bacroix, Giovanni Zanzotto, Nikolai Gorbushin and Lev Truskinovsky

Discontinuous yielding of pristine micro-crystals

Online first

<https://doi.org/10.5802/crphys.77>

Part of the Special Issue: Plasticity and Solid State Physics

Guest editors: Samuel Forest (Mines ParisTech, Université PSL, CNRS, France) and David Rodney (Université Claude Bernard Lyon 1, France)

Les Comptes Rendus. Physique *sont membres du Centre Mersenne pour l'édition scientifique ouverte*
www.centre-mersenne.org

Comptes Rendus
Physique
Online first
https://doi.org/10.5802/crphys.77

Plasticity and Solid State Physics / *Plasticité et Physique des Solides*

Discontinuous yielding of pristine micro-crystals

Oguz Umut Salman[*], [a], **Roberta Baggio** [a], **Brigitte Bacroix** [a], **Giovanni Zanzotto** [b], **Nikolai Gorbushin** [c] **and Lev Truskinovsky**[*], [c]

[a] CNRS, LSPM UPR3407, Université Sorbonne Paris Nord, Villetaneuse, 93430, France

[b] DPG, Université di Padova, Via Venezia 8, 35131 Padova, Italy

[c] PMMH, CNRS-UMR 7636, ESPCI PSL, F-75005 Paris, France

E-mails: umut.salman@lspm.cnrs.fr (O. U. Salman), robi.bagg.colpi@gmail.com (R. Baggio), brigitte.bacroix@lspm.cnrs.fr (B. Bacroix), zanzotto@dmsa.unipd.it (G. Zanzotto), nikolai.gorbushin@espci.fr (N. Gorbushin), lev.truskinovsky@espci.fr (L. Truskinovsky)

Abstract. We study the mechanical response of a dislocation-free 2D crystal under homogenous shear using a new mesoscopic approach to crystal plasticity, a Landau-type theory, accounting for the global invariance of the energy in the space of strain tensors while operating with an infinite number of equivalent energy wells. The advantage of this approach is that it eliminates arbitrariness in dealing with topological transitions involved, for instance, in nucleation and annihilation of dislocations. We use discontinuous yielding of pristine micro-crystals as a benchmark problem for the new theory and show that the nature of the catastrophic instability, which in this setting inevitably follows the standard affine response, depends not only on lattice symmetry but also on the orientation of the crystal in the loading device. The ensuing dislocation avalanche involves cooperative dislocation nucleation, resulting in the formation of complex microstructures controlled by a nontrivial self-induced coupling between different plastic mechanisms.

Keywords. Plasticity, Dislocations, Landau theory, Nucleation, Pattern formation, Brittleness.

1. Introduction

With the advance of nanotechnology and broad fabrication of nano-scale structures, the focus in the study of plastic deformation has shifted to atomic dimensions. The emerging science of nano-materials deals, for instance, with machine parts printed by chemical vapor deposition or made of nano-grained metals. At these manufacturing scales, external and internal (microstructural) lengths become comparable, and the dislocation-based description of plasticity comes to the forefront in providing design guidelines for miniaturized mechanical devices [1–3]. It was found, for instance, that sub-micron size objects, serving as components of such systems, are characterized by remarkably high strength. This opened a way to a broad range of *novel* engineering applications, including nano-metric machining and hierarchical steels, e.g. [4].

[*] Corresponding authors.

Considerable research efforts have been focused on the study of dislocation plasticity in sub-micron crystals in an attempt to assess the extent of the failure of traditional inelastic constitutive models at these scales [5–9]. As a result of these efforts, it has become clear that the deformation mechanisms, which we habitually associate with plastic flows, change dramatically once the sample size is reduced below the micrometer range. It was found that the strength of such crystals reaches theoretical (ideal) limit [10–13] and that the plastic flow proceeds through stress drops reminiscent of brittle fracture [14–17]. The attendant intermittency compromises the reliable functioning of ultra-small machinery and jeopardizes our ability to ensure the predictable performance of MEMS and other similar systems [18–22].

Of primary interest to our study will be the phenomenon of *discontinuous yielding* in sub-micron (initially) dislocation free volumes. According to the classical continuum paradigm, the elastic deformation in strained crystals must be followed by either an abrupt brittle-like failure or gradual plastic deformation. Instead, loading of sub-micron crystals revealed a mixed, fracture-type plastic behavior. Micro-crystals, exhibiting smooth classical yield at macro-scales, were shown to fail catastrophically, with conventional work hardening replaced by a sequence of intermittent plastic events [23].

The precipitous brittle yield, revealing a high level of dislocation correlations and manifesting plastic collapse, was first discovered in metal whiskers [24, 25]. Brittleness of this type has been since routinely observed in nanoparticles, which "break plastically" while generating a large number of dislocations [26, 27]; similar global plastic instabilities have also been recorded during nanoindentation [28, 29]. The implied system size plastic avalanches result from a large number of highly cooperative individual dislocation nucleation and dislocation glide events, taking place almost simultaneously [13, 18, 30, 31].

The distinctive features of crystal plasticity at sub-micron scales can be attributed to the high degree of structural perfection of such samples, which are usually almost pristine [32, 33]. In particular, the catastrophic yield depends critically on the absence of dislocations before straining. Despite the global, system-spanning scale of experienced plastic deformation, such samples produce nearly pristine postmortem microstructures. Almost all dislocations mediating the explosive stress drop manage to escape to the boundaries, sometimes even producing pristine-to-pristine transition [16, 34]. It was also observed that as the deformation volume of a material decreases, the effect of crystal orientation on the operative deformation mechanisms increases; in particular, the mechanical response of sub-micron defect-free nanopillars is different depending on whether they are deformed along high symmetry orientations or low symmetry orientations [35, 36]. The compression tests on confined micropillars revealed higher (and therefore closer to theoretical limit) stresses of massive dislocation nucleation than in the presence of free surfaces [36, 37].

In this paper, addressing the mechanical response of dislocation-free 2D crystals under homogenous shear, we attempt to rationalize the above observations using the mesoscopic model of crystal plasticity [38–40]. We use discontinuous yielding of pristine micro-crystals as a benchmark problem for this new theory and study in detail how the nature of the catastrophic instability depends on the lattice symmetry and the orientation of the crystal in the loading device. The initial plasticity in pristine nano-scale volumes is of particular *theoretical* importance as the process dominated by cooperative dislocation nucleation vs more conventional flow mechanisms involving multiplication and glide of pre-existing dislocations.

The rest of the paper is organized as follows. In Section 2, we motivate our study reviewing the problem from the viewpoint of materials science of sub-micron crystals. We then briefly discuss the existing computational tools. The new mesoscopic model is introduced in Section 3, where we recall the geometrically nonlinear kinematics of crystal lattices and discuss the construction of strain-energy density respecting the finite strain symmetry of the crystal lattice. In Section 4,

we present the macroscopic picture of the discontinuous yield revealed by our numerical experiments and, to justify these results, compute the theoretical (ideal) shear strength for perfect crystals with different point groups. In Section 5, we study post-bifurcation behavior of pristine crystals and compare the post avalanche dislocation patterns. Along with their representation in the physical space, we also visualize such patterns in the configurational space of lattice strains. In Section 6, we briefly discuss the mechanical response of the simulated crystals beyond the catastrophic brittle event. Finally, in Section 7 we present our conclusions.

2. Some background

Plastic deformation in crystalline solids involves discontinuous changes in the configuration of nearest neighboring atoms as some stress/strain thresholds are exceeded upon external loading. The associated relative movement can be interpreted as the creation and propagation of topological lattice defects. The most prominent among them are dislocations, moving along crystallographic planes and leaving behind quantized lattice slip [41–43]. Understanding the collective motion of dislocations is the key to control the ductile failure of crystals as these linear defects are involved in shear band formation, fatigue, and even fracture [44–46].

Plastic flow is inherently complex due to long-range elastic interactions of dislocation lines and strongly nonlinear, threshold type short-range interactions of dislocation cores [47, 48]. Facilitated by lattice trapping, transient and sessile dislocation patterns cover a broad range of scales from microscopic (junctions) to macroscopic (grains) [49–51].

Despite the presence of microscopic heterogeneities, plastic flows appear at the scale of bulk materials as smooth phenomena amenable to continuous description [52]. Therefore, macroscopic crystal plasticity is usually formulated within classical continuum mechanics and involves macroscale constitutive relations. The inelastic component of strain tensor is parametrized by a finite number of order parameters representing amplitudes of pre-designed plastic mechanisms; in rate independent limit each of them is assumed to be governed by dry friction dynamics [53–58]. The fact that fluctuations are effectively averaged out,[1] opens for continuum plasticity (CP) access to macroscopic time and length scales and allows one to model realistic 3D structures with complex geometries while accounting phenomenologically for such complex effects as hardening, rate-dependence and polycrystallinity [55, 61–64].

However, it has been recently realized that plastic flows in ultra-small samples are beyond the reach of such theories. A description of the cross-over from a “mild” plastic flow in bulk materials to a “wild” scale-free intermittent plastic response at the sub-micron scale requires significant paradigm change [59]. In particular, the current CP theory fails to resolve intermittent stress-drops (or strain-jumps) at submicron scales [11, 13, 22] and is also unable to explain catastrophic events accompanying plastic flows in nanoparticles [16], nanowires [65] and nanopillars [14, 66–68]. None of these phenomena can be rationalized without a direct reference to dislocation motion.

If in bulk materials dislocation motion is largely uncorrelated and fluctuations can be indeed averaged out, plastic flows in sub-micron crystal involve highly cooperative dislocational rearrangements. The most striking effect of such cooperativity is provided by intermittent system size dislocation avalanches, which defy self-averaging and challenge any attempt of continuous description. More generally, the scale-free CP fails at sample sizes comparable to the emerging microstructural scale of defect patterning, simply because the latter is assumed to be zero in the CP theory. The attempts to regularize the CP and link the internal length scale with the presence

[1] Recently continuum models were proposed with internal fluctuations accounted for through stochastic constitutive equations [59, 60].

of "geometrically necessary" strain gradients have been so far only partially successful as the size effect was also observed in the absence of strain gradients, e.g. [69].

An alternative approach to the rationalization of the size effect was to shift the attention from the role of gradients in dislocation arrangements to the scarcity of dislocation sources in small crystals. It was noticed that when sufficiently small crystals were strained to the bulk yield stresses, the rate of dislocation escape to the surfaces grew to become larger than the rate of dislocation multiplication, and therefore, plasticity could proceed only by the nucleation of new dislocations at considerably higher stresses [70]. The implied "dislocation starvation" was therefore linked to the fact the "breeding" distance for dislocation multiplication becomes larger than the system size [23, 70, 70–74].

Following this logic, the "brittle" response of pristine ultra-small samples after they reached the level of theoretical (ideal) strength, can be explained by massive homogeneous nucleation of dislocations [75–77]. In other words, in such "starved" samples yielding can be expected to proceed as a dislocation nucleation avalanche which can reach the size of the system [19, 78–81]. The implied cooperative response becomes possible because the defect-free environment allows the nucleated dislocations to dynamically self-organize, taking full advantage of the un-screened long-range elastic interactions [82–84]. The emerging mechanical instability ultimately originates from strain softening whose origin will be revealed as a part of this study.

We note that sharp peak stresses at yielding have been also observed in some *macroscopic* samples where the large yield drop is usually followed by a Luders-like flow instability, e.g. [85,86]. In such cases the initial mobile dislocation density is usually low either because dislocations were annihilated during the annealing process or because they were blocked by solute atoms; in both cases the discontinuous yielding is associated with either collective depinning from Cottrell atmosphere or explosive nucleation from nano-sized grain boundary sources. A theoretical explanation of discontinuous yielding in the prototypical context of transformational plasticity was proposed in [87] where the stress peaks were linked to the difference between (homogeneous) nucleation and propagation thresholds for internal instabilities.

The development of the computational tools accounting for the dislocational nature of plastic flows has become a priority because the inadequacy of the conventional methods based on CP was placing severe restrictions on the possibility to model plastically deforming ultra-small structural elements [22, 88–90]. In particular, it was realized that to simulate *discontinuous yielding* in sub-micron crystals which involves massive nucleation of dislocations, the modeling approach cannot ignore lattice effects and must necessarily account for phenomena at the scale of dislocation cores. Capturing the attendant pattern formation is challenging because the nucleated dislocations continue to interact strongly at many different scales [91–95].

Numerous computational alternatives to CP have been developed targeting different time and length-scales. They range from molecular dynamics (MD) [96, 97] and similarly microscopic phase-field crystal (PFC) method [98, 99], to the more coarse grained phase-field dislocation dynamics (PFDD) [100–102], discrete dislocation dynamics (DDD) [103–106], and continuum dislocation dynamics (CDD) [107–109]. The multi-scale quasi-continuum model (QC) attempts to bridge all the scales while accounting for each of them fully comprehensibly [110, 111].

MD approaches, including Molecular Statics (MS), and Density Functional Theory (DFT), accurately represent micro-mechanisms of plastic response while relying minimally on phenomenology [112]. MD simulations have been particularly instrumental in the study of the homogeneous and heterogeneous dislocation nucleation [76, 90, 97]. The only relative shortcoming of the atomistic simulations is that they are still computationally rather expensive in most applications, even at the small time and length scales of interest; also the problem of mapping to the macroscopic description in terms of the measurable quantities like stresses and strains is apparently not yet fully resolved [113–116]. Partial temporal averaging of atomistic molecular

dynamics has emerged in the form a coarse-grained continuum PFC theory [117]. The PFC approach was applied to the description of an ensemble of few interacting dislocation dipoles and was able to capture some cooperative features of crystal plasticity [98, 99, 118]. However, such a detailed description of atomic lattices still remains rather demanding in terms of computer time, at least in the case of developed plastic flows with realistic number of interacting dislocations.

Discrete dislocation dynamics (DDD) approach was created to overcome the short time and length scales of atomistic methods. This model treats adequately long range interaction of dislocations without resolving the fine structure of the dislocation cores. To account for short range interactions, specific "local rules" must be added governing, for instance, intersections and locks. Even some particular lattice scale effects have been successfully modeled with the help of such additional phenomenological constructs, typically motivated by atomistic simulations [119–125]. Being reinforced in this way, the DDD has emerged as an extremely useful approach for modeling evolution of many interacting dislocations [126, 127]. However, it still remains challenging to account in the DDD framework for large deformations, crystal symmetry, lattice rotation, as well as the emergence of non-dislocational defects. Coarse graining of DDD, which opens the way towards modeling of dislocation patterning, has been attempted in the framework of the mesoscopic CDD methods where dislocation microstructures are modeled by continuum dislocation density fields [128–130]. While various phenomenological closure relations have been proposed to model the evolution of the dislocation density, the systematic development of this approach is hindered by the fact that *rigorous* statistical averaging in the ensemble of strongly interacting dynamic defects is still a big challenge [131].

In search of a micro–macro compromise a QC approach was proposed in [132] and then significantly developed in [110, 111, 133–135]. It is based on the observation that a fully atomistic resolution is necessary only in small spatial regions, while in most of the modeling domain the deformation fields can be represented by the classical continuum theory. A necessity of patching the continuum and discrete subdomains poses, however, a complex problem [111, 136]. The QC method has been successfully used in many applications, including the study of nanoindentation, deformation of grain-boundaries and crack tip evolution [137–140].

Of particular interest to our study is the local version of the QC method representing a mesoscale compromise between continuum and atomistic approaches [132, 134]; a closely related approach is the interatomic potential FEM (IPFEM) [141, 142]. In these effectively single scale methods the spatial domain is subdivided into discrete elements, as in a finite element method (FEM), and the deformation in each element is taken to be piece-wise affine. The energy density of an element, which then depends only on the displacement gradient at this point, is evaluated using interatomic potentials and the Cauchy–Born rule [143–146]. These approaches were shown to capture adequately the basic structure of dislocation cores, even though they can misrepresent some truly atomistic features like deformations varying rapidly within the cut-off distance of the interatomic potential.

A mesoscale approach to crystal plasticity, which also allows one to treat dislocations in a fully continuum framework, and which is relevant for our own development, is the phase-field dislocation dynamics (PFDD) [101, 147–149]. This method has evolved from the original Landau approach to the modeling of phase transitions [150–155]. In PFDD lattice slips are described by scalar order parameters and the energy wells represent quantized lattice invariant shears [147, 156, 157]; transition layers, separating regions with different amount of shear, represent the locations of dislocation lines. The Landau energy functional couples the *tensorial* linear elastic energy with the *scalar* lattice energy whose periodic structure is usually informed by atomic scale simulations based on the Cauchy–Born rule. The PFDD method enables simulations of much larger crystal sizes and much longer time scales than atomistic simulations [150, 158–160]. While the extensions of PFDD to finite strains have recently appeared [161, 162], the remaining

challenge is that the structure of lattice invariant shears is resolved by scalar order parameters only approximately [98, 163, 164].

3. Mesoscopic tensorial model (MTM)

We have seen that despite many important advances in various specific problems, the sufficiently versatile computational method, allowing for natural coupling of different plastic "mechanisms" while addressing realistic space and time scales,[2] is still missing. The challenge is then to build a synthetic mesoscopic tensorial approach dealing with large strains, while accounting correctly for both anisotropy and discreteness of the simplest Bravais lattices.

Different attempts along these lines can be found in the literature. The corresponding scalar approaches [38, 165, 166] can be viewed as generalizations of the minimalistic 1D Frenkel–Kontorova model [167–169] for the 2D case when only one slip system is activated. Despite their simplicity such models have been successful in describing dislocation cores [170], in simulating dislocation nucleation [75, 171–174] and even in modeling of plastic intermittency [39, 68]. The tensorial models with *linearized* kinematics were proposed in [175–178]. They produced a more realistic picture of plastic flows but still could not account adequately for lattice-invariant shears associated with finite plastic slip [179].

The first attempts to incorporate the effects of geometrical nonlinearity were made in the context of a model of reconstructive phase transitions allowing for partial plastic accommodation [180]. A finite strain model focused directly on the modeling of plastic deformation was first developed for the case of highly anisotropic lattices of HCP type with a single slip system [38]. Both of these papers can be viewed as different realizations of the original program of Ericksen who proposed that in nonlinear elasticity the energy periodicity should be made compatible with geometrically nonlinear kinematics of Bravais lattices [181–184], see also the subsequent important developments of the mathematical formalism in [185–188].

Behind the coarse-grained approach of Ericksen was the general assumption that meso-scale material elements are exposed to an effective energy landscape which is globally periodic due to the presence of lattice invariant shears. From the perspective of such Landau-type continuum theory with an infinite number of equivalent energy wells, plastically deformed crystal can be seen as a multi-phase mixture of equivalent "phases". Plastic yield can be then interpreted as an escape from the reference energy well and plastic "mechanisms" can be linked to low-barrier valleys in the energy landscape. Friction type dissipation controlling dynamics in continuum crystal plasticity emerges in such theory as a result of a homogenized description of an overdamped athermal dynamics in a rugged energy landscape [189, 190].

The 2D scalar model of crystal plasticity presented in [38,39] was effectively a single slip system version of such theory. Building upon [180], a 2D tensorial version was presented in [40]. Its main advantage is that it incorporates adequately the full symmetry of the Bravais lattices [181, 184]. We recall that the invariance described by the *infinite* group $GL(2,\mathbb{Z})$ is different from the one associated with the classical *finite* point group limited to orthogonal transformations. The global group $GL(2,\mathbb{Z})$ is much broader, accounting not only for orthogonal transformations but also for non-orthogonal transformations representing lattice invariant shears. For example, in 2D a Bravais lattice can be viewed as an infinite integer translation of two linearly independent vectors or, more formally, it is a set of vectors $\mathbf{x} \in \mathbb{R}^2$ such that $\mathbf{x} = \nu_K \mathbf{e}_K$, with $\nu_K \in \mathbb{Z}$. For a given Bravais lattice, there are infinite choices for the basis $\{\mathbf{e}_K\}$. The associate global symmetry group is the maximal subgroup of the group of invertible linear mappings leaving the lattice invariant. In

[2] Allowing one, for instance, to resolve the system size dislocation nucleation avalanche for micron size crystals.

particular, for 2D Bravais lattices it is $GL(2,\mathbb{Z}) = \{M_{KL} \in \mathbb{Z}, \det(\mathbf{M}) = \pm 1\}$, where $K, L = 1, 2$. In words, the global symmetry group of a 2D Bravais lattice is represented by 2×2 invertible matrices with integer entries and determinant ± 1.

In the kinematically nonlinear Landau type theory with $GL(2,\mathbb{Z})$ symmetry the role of the order parameter is played by the metric tensor (defined below), and the bottoms of the energy wells correspond to lattice invariant deformations. Since the ground state in the continuum theory of this type is necessarily degenerate (hydrostatic) [182, 191], the regularization is necessary, as in the case of PFDD or any other Landau-type theory. In [40] such regularizing internal length scale was associated with the size of the mesh generating discrete elastic *elements*. In other words, the mesh scale was treated as a *physical* parameter which defines the meso-scale. Given the large magnitude of the "transformation strain", different "phases" ended up being localized at the scale of such mesoscopic *elements* and the domain boundaries appeared macroscopically as linear defects mimicking dislocations.

In what follows we refer to the approach proposed in [40] as the mesoscopic tensorial model (MTM). The main advantage of this approach is that it is formulated in terms of macroscopically measurable quantities (stress and strain) while being able to distinguish between different symmetry induced configurations of dislocation cores. It can therefore account adequately for both long- and short-range interactions between dislocations. Most importantly, it allows for topological transitions associated with dislocation nucleation and annihilation even though the corresponding "reactions" appear as blurred on the scale of regularization. Last but not least, in the MTM approach the interaction of dislocations with various obstacles, including pinning by impurities and depinning from nucleation sources, can be handled without introducing ad-hoc relations.

In this paper the MTM is used to conceptualize the brittle-like response of nominally ductile sub-micron crystals. Through a series of numerical experiments we uncover the origin of the correlated dislocational response of crystals with different symmetry at loading levels approaching the theoretical (ideal) strength. In particular, we reveal the mechanism of the observed orientation dependence of the degree of "brittleness" and rationalize the system size dependence of the associated collective nucleation event.

3.1. $GL(2,\mathbb{Z})$ *energy density*

For simplicity, we deal in this paper with the two dimensional Bravais lattices: square (with lower, square symmetry) and triangular (with higher, hexagonal symmetry). In addition to its theoretical interest, the study of plasticity in 2D crystals is technologically relevant because such crystals have been recently found important in many applications [192–200].

The main ingredient of the MTM approach is the objective elastic energy density which respects the $GL(2,\mathbb{Z})$ symmetry. To construct such energy, we need to first introduce the deformation of a continuum body $\mathbf{y} = \mathbf{y}(\mathbf{x})$, where $\mathbf{y}$ and $\mathbf{x}$ are the position vectors in the current (Eulerian) configuration and the reference (Lagrangian) configuration, respectively. If $\mathbf{F}$ is the deformation gradient $\nabla\mathbf{y} = \partial\mathbf{y}/\partial\mathbf{x}$, the frame indifferent elastic energy density $\Phi(\mathbf{C})$ can depend on $\mathbf{F}$ only through the metric tensor $\mathbf{C} = \mathbf{F}^T\mathbf{F}$. To account adequately for all deformations that map a Bravais lattice onto itself, we require that the strain energy density satisfies $\Phi(\mathbf{C}) = \Phi(\mathbf{M}^T\mathbf{C}\mathbf{M})$ for any matrix $\mathbf{M}$ in $GL(2,\mathbb{Z})$. We recall that this invariance follows from the fact that the same lattice can be generated by the two sets of lattice vectors $\bar{\mathbf{e}}_K$ and $\mathbf{e}_K$ if and only if $\bar{\mathbf{e}}_K = M_{KL}\mathbf{e}_L$. In the presence of such symmetry, the space of metric tensors $\mathbf{C}$ with components $C_{KL} = \mathbf{e}_K \cdot \mathbf{e}_L$ partitions into periodicity domains. Therefore, when the energy is known in one of the domains, it can be automatically extended to all other equivalent domains by the use of global tensorial periodicity.

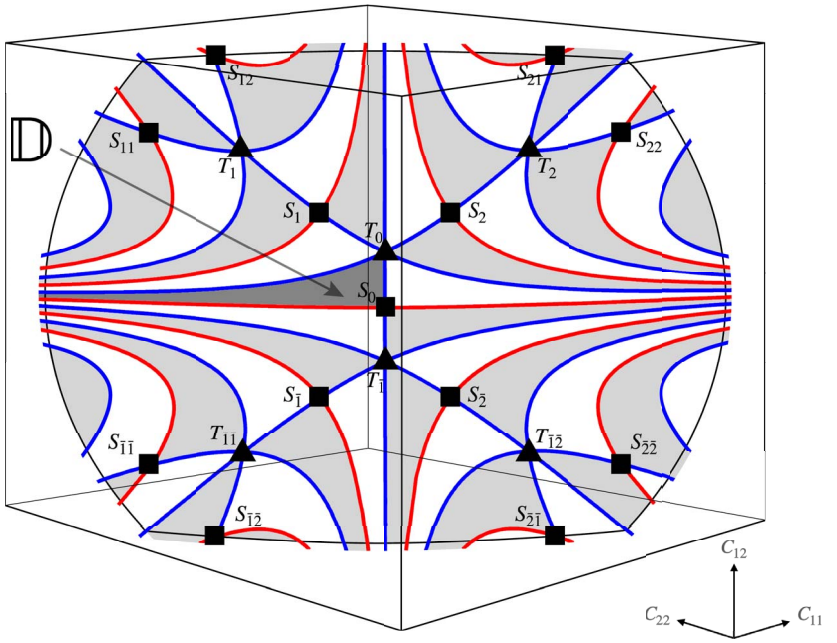

Figure 1. The structure of the $GL(2,\mathbb{Z})$ periodicity domains in the space of metric tensors $\mathbf{C}$. The shown portion of the infinite surface $\det\mathbf{C}=1$ represents simple lattices with $\det\mathbf{C}>0$. The projected section of the original hyperbolic surface is defined by the inequalities $0<C_{11}<6$, $0<C_{22}<6$, and $-3<C_{12}<3$.

The space of metric tensors in the 2D case is three dimensional and in Figure 1 we show a two dimensional section of this space defined by the condition $\det\mathbf{C}=1$. For better visibility equivalent tensorial periodicity subdomains are shown in two alternating colors, gray and white. Each of these subdomains contains necessarily one and only one copy of a particular Bravais lattice. In this figure, equivalent zero-parametric families of square lattice configurations are marked with solid squares $S_{\mathrm{i}}, S_{\mathrm{ij}},\ldots, S_{\bar{\mathrm{i}}}, S_{\bar{\mathrm{i}}\bar{\mathrm{j}}},\ldots$ while solid triangles $T_{\mathrm{i}}, T_{\mathrm{ij}},\ldots, T_{\bar{\mathrm{i}}}, T_{\bar{\mathrm{i}}\bar{\mathrm{j}}},\ldots$ correspond to similar families of equivalent triangular lattices. Red lines indicate one-parametric families of rectangular lattices and blue lines correspond to similar families of rhombic lattices. Finally, the open 2D domains correspond to two-parametric families of equivalent oblique (monoclinic) lattices, see also [201–204]. Note that in this representation we do not see the "volumetric" part of the metric tensor responsible, for instance, for void formation [205].

The darkened area in Figure 1, denoted by $\mathbb{D}$, is known as the "fundamental" domain [206]. Among all the equivalent metric tensors describing symmetry-related lattices, this domain contains the "minimal" ones, known as "reduced forms of Lagrange". An arbitrary basis $\mathbf{e}_i$ producing an arbitrary metric $\mathbf{C}$ has its unique "Lagrange reduced" copy $\tilde{\mathbf{e}}_i$ with the corresponding metric $\tilde{\mathbf{C}}$ in $\mathbb{D}$.

The Lagrange reduction is obtained using the following rule: among all symmetry related copies of the original basis, the reduced one is formed by the shortest non-colinear vectors with an acute angle between them, see for instance [180]. Therefore, the domain $\mathbb{D}$ can be defined as:

$$\mathbb{D}=\left\{0<C_{11}\le C_{22}, 0<C_{12}\le\frac{C_{11}}{2}\right\}. \tag{1}$$

Inside this domain, the "Lagrange reduced" square lattice, with basis vectors aligned with the close-packed directions $\mathbf{e}_1=(1,0)$, $\mathbf{e}_2=(0,1)$, corresponds to point S_0 in Figure 1. Instead, the

"Lagrange reduced" triangular lattice with its basis vectors $\mathbf{h}_1 = \gamma(1,0)$ and $\mathbf{h}_2 = \gamma(1/2, \sqrt{3}/2)$, where $\gamma = (4/3)^{1/4}$, corresponds to the point T_0 in Figure 1.

In view of the $GL(2,\mathbb{Z})$ periodicity, it is sufficient to know the elastic energy for $\tilde{\mathbf{C}} \in \mathbb{D}$. One can then use the symmetry to write $\Phi(\mathbf{C}) = \Phi^0(\tilde{\mathbf{C}})$, where $\tilde{\mathbf{C}} = \mathbf{M}^T\mathbf{C}\mathbf{M}$ is the Lagrange reduced metric, and the function Φ^0 is defined only inside $\mathbb{D}$. The condition that the function Φ^0 is twice-differentiable can be satisfied if the deviatoric part of Φ^0 is a sixth order polynomial [185, 187]. With hexagonal symmetry chosen as global, one can write the minimal expression for such polynomial [180]

$$\Phi^0_d(\tilde{\mathbf{C}}/(\det\mathbf{C})^{1/2}) = \beta\psi_1(\tilde{\mathbf{C}}/(\det\mathbf{C})^{1/2}) + \psi_2(\tilde{\mathbf{C}}/(\det\mathbf{C})^{1/2}), \tag{2}$$

where, $\psi_1 = {I_1}^4 I_2 - 41\,{I_2}^3/99 + 7\,I_1 I_2 I_3/66 + {I_3}^2/1056$, and $\psi_2 = 4\,{I_2}^3/11 + {I_1}^3 I_3 - 8\,I_1 I_2 I_3/11 + 17\,{I_3}^2/528$. and we used the following hexagonal invariants $I_1 = 1/3(\tilde{C}_{11}+\tilde{C}_{22}-\tilde{C}_{12})$, $I_2 = 1/4(\tilde{C}_{11}-\tilde{C}_{22})^2 + 1/12(\tilde{C}_{11}+\tilde{C}_{22}-4\tilde{C}_{12})^2$, and $I_3 = (\tilde{C}_{11}-\tilde{C}_{22})^2(\tilde{C}_{11}+\tilde{C}_{22}-4\tilde{C}_{12}) - 1/9(\tilde{C}_{11}+\tilde{C}_{22}-4\tilde{C}_{12})^3$. The elastic energy density (2) depends on a single parameter β that may be used to enforce a particular symmetry on the reference state. For instance, the choice $\beta = -1/4$ guarantees that the global energy minimizers correspond to square lattices while the choice $\beta = 4$ shifts the bias towards the triangular lattice. In what follows, the total elastic energy will be then taken in the form $\Phi^0(\tilde{\mathbf{C}}) = \Phi^0_d(\tilde{\mathbf{C}}/(\det\mathbf{C})^{1/2}) + \Phi_v(\det\mathbf{C})$. The additive volumetric part of the energy density, which plays only minor role in this study by affecting the structure of dislocation cores and controlling the formation of voids, will be chosen in the form $\Phi_v(s) = \mu(s - \log(s))$. This choice, instead of a more realistic Lennard-Jones type potential, will allow us to avoid various volumetric instabilities while still excluding infinite compression. In particular, to ensure that the strain field remains close to the surface $\det\mathbf{C} = 1$ in our numerical experiments we choose large value of the bulk modulus by setting $\mu = 25$.

We remark that the particular potential (2) was chosen for illustrative purposes only and for most applications in crystal plasticity the piece-wise quadratic potentials with $GL(2,\mathbb{Z})$ symmetry would be sufficient, see for instance [39, 68]. Outside crystal plasticity, the general approach of MTM can be used as well with potentials satisfying less restrictive symmetry constraints, see for instance, [207].

3.2. *Energy landscape*

To visualize the local energy landscape we use the plane with coordinates $((C_{11}-C_{22})/\sqrt{2}, C_{12})$. In Figure 2(a) we illustrate the potential (2) with $\beta = -1/4$ describing an energy landscape whose absolute minima are the equivalent square lattices. To model plastic flows in triangular lattices with higher, hexagonal symmetry, we choose in (2) the parameter value $\beta = 4$ and the resulting elastic potential is illustrated in Figure 3(a).

In Figures 2(a) and 3(a) one can clearly distinguish between the "soft" directions located inside the deep valleys of the energy landscape (marked in blue), and the "hard" directions pointing away from the valleys and forcing the system to climb high energy barriers separating the valleys (yellow and red regions). Inside each low energy valley the energy is periodic with the bottoms of the energy wells corresponding to equivalent lattices. Thus, in the case of square lattices (Figure 2(a) the equivalent minima are denoted by $S_{\mathrm{i}}, S_{\mathrm{ij}}, \ldots, S_{\bar{\mathrm{i}}}, S_{\overline{\mathrm{ij}}}, \ldots$ and in the case of triangular lattices (Figure 3(a)), by $T_{\mathrm{i}}, T_{\mathrm{ij}}, \ldots, T_{\bar{\mathrm{i}}}, T_{\overline{\mathrm{ij}}}, \ldots$.

Note that while the energy is locally convex near the bottom of each energy well and can be approximated by the standard Hookean paraboloid, the global energy landscape is highly non-convex and can be characterized as rugged. In particular this means that outside the immediate vicinity of the energy wells bottoms the system finds itself in spinodal regions where the constitutive behavior *softens* opening the possibility for various mechanical instabilities. Note that the local maxima of the one parametric energy landscape along the low energy valleys turn out to

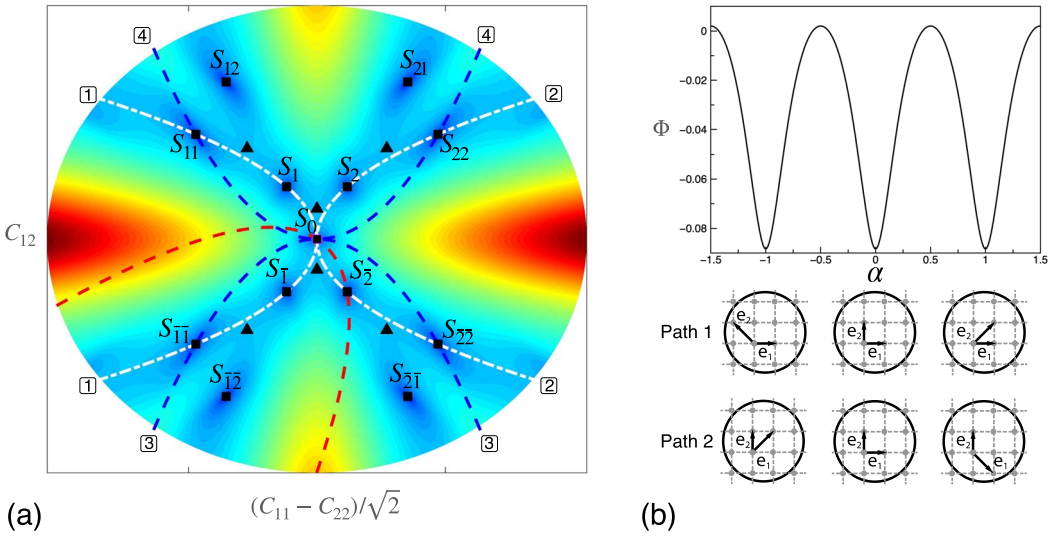

Figure 2. (a) The level sets of the strain-energy density (2) with $\beta = -1/4$. Colors indicate the energy level: blue, low; red, high. Dashed lines correspond to the simple shear loading paths $\mathbf{F}(\alpha, \phi)$ defined in (3). (b) The periodic strain-energy profile along the two symmetric paths 1–1 and 2–2 and the current state of lattice vectors.

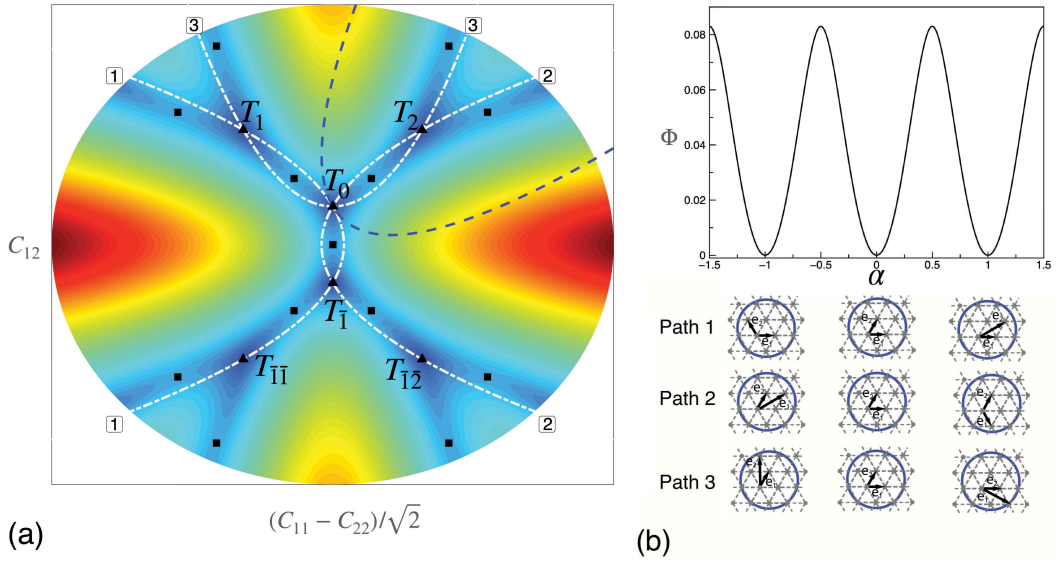

Figure 3. (a) The level sets of the strain-energy (2) with $\beta = 4$. Colors indicate the energy level: blue, low; red, high. Dashed lines correspond to the simple shear loading paths $\mathbf{F}(\alpha, \phi)$ defined in (4). (b) The periodic strain-energy profile along the three symmetric paths 1–1, 2–2, and 3–3 and the current state of lattice vectors.

be located very close to the configurations corresponding to saddles describing perfect lattices with alternative symmetries: triangular lattices, in the case when we shear a square lattice (see triangles near the local maxima along the white dashed paths in Figure 2(a)) and square lattices, in the case when we shear a triangular lattice (see squares near the local maxima along the white

dashed paths in Figure 3(a)).

CP theory obviously appreciates the implied complexity of the energy landscape but not in the same way as MTM. Thus, the low energy valleys are modeled as zero energy plastic "mechanisms". The periodicity of the energy inside the valleys is neglected and instead the phenomenological friction type lays are introduced to govern the "working" of such mechanisms. Elasticity is usually assumed to be linear and is only accounted for around the reference energy well, which is then extended globally. This does not create problems in CP because at large strains plastic deformation along the valleys always wins against elasticity which becomes at such strains prohibitively expensive energetically. To describe in the CP framework the coupling between different plastic "mechanisms", involved for instance in latent hardening [208], additional phenomenological relations have to be formulated. In MTM those will be automatically accounted for due to the presence of various saddle points (mountain paths) that are apparent in Figures 2(a) and 3(a).

To illustrate a more detailed structure of the energy landscape along the particular low energy valleys we now consider two parametric families of square lattices transformed to one another by the volume preserving shear deformations of the form

$$\bar{\mathbf{F}}(\alpha,\phi) = \mathbb{1} + \alpha \mathbf{a}(\phi) \otimes \mathbf{a}^{\perp}(\phi), \tag{3}$$

where α is the amplitude of shear, $\mathbf{a}(\phi) = \mathbf{R}(\phi)\mathbf{e}_1$, $\mathbf{R}(\phi)$ is a matrix describing a counterclockwise rotation by the angle ϕ, $\mathbf{e}_1$ is a unit vector of the Cartesian coordinate system directed along the close-packed x direction and $\mathbf{a}^{\perp}$ is a vector orthogonal to $\mathbf{a}$.

For instance, if we fix $\phi = 0$ and consider a one parametric family involving the metric tensors $\mathbf{C}(\alpha)$, we obtain the path 1–1, shown in Figure 2(a) by a dashed white line facing left. It starts at the reference state S_0, corresponding to the unstressed square lattice, and at integer values of parameter α generates an infinite sequence of equivalent unstressed replicas of the same square lattice. For instance, the "closest" lattices configurations S_1 and $S_{\bar{1}}$ can be reached from S_0 by the elementary shear deformations $\bar{\mathbf{F}}(\pm 1, 0)$.

If we choose instead $\phi = \pi/2$, we obtain another one parametric family of simple shears described by the path 2–2, shown in Figure 2(a) by a dashed white line facing right. It also starts at the reference state S_0 and produces at integer values of parameter α an infinite sequence of equivalent unstressed configurations of the square lattice. Once again, the "closest" lattices S_2 and $S_{\bar{2}}$ can be reached through the shear deformations $\bar{\mathbf{F}}(\mp 1, \pi/2)$.

The energy landscapes along these symmetric paths are the same, see Figure 2(b). Note that around the symmetric energy minima $\alpha = 0$ and $\alpha = \pm 1$, visible in such a graph, the energy is quadratic but then it loses convexity and the corresponding mechanical response starts to soften. Such softening is ultimately behind the break up of elastic response and the emergence of yield. If the system is quasi-statically driven through such an energy landscape, it undergoes a succession of snap-back instabilities which, under overdamped dynamics, merge into the dissipative plastic response which is postulated phenomenologically in the classical CP approach, see [189] for details.

Note that a *composition* of shear deformations from the paths 1–1 and 2–2 can be interpreted as an activation of a double-slip. For instance, the mapping $\bar{\mathbf{F}}(-1, \pi/2)\bar{\mathbf{F}}(1, 0)$ brings the system from the reference lattice configuration S_0 to the equivalent lattice configuration S_{12} after it slips in two perpendicular directions. In fact, all the bottoms of the energy wells $S_{\mathrm{ij}}, \ldots, S_{\bar{\mathrm{i}}\bar{\mathrm{j}}}, \ldots$, corresponding to equivalent square lattices, can be reached similarly by combining quantized simple shears (3) with $\phi = 0$ or $\phi = \pi/2$. Moreover, as we have already mentioned, a simple shear path leading away from one of the energy wells passes near the saddles corresponding to ideal lattices with different symmetries. It is then natural to conclude that these saddles serve as a switching points activating double slip and inciting composite shears. Based on these observations, one can argue that multiple alternative lattice symmetries, that are virtually invisible in the

"single symmetry" classical CP approach, may be contributing fundamentally to the complexity of plastic flows in crystals.

Periodicity of the energy along the particular *tensorial* directions, illustrated in Figure 2(b), is usually directly postulated in PFDD, with each of these directions bringing in a *scalar* order parameter of its own. To describe a *composition* of the corresponding shear deformations, the PFDD order parameters need to be coupled phenomenologically. Instead, in the MTM, such coupling is automatic due to the global symmetry requirements. Moreover the MTM approach allows one to assess the height and the structure of the barriers separating the corresponding valleys and controlling the activation of double-slip. Note also, that a combination of scalars can represent a globally defined tensorial variable (metric tensor) only approximately.

Turning back to Figure 2(a), we observe that the two other symmetric paths 3–3 and 4–4, shown by dashed blue lines, correspond to simple shears applied to the rotated crystal with $\phi = \pi/4$ and $\phi = 3\pi/4$. While these symmetric shears are no longer aligned with the dense planes of our square lattice, the corresponding loading paths are still special since they bring the system from the reference energy well S_0 directly to the second nearest energy wells, represented in Figure 2(a) by the small squares S_{11}, S_{22}, $S_{\bar{1}\bar{1}}$ and $S_{\bar{2}\bar{2}}$. Along such paths the energy landscape is also periodic but the period doubles and the separating barriers become much higher as these paths are largely located outside the low energy valleys. While in CP such paths are not viewed as plastic "mechanisms" that can be activated, they are still accounted for in the MTM which deals with the whole tensorial landscape and therefore encompasses all possible paths.

Finally, the red dashed line in Figure 2(a) illustrates a non-symmetric loading path with $\phi = \arctan(1/2)$, also originating in S_0. This path exhibits the characteristic loading–unloading asymmetry of *generic* simple shear deformations. In particular, along this path the equivalent square energy well $S_{\bar{2}}$ can be reached through "unloading" at $\bar{\mathbf{F}}(-1, \arctan(1/2))$ but none of the nearest square wells are reached upon "loading" with α positive.

The analysis above suggests the strong dependence of the plastic response on the orientation of the crystalline sample inside a hard loading device, even if it always applies the same simple shear deformation. The fact that there are soft and hard orientations has been long known in crystal plasticity. MTM approach presents a more nuanced picture, showing that the soft paths may come not only with different size of the periodically placed barriers but also with different periodicity, while along the hard paths one may expect extremely high barriers and generic loading–unloading asymmetry. The crucial advantage of the MTM is that all this complexity does not have to be postulated and emerges directly from the global symmetry of the energy landscape.

The obtained general picture is confirmed if we turn from square to triangular lattices, however, as the analysis below shows, the important differences between the energy landscape in lower symmetry (square) and higher symmetry (triangular) lattices exist.

In the case of triangular lattices we can again illustrate the available plastic "mechanisms" by considering the one parametric simple shear paths. The single slip plasticity in triangular lattices can be modeled by the shears

$$\bar{\mathbf{F}}(\alpha, \phi) = \mathbb{1} + \alpha \mathbf{b}_1(\phi) \otimes \mathbf{b}^2(\phi), \tag{4}$$

where $\mathbf{b}_A(\phi) = \mathbf{R}(\phi)\mathbf{h}_A$ with $A = 1, 2$. The (non-unit) lattice vectors $\mathbf{h}_A$ have been introduced earlier and the vectors $\mathbf{b}^A$ are their *duals* defined by the conditions $\mathbf{b}_A \cdot \mathbf{b}^B = \delta_A^B$.

Using (4), we can generate three symmetric shear paths originating in the unstressed lattice T_0 and describing plastic slips along the three close-packed directions. They correspond to crystal orientations $\phi = 0, \pi/3, 2\pi/3$, see the white dashed lines in Figure 3(a). Here again, for the integer values of α we obtain infinite families of equivalent replicas of the original triangular lattice. In particular, the lattice configurations T_1 and $T_{\bar{1}}$, located on the path 1–1, can be reached by the shear deformations $\bar{\mathbf{F}}(\pm 1, 0)$ starting from the lattice configuration T_0 (see the dashed white

line facing left). Upon further "unloading" $\bar{\mathbf{F}}(-2,0)$, another triangular lattice $T_{\bar{1}\bar{1}}$ can be reached, while the lattice configuration T_{11} is reachable by the matching additional "loading" $\bar{\mathbf{F}}(2,0)$ (not visible in Figure 3(a)).

The symmetry related paths 2–2 and 3–3, also shown in Figure 3(a) by dashed white lines, correspond to the shear deformations $\bar{\mathbf{F}}(\alpha,\pi/3)$ and $\bar{\mathbf{F}}(\alpha,2\pi/3)$. Both of them also originate in the point T_0 and produce at integer values of α infinite families of equivalent replicas of the original triangular lattice. Thus, along the path 2–2, one can reach the equivalent lattices T_2, $T_{\bar{1}}$, and $T_{\bar{1}\bar{2}}$, all visible in Figure 3(a). Similarly, the equivalent lattice configurations T_1 and T_2 are reachable along the path 3–3.

For each of these paths, which all correspond to the known plastic "mechanisms", the one dimensional periodic energy landscape is exactly the same, see Figure 3(b). The maxima of such energy landscapes are located close to the saddle points of the global energy landscape corresponding to square lattice configurations. Because they follow the low energy valleys of the global energy landscape (shown in blue in Figure 3(a)), these simple shear paths correspond to "soft" loading directions for a triangular lattice. Observe that such valleys are splitting into two in each of the energy wells which is clearly an easy mechanism for the activation of multi-slip in such higher symmetry lattices.

A non generic path with $\phi = \pi/2$ is also shown in Figure 3(a) (see the blue dashed line). In this case, the crystal is not driven along one of the low energy valleys, however it does pass through the bottoms of the energy wells (with period 3). If we load the crystal in shear along this "hard" direction, we can expected to reach the "yellow" and even "red" zones in Figure 3(a) and therefore acquire considerable elastic energy before the ultimate breakdown of an elastic state. Curiously enough, as we show below, this does not happen.

Since we use in this paper a particular expression for the energy (2), one may think that, given that the results depend on this choice, we cannot obtain generic picture for square and tetragonal crystals. However, the proposed energy has several universal features such as the exact location of the energy wells and the fact that they are quadratic close to lattice invariant shears. Moreover, the configuration of the low energy valleys and the connecting saddle points is also universal in the sense that it is dictated exclusively by the $GL(2,\mathbb{Z})$ symmetry. Of course, the potential-specific features of the energy landscape, like the curvatures of the wells and the height of the energy barriers, remain. In fact, such *quantitative* ambiguity is the element which MTM shares with all other Landau type theories. To assess this ambiguity, we have conducted a preliminary comparison of the results presented here with the outcome of the MTM, where the energy was constructed directly from an atomic model. While the fine structure of the dislocation cores was affected, we did not record any qualitative differences as far as the global post yield dislocation pattern is concerned [209].

Note also that the level of smoothness of the Landau potential can be improved if we replace the six order polynomials used in (2), by the higher order polynomials. Various exponential approximations were discussed in [186] and an example of an analytic function with $GL(2,\mathbb{Z})$ symmetry was presented in [40]. However, in general, such potentials are analyzed numerically and the possibility of a relatively simple analytic representation is not an issue. Therefore, physically relevant potentials can be constructed directly inside the fundamental domain $\mathbb{D}$ by analyzing homogeneous deformations of atoms and applying the Cauchy–Born rule. To this end one can use interatomic potentials, embedded atom methods and even quantum mechanics. Such numerically constructed energy potentials can be then continued by symmetry using the Lagrange reduction mentioned above or other similar approaches [206,210,211].

3.3. *Computational approach*

We now turn to the numerical implementation of the MTM approach. Its underlying idea is that rate-independent crystal plasticity can be modeled within the framework of the appropriately discretized nonlinear elasticity combined with athermal, overdamped dynamics. If the loading is sufficiently slow, the exact nature of such dynamics is not essential as long as it effectively performs incremental energy minimization [189,190]. As the loading evolves the system remains on the same branch of local minima of the energy till the latter ceases to exist and then it switches to another equilibrium branch. Such switching is a dynamic process (avalanche) which can be considered instantaneous at the time scale of the loading but it still contributes to dissipation. In this representation, plastic flow emerges as a set of equilibrium solutions of nonlinear elasticity with dissipation taking place exclusively during the abrupt branch switching events [189].

We recall that solution of an elastic problem implies local minimization of the energy

$$W = \int_{\Omega} \Phi(\nabla \mathbf{y}) \mathrm{d}\mathbf{x},$$

which is prescribed on a reference domain Ω with unit volume. We assume that the system is loaded by an affine displacement field prescribed on $\partial\Omega$ (hard device). The conditions of mechanical equilibrium can be formulated in terms of the first Piola-Kirchhoff stress tensor $\mathbf{P} = \partial\Phi/\partial\mathbf{F}$. In the index free form they can be written as

$$\nabla \cdot \mathbf{P} = 0.$$

Using the Eulerian $i, j = 1,2$ and the Lagrangian $K, L = 1,2$ indexes and assuming summation on repeated indexes, we can rewrite these equations in the form

$$A_{iKjL} y_{j,KL} = 0,$$

where

$$A_{iKjL} = \frac{\partial^2 \Phi^0(\tilde{\mathbf{C}})}{\partial F_{iK} \partial F_{jL}}. \tag{5}$$

Here $\tilde{\mathbf{C}} = \mathbf{M}^T \mathbf{C} \mathbf{M}$, where the integer-valued matrix $\mathbf{M}$ with determinant equal to one is computed for each value of $\mathbf{C}$ using the Lagrange reduction algorithm. The matrix $\mathbf{M}$ depends on the current state of deformation $\mathbf{F}$ in a piece-wise constant manner and therefore can be considered as constant in (5) which can be then rewritten as

$$A_{iKjL} = \mathrm{M}_{MN}\mathrm{M}_{PQ}\left[\frac{\partial C_{MP}}{\partial F_{jL}}\frac{\partial C_{AB}}{\partial F_{iK}}\mathrm{M}_{AC}\mathrm{M}_{BD}\mathrm{H}_{MQCD} + \frac{\partial^2 C_{MP}}{\partial F_{iK}\partial F_{jL}}\Sigma_{NQ}\right]. \tag{6}$$

Here we introduced the tensors

$$\mathbf{\Sigma} = \begin{bmatrix} \dfrac{\partial \Phi^0}{\partial \widetilde{C}_{11}} & \dfrac{1}{2}\dfrac{\partial \Phi^0}{\partial \widetilde{C}_{12}} \\ \dfrac{1}{2}\dfrac{\partial \Phi^0}{\partial \widetilde{C}_{12}} & \dfrac{\partial \Phi^0}{\partial \widetilde{C}_{22}} \end{bmatrix}, \tag{7}$$

and

$$\mathbf{H} = \begin{bmatrix} \begin{bmatrix} \dfrac{\partial^2 \Phi^0}{\partial \widetilde{C}_{11}^2} & \dfrac{1}{2}\dfrac{\partial^2 \Phi^0}{\partial \widetilde{C}_{12}\partial \widetilde{C}_{11}} \\ \dfrac{1}{2}\dfrac{\partial^2 \Phi^0}{\partial \widetilde{C}_{12}\partial \widetilde{C}_{11}} & \dfrac{\partial^2 \Phi^0}{\partial \widetilde{C}_{22}\partial \widetilde{C}_{11}} \end{bmatrix} & \dfrac{1}{2}\begin{bmatrix} \dfrac{\partial^2 \Phi^0}{\partial \widetilde{C}_{11}\partial \widetilde{C}_{12}} & \dfrac{1}{2}\dfrac{\partial^2 \Phi^0}{\partial \widetilde{C}_{12}^2} \\ \dfrac{1}{2}\dfrac{\partial^2 \Phi^0}{\partial \widetilde{C}_{12}^2} & \dfrac{\partial^2 \Phi^0}{\partial \widetilde{C}_{22}\partial \widetilde{C}_{12}} \end{bmatrix} \\ \dfrac{1}{2}\begin{bmatrix} \dfrac{\partial^2 \Phi^0}{\partial \widetilde{C}_{11}\partial \widetilde{C}_{12}} & \dfrac{1}{2}\dfrac{\partial^2 \Phi^0}{\partial \widetilde{C}_{12}^2} \\ \dfrac{1}{2}\dfrac{\partial^2 \Phi^0}{\partial \widetilde{C}_{12}^2} & \dfrac{\partial^2 \Phi^0}{\partial \widetilde{C}_{22}\partial \widetilde{C}_{12}} \end{bmatrix} & \begin{bmatrix} \dfrac{\partial^2 \Phi^0}{\partial \widetilde{C}_{11}\partial \widetilde{C}_{22}} & \dfrac{1}{2}\dfrac{\partial^2 \Phi^0}{\partial \widetilde{C}_{12}\partial \widetilde{C}_{11}} \\ \dfrac{1}{2}\dfrac{\partial^2 \Phi^0}{\partial \widetilde{C}_{12}\partial \widetilde{C}_{11}} & \dfrac{\partial^2 \Phi^0}{\partial \widetilde{C}_{22}^2} \end{bmatrix} \end{bmatrix}, \tag{8}$$

which are assumed as known inside the fundamental domain $\mathbb{D}$. We also recall here for convenience that $\partial C_{KL}/\partial F_{ij} = \delta_{Kj}F_{iL} + \delta_{Lj}F_{iK}$, and $\partial^2 C_{KL}/\partial F_{iM}\partial F_{jN} = (\delta_{KM}\delta_{LN} + \delta_{KN}\delta_{LM})\delta_{ij}$.

As we have already mentioned, the continuum elasticity problem, formulated above, is highly degenerate which is the property the MTM shares with other similar Landau type theories. Usually such theories are regularized through the introduction of an internal length scale. In contrast to the conventional Ginzburg–Landau approaches like PFDD, relying for regularization on higher gradients of the order parameters, in MTM the regularization is achieved by spatial discretization. More precisely, deformation is assumed to be piecewise linear and the elastic response is attributed to discrete material elements whose size is viewed as a physical parameter of the model [38, 40, 180].

We therefore need to reduce the space of admissible deformations to compatible piecewise-affine mappings. To this end we build a network whose discrete nodes are labeled by integer valued coordinates $a = 1, \dots, N^2$. We assume that each element of the network is a deformable triangle and write the displacement field in the form $\mathbf{u}(\mathbf{x}) = \mathbf{u}^a \mathcal{N}^a(\mathbf{x})$, where $\mathcal{N}^a(\mathbf{x})$ are the compactly supported shape functions, $\mathbf{u}^a$ are the amplitudes of nodal displacements and summation over repeated indexes effectively extends over elements containing or bounding point $\mathbf{x}$. The mesoscopic deformation gradient is then $\mathbf{F}(\mathbf{x}) = \mathbb{1} + \nabla\mathbf{u}(\mathbf{x})$, and the equilibrium equations can be written in the form

$$\frac{\partial W}{\partial \mathbf{u}^a} = \int_\Omega \mathbf{P}(\mathbf{F})\nabla\mathcal{N}^a(\mathbf{x})\,\mathrm{d}\mathbf{x} = 0, \tag{8}$$

where $\mathbf{P} = 2\mathbf{F}\mathbf{M}\boldsymbol{\Sigma}\mathbf{M}^T$. This problem can be solved by quasi-Newton method followed by the so called NR "refinement" when the initial guess is too far from the solution for Newton–Raphson method to converge initially [132].

More specifically, to solve (8) for $\mathbf{u}^a$ we first use the L-BFGS algorithm [212] which builds a positive definite linear approximation of (8) allowing one to make a quasi-Newton step lowering W. Such iterations continue till the increment in total energy W becomes sufficiently small. The obtained approximate solution is then used as an initial guess $\mathbf{w}^a$ to solve, using LU factorization [213, 214], the equations for the correction $\mathrm{d}\mathbf{w}^a$

$$K_{ij}^{ab}\,\mathrm{d}w_j^b + R_i^a = 0, \tag{9}$$

where

$$K_{ij}^{ab} = A_{iKjL}(\mathbf{F})\frac{\partial\mathcal{N}^a}{\partial x_K}\frac{\partial\mathcal{N}^b}{\partial x_L}, \quad R_i^a = P_{iK}(\mathbf{F})\frac{\partial\mathcal{N}^a}{\partial x_K}. \tag{10}$$

The displacement field can be updated in this way till the value of the integral in (8) is sufficiently small and then the loading parameter can be advanced again. In the case when the applied deformation is, a homogeneous shear $\bar{\mathbf{F}}(\alpha,\phi)$ with fixed orientation ϕ, the loading parameter is the shear amplitude α. By changing this parameter in increments of 10^{-4}, we advance the displacement field $\mathbf{u}(\alpha,\phi) = (\bar{\mathbf{F}}(\alpha,\phi) - \mathbb{1})\mathbf{x}$ for all nodes a on the boundary of the body $\partial\Omega$.

The outcome of such numerical experiments depends on the value of the internal length scale entering the discrete problem through the finite element size h. Each element contains n^2 interacting atoms, where $n = h/a$ and a is a fixed atomic scale. For such element deformed in simple shear we can use one of the known ab initio methods to compute its energy, which becomes close to periodic as we increase h. The value of this internal length scale used in MTM depends on the smallest range of energy periodicity required in the problem; in considered cases the periodicity at the level of the few first energy wells could be captured already for $h \sim 10a$.

Since the linear size of the macroscopic sample is $L = 1$, the small dimensionless parameter of the MTM is $h/L = 1/N$ where N^2 is the number of the nodes. Thus, if h is in nm size range, the simulations with $N \sim 10^3$ would describe a micrometer size crystal. When N is small, dislocation

cores emerge as *blurred* because the scales smaller than $1/N$ are homogenized out. While such cut-offs may compromise the short-range interaction of dislocations, long-range interactions at distances larger than $1/N$ will be captured correctly.

4. Numerical experiments

To understand the paradoxical crack-free brittle behavior of very small, initially dislocation-free crystals, we used MTM and conducted a series of numerical experiments with square and triangular crystals. The samples were subjected to simple shear, and we performed experiments with several different orientations of the same samples in the same hard loading device. We used square cut samples in all our experiments and could vary the system size up to $N = 1024$.

4.1. *Macroscopic response*

The obtained macroscopic responses for crystals described by the piece-wise smooth potential (2) are summarized in Figures 4(a) and (b). We show separately the energy–strain and the stress–strain responses for square and triangular crystals loaded in different orientations. The energy was obtained by incremental local minimization starting from the reference state. To compute the stress–strain curve, we define the resolved-shear stress in the direction of loading as $\tau(\alpha) = \mathrm{d}W/\mathrm{d}\alpha = \int_\Omega \mathbf{P} : (\mathrm{d}\bar{\mathbf{F}}/\mathrm{d}\alpha)\mathrm{d}x$.

In each of our numerical experiments, the initial phase of the deformation history is (non-linear) elastic. During this stage, all elements have associated metrics that remain inside the extended fundamental neighborhood of the initial phase (Pitteri neighborhood [188]), comprised of four (in case of square symmetry) or six (in case of triangular symmetry) symmetric replicas of the fundamental domain. While the response of the crystal inside such domain is nominally elastic, our experiments show that the affine deformation becomes unstable before the boundary of this neighborhood is reached. The instability takes place at a critical value of the loading parameter $\alpha = \alpha_c^*$ which depends not only on crystal symmetry and crystal orientation, see Figure 4, but also on the value of N (see below). The breakdown of affine elastic regime takes the form of a catastrophic drop in both stress and energy. While these drops are still associated with plastic deformation, they are highly reminiscent of brittle fracture.

We now discuss how the macroscopic mechanical behavior during such discontinuous yield depends on crystal symmetry and how it varies when crystals of the same symmetry are differently orientated in the loading machine.

We start with a pristine square crystal that we load along the principal slip direction with $\phi = 0$. In such an "easy" glide direction, the instability is preceded by the purely elastic softening, and the yield takes place near the maximal load. However, instead of conventional continuous yielding, the crystal experiences discontinuous yield as it abruptly loses almost all accumulated energy with stress dropping almost to zero. This means that the crystal manages to expel almost all nucleated dislocations away from its bulk, either by annihilating or sending them towards the boundaries. If the boundaries were unconstrained, the transition would be pristine-to-pristine, but in the hard-device loading conditions, at least some of the nucleated dislocations end up forming low energy piles-up near the boundaries (see more about this in the next section).

A similar almost pristine-to-pristine discontinuous-yield occurs in the case of a less symmetric but still non-generic shear with $\phi = \pi/4$ but only after both the elastic energy and the stress reach a much higher value. As we have already seen, along this loading path, the periodicity strain doubles, and the barriers become much higher than in the case of shear loading directed along the low energy valley. The crystal is first driven away from such valley and, before yielding, manages to accumulate a considerable amount of energy without an apparent softening. It is then

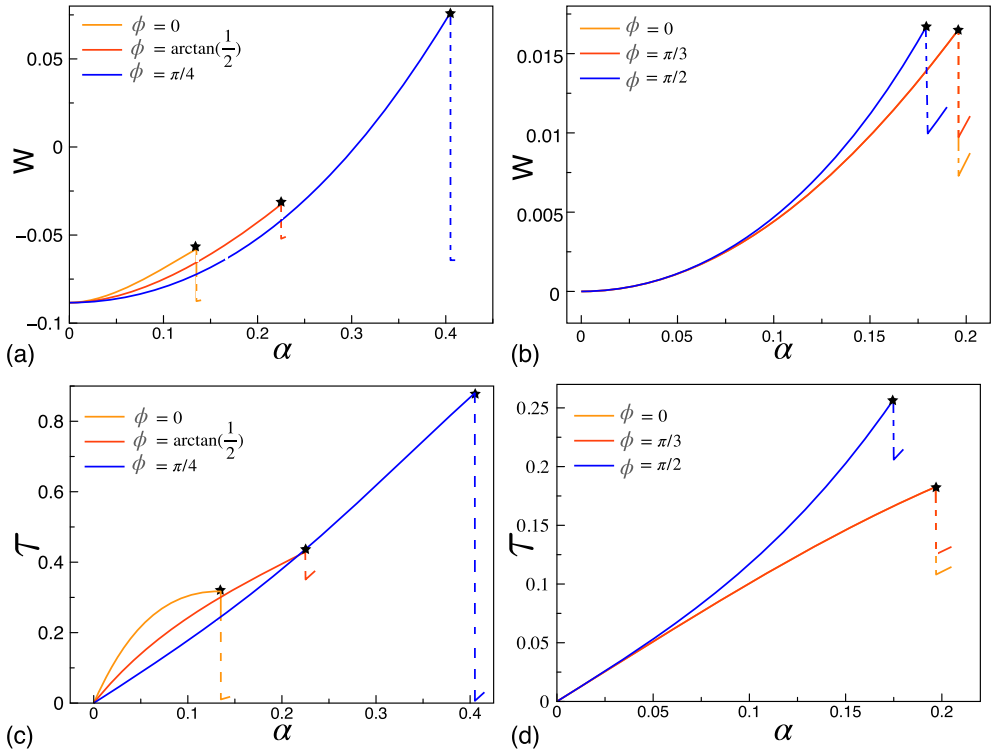

Figure 4. Macroscopic mechanical response of square (a–c) and triangular crystals (b–d) subjected to simple shear loading: (a,b) the equilibrium elastic energy $W(\alpha)$ (c,d); the equilibrium stress $\tau(\alpha)$.

rather remarkable that the eventual breakdown of the elastic state leads to almost complete relaxation of considerable elastic stress. The explanation probably lies in the fact that the crystal's orientation is still special vis a vis the applied load.

Loading of the crystal in a non-generic tensorial direction $\phi = \arctan(1/2)$ leads to a moderate softening in the elastic range, which again ends with a discontinuous yield. The resulting dislocation avalanche relaxes the stored elastic energy only minimally. This suggests that the crystal is left with considerable amount of dislocations which may not be strongly correlated.

In triangular lattices with hexagonal crystallographic symmetry, the macroscopic mechanical response is different. For two loading paths with $\phi = 0$ and $\phi = \pi/3$, passing inside the low energy valleys, the overall softening nonlinear elastic response terminates with a yielding avalanche which takes place at exactly the same level of energy and the same value of the loading parameter. The pristine state is not recovered after the discontinuous yield because higher symmetry gives rise to geometric frustration, and the stored elastic energy cannot be fully resolved through dislocation self-organization. However, the resulting stress drop is considerable, which suggests that long-range correlations have been created. The slight difference in the terminal post-avalanche state for the paths with $\phi = 0$ and $\phi = \pi/3$ is a finite size effect suggesting that the corresponding instability modes interact differently with the incommensurate square shape of the sample.

Along the non-generic "hard" loading path with $\phi = \pi/2$, the crystal shows hardening nonlinear elastic response, however, the yielding stress is only slightly higher than in the case of the "soft" paths considered above. The discontinuous yield leads again to relatively small energy relaxation, suggesting that a high symmetry environment favors the considerable accu-

mulation of dislocations. However, the stress drop is smaller than along more symmetric "soft" paths, which hints towards a higher level of frustration and weaker long-range correlations in the post-buckling equilibrium state.

To summarize, our numerical experiments suggest that nominally ductile crystals, which are expected to yield continuously in the bulk form (large N, pre-existing defects), can undergo a brittle-to-ductile (BD) transition when the value of N and the initial dislocation density both drop below certain thresholds. Such brittleness has been indeed realized to be a characteristic feature of sub-micron samples with high initial purity (absence of solutes, precipitates, and dislocations). The implied discontinuous yield results from massive homogeneous nucleation of dislocations in the form of a highly cooperative avalanche. As we have shown, the MTM can successfully simulate such avalanches and captures not only the catastrophic stress drop but also, in some cases, the recovery of almost pristine post-avalanche states. Even more importantly, MTM allows one to study the *subtle* quantitative dependence of the parameters of such discontinuous yield on crystal symmetry and sample orientation. Some features of the observed behavior may depend on our particular choice of the Landau potential, like for instance, the crossover from elastic softening to elastic hardening depending on the orientation of the sample; the question whether such behavior is instead a generic property of all $GL(2,\mathbb{Z})$ symmetric potentials will be addressed elsewhere.

4.2. *Ideal shear strength*

To rationalize the observed behavior, we now study analytically the linear stability of an affine elastic response in homogeneously deformed crystals. From the classical continuum elasticity standpoint, the instability would mean that a homogeneous configuration is no longer a weak local minimum of the elastic energy. In a hard device, such instability results from the local loss of rank-1 convexity of the elastic energy density which also means the loss of strong ellipticity of the equilibrium equations [215, 216]. The instability in the regularized model is necessarily delayed which is one of the sources of the "smaller is stronger" size effect in sub-micron crystals.

Consider a homogeneous configuration of an elastic crystal with deformation gradient $\mathbf{F}$ rigidly imposed on its boundary. Suppose that this state becomes linearly unstable at the critical value of the imposed strain $\bar{\mathbf{F}}^c$. To find this threshold, we need to linearize the equilibrium equations around the homogeneous state. If we write them in terms of small incremental displacements $\mathbf{u}$ superimposed on the homogeneous state $\mathbf{F}$ (used as the reference state), we obtain the system

$$\mathcal{A}_{piqj}(\mathbf{F})u_{j,pq} = 0,$$

where $\mathcal{A}_{piqj}(\mathbf{F}) = F_{pK}F_{qL}A_{KiLj}$ is the (Eulerian) tensor of incremental moduli. The unstable mode can be represented as a combination of Fourier components $\mathbf{u} = \boldsymbol{\eta}\exp(\mathrm{i}k\boldsymbol{n}\mathbf{x})$, where $\boldsymbol{n}$ is the unit normal selecting the modulation direction, $\boldsymbol{\eta}$ is the amplitude, and k is the wave number. In the Fourier space, this equation can be re-written as

$$[\boldsymbol{\Omega}(\mathbf{F},\boldsymbol{n})\boldsymbol{\eta}]\boldsymbol{\eta} = 0,$$

where $\Omega_{jl}(\mathbf{F},\boldsymbol{n}) = \mathcal{A}_{ijml}n_i n_m(\mathbf{F})$ is the Eulerian acoustic tensor [217, 218]. Stability of the homogeneous state $\mathbf{F}$ is lost when there exists a non-trivial $\boldsymbol{n}$ such that

$$\mathtt{det}\,\boldsymbol{\Omega}(\mathbf{F},\boldsymbol{n}) = 0.$$

This condition can be used to identify the unstable values of $\mathbf{C}$ [219–221]. Generalizing the classical definition of Frenkel [222], we can associate the ideal shear strength with such $\mathbf{C}$ and compute them by performing a sequence of monotone loading tests. The ensuing critical

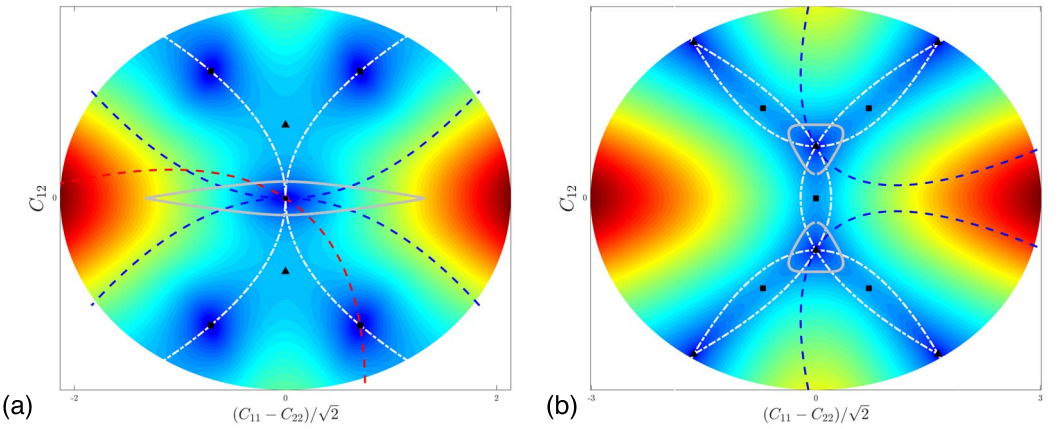

Figure 5. Surfaces of ideal shear strength for square (a) and triangular (b) crystals. Silver contours delimit the domains of linear stability for homogeneous states. The strain-energy density is taken from (2).

orientation $\boldsymbol{n}$ and the associated polarization $\boldsymbol{\eta}$ can be interpreted as the characteristics of the incipient defects, see, for instance, [76, 77, 141, 142, 223, 224].

To identify the sub-domain in the space of reduced metric tensors (inside the extended fundamental domain) where the homogeneous deformations are stable, we conducted a series of numerical experiments with differently oriented lattices loaded by shear deformations of the form (3) and (4). Interpolating over a family of one parametric paths we obtained the surfaces of ideal strength for both square and triangular lattices, see the light grey contours in Figures 5(a) and 5(b), respectively. These contours represent upper bounds for the sets which can be interpreted as continuum yield surfaces.

Observe that such surfaces may have rather different shapes: more elongated in the case of less symmetric square lattices and more round in the case of more symmetric triangular lattices. To maintain the symmetry of the configurational space, we showed in the case of triangular lattice two symmetric yield surfaces. Similar stability boundaries can be, of course, constructed around each of the equivalent replicas of the unstressed lattices [40].

The strong asymmetry of such yield surface in the case of square lattices, see Figure 5(a), shows that if an anisotropic crystal is loaded in "soft" and "hard" tensorial directions it can exhibit very different strength. Thus, the instability can take place either inside the low energy valley or get delayed till after the crystal has first stored considerable amount of elastic energy. Instead, in high symmetry crystals the apparent yield surface is almost isotropic, see Figure 5(b), and since in this case all tensorial loading directions are almost equally "soft", the expected theoretical strength is low independently of the orientation of the applied shear.

In our numerical experiments, the parameters of discontinuous yield were practically indistinguishable from the computations based on the idea of ideal shear strength, see small stars on the stress–strain and energy–strain graphs in Figure 4. This means that inside the elastic range the system with $N = 1024$ is adequately described by the continuum limit. This also justifies the experimental observations that pristine sub-micron crystals yield close to the limits of theoretical strength which therefore cannot be improved without changing the nature of the crystal.

It is instructive to look in more detail at the instability modes for crystals reaching different points $\alpha = \alpha_c(\phi)$ along the surface of ideal strength. The knowledge of the corresponding vectors $\boldsymbol{n}_c$ and $\boldsymbol{\eta}_c$ allows one to identify the primary instability modes which, at least for sufficiently large

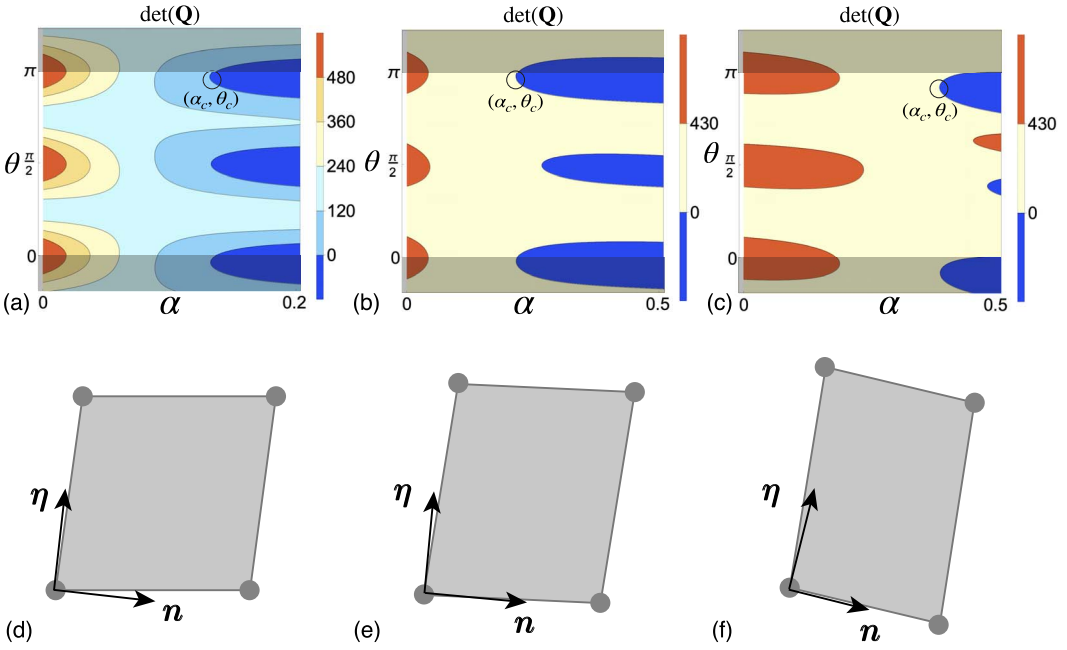

Figure 6. Instability limits for square lattices: (a–c) level sets for the determinant of the Eulerian acoustic tensor, (d–f) parameters of the unstable modes vis a vis the deformed lattice vectors. (a) $\phi = 0$, (b) $\phi = \arctan 1/2$ and (c) $\phi = \pi/4$. The parameters (α_c, θ_c) are calculated from the condition $\det(\mathbf{Q}) = 0$.

N, guide the eventual nucleation of dislocational dipoles. Since the value of the bulk modulus μ in the strain-energy density was chosen to be sufficiently large, our crystals are effectively incompressible and therefore we can always expect that approximately $\boldsymbol{n}_c \perp \boldsymbol{\eta}_c$ and the instability mode is close to a simple shear.

Consider first square lattices, and assume that the macroscopic loading paths are again given by (3) with $\phi = 0, \arctan(1/2), \pi/4$, see Figure 2. In Figure 6(a–c) we show the evolution of the determinant of the Eulerian acoustic tensor along each of these path as a function of the parameter θ defining the orientation of the unit vector $\boldsymbol{n} = (\cos\theta, \sin\theta)$. The external boundaries of the dark blue regions define the stability limits and the smallest value of the loading parameter α on one of such boundaries, defines the maximal homogeneous strain achievable along the corresponding loading path. Note that the whole pattern is periodic in θ and only one period is shown in Figure 6(a–c).

We recall that the "soft" path with $\phi = 0$ corresponds to a simple shear along one of the dense planes of the square lattice. According to Figure 6(a), at the critical value of the loading parameter $\alpha_c \approx 0.134$, the associated $\theta_c \approx 3.035$ rad. Since the unit vectors $\boldsymbol{n}_c$ and $\boldsymbol{\eta}_c \approx \boldsymbol{n}^{\perp}$ are almost parallel to the current (deformed) lattice vectors, see Figure 6(d), the unstable mode essentially activates a single slip in the "vertical" direction. This is illustrated in Figure 7 where we show the orientation of the unstable mode. Note that the red arrow in Figure 7 points to the right of the pure shear path. This, together with the global topography of the energy surface suggests that the instability will develop in the direction of the energy well S_2 rather than S_1.

The fact that this first unstable mode is not the one associated with $\theta_c \approx \pi/2$, which would mean a single slip in the "horizontal" direction, may be thought as counter-intuitive based on the naive application of the plastic "mechanisms" approach of CP. And indeed, the mode

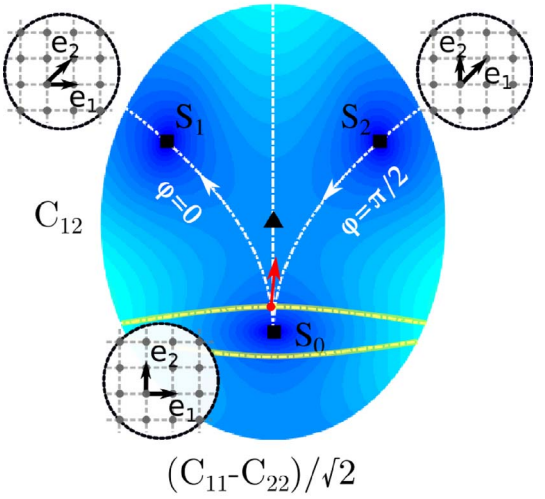

Figure 7. The orientation (in the configurational space of metric tensors) of the first unstable mode along the simple shear loading path $\phi = 0$ originating in S_0 (red arrow). Yellow curve is the theoretical strength threshold. The white dashed path passing through the black triangle (traingular lattice T_0) corresponds to pure shear. Shades of blue show the level sets of the potential. White arrows point in the direction of growing simple shear amplitude α.

with $\theta_c \approx 1.5746$ rad, which corresponds to the anticipated "horizontal" direction of slip, is destabilized right after the mode with $\theta_c \approx 3.035$ rad. The *splitting* of these two modes is the effect of geometric nonlinearity. Thus, if kinematics is linearized, which essentially means that the terms of the order of α^2 are neglected, simple shears along the tensorial directions $\phi = 0$ and $\phi = \pi/2$ become indistinguishable since

$$\mathbf{C}(\alpha,0) = \begin{bmatrix} 1 & \alpha \\ \alpha & 1+\alpha^2 \end{bmatrix}, \quad \mathbf{C}(-\alpha,\pi/2) = \begin{bmatrix} 1+\alpha^2 & \alpha \\ \alpha & 1 \end{bmatrix}. \tag{11}$$

The geometrically linearized theories, neglecting the terms *quadratic* in α, are confined to the plane $\mathtt{tr}\,\mathbf{C} = 2$, which is tangential to the hyperboloid $\det\mathbf{C} = 1$ at S_0, see Figure 8. In such theories, see, for instance, [174, 176–178], the strain paths corresponding to the simple shearing deformations $\bar{\mathbf{F}}(\alpha,\phi = 0)$ and $\bar{\mathbf{F}}(-\alpha,\phi = \pi/2)$ would merge into a single line $C_{11} = C_{22} = 1$. As a result, for instance, the two minima S_1 and S_2 would collapse on each other, see Figure 8. In our geometrically nonlinear approach the applied simple shear biases one of these modes and, as we have seen above, the two plastic "mechanisms" end up activated *consecutively* rather than *simultaneously* as the linearized theory (as well as classical CP) would suggest. Similar degeneracy occurs also in the case of triangular lattices if the configurational space is reduced to the plane tangent to the point T_0 as in [225].

For our two other loading paths with $\phi = \arctan(1/2)$ and $\phi = \pi/4$, see Figure 6(b,c), a single unstable mode can be clearly isolated. The vectors $\boldsymbol{n}_c$ and $\boldsymbol{\eta}_c \approx \boldsymbol{n}_c^{\perp}$ are again almost parallel to the deformed lattice vectors in the case of $\phi = \arctan(1/2)$ path, see Figure 6(e). The ensuing instability is close to the one along the path $\phi = 0$. In particular, a single slip system is activated ("vertical") and initially nucleated dislocation dipoles is of one type only. The post-bifurcational localization can be then again expected to take the form of the nucleation of dislocation pairs along the plane selected by the condition of continuum instability as in Peierls–Nabarro model [169].

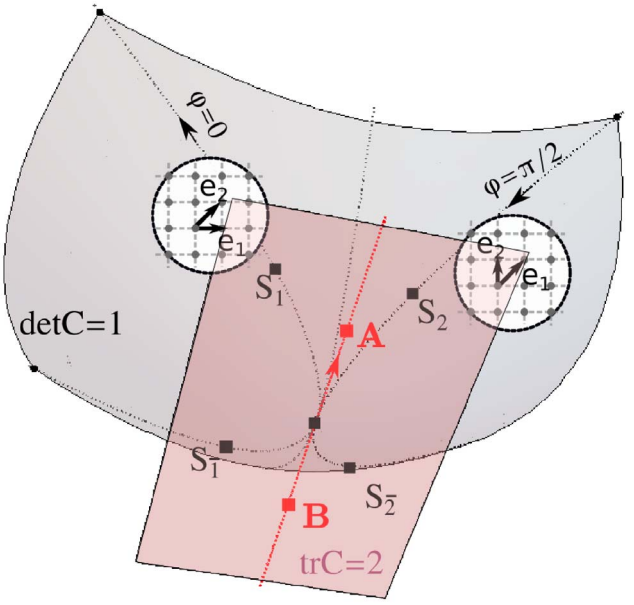

Figure 8. The effect of the geometric linearization of MTM around the square energy well S_0. In such approximation the (gray) hyperbolic surface $\det\mathbf{C} = 1$ is replaced by the (pink) tangent plane $\mathtt{tr}\,\mathbf{C} = 2$. The two simple shear paths with $\phi = 0$ and $\phi = \pi/2$ as well as the pure shear path (shown by a separating gray dashed line) collapse into a single path shown by the red straight line AB. Here a single point A describes the two square lattices S_1 and S_2, while a single point B stands for the two square lattices $S_{\bar{1}}$ and $S_{\bar{2}}$.

In the case of $\phi = \pi/4$ path, see Figure 6(f), the situation is different because the pre-instability lattice is strongly distorted and is almost rectangular. The instability mode is no longer aligned with the low energy valleys of the energy landscape which should lead to the simultaneous activation of both slip systems and the emergence of both "vertical" and "horizontal" dislocations. Overall, as we move away from the "soft" path $\phi = 0$, the loading directions become progressively "harder" and along such paths the instability takes place at higher values of energy density. Given that the corresponding unstable modes are not perfectly aligned with deformed lattice vectors, the ensuing geometrical frustration should lead to higher complexity of the dislocation patterns.

In the case of triangular lattice, we again consider non-generic simple shear loading paths along the dense crystallographic planes with $\phi = 0$ and $\pi/3$ and a generic path with $\phi = \pi/2$, see (4). The first two represent "soft" shearing directions, while the last one is the "hard" one facing potentially higher energy barrier. Figure 9(a,b,c) show the level sets of the determinant of the Eulerian acoustic tensor in the plane of parameters α and θ for each of the three paths.

Note first that, in contrast to the case of square symmetry, here the instability thresholds along different paths do not differ considerably. Moreover, the apparently "hard" path with $\phi = \pi/2$, which does not correspond to any straightforward plastic "mechanism", gets destabilized before the apparently "easy" ones with $\phi = 0$ and $\phi = \pi/3$. We reiterate that such quasi-uniformity of the instability conditions is a natural property of higher symmetry lattices with all thresholds collapsing onto one in the case of ideal isotropic solids (with superimposed fluctuations in the case of amorphous glasses or polycrystals).

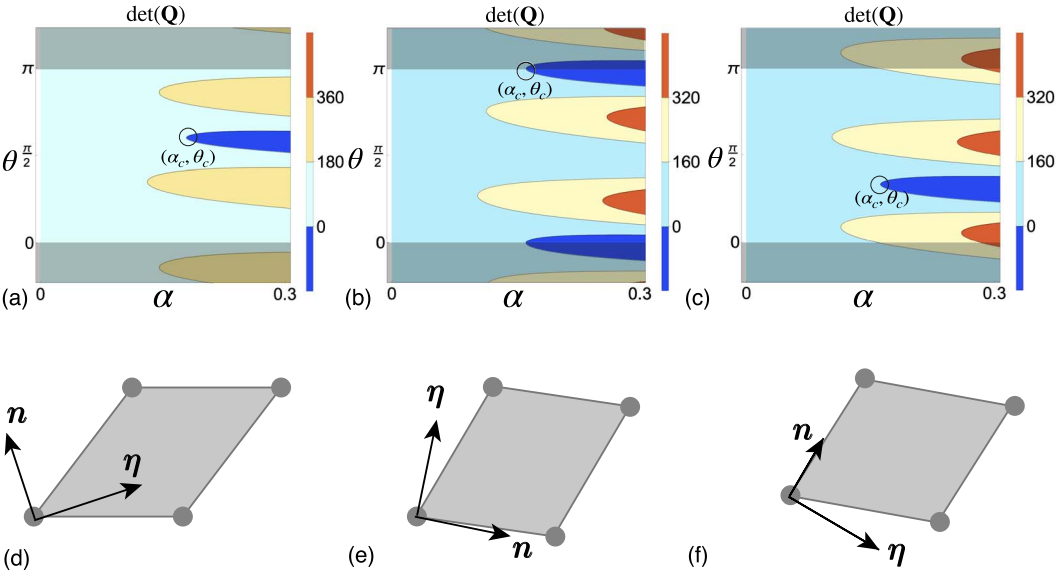

Figure 9. Instability limits for triangular lattices: (a–c) level sets for the determinant of the Eulerian acoustic tensor, (d–f) parameters of the unstable modes vis a vis the deformed lattice vectors. (a) $\phi = 0$, (b) $\phi = \pi/3$ and (c) $\phi = \pi/2$. The parameters (α_c, θ_c) are calculated from the condition $\det(\mathbf{\Omega}) = 0$.

We also observe that in all three cases the instability modes are characterized by the vectors $\boldsymbol{n}_c$ and $\boldsymbol{\eta}_c \approx \boldsymbol{n}_c^{\perp}$ that are no longer co-linear with the orientation of the deformed lattice basis. This suggests that the initial patterning, controlled by the continuum instability, is incommensurate with lattice slips and therefore the mechanism of dislocation nucleation may be rather different from the one predicted by the Peierls–Nabarro model [169]. The fact that still $\boldsymbol{\eta}_c \approx \boldsymbol{n}_c^{\perp}$ suggests that the macroscopic instability will appear in the form of simple shear, however, the misalignment of the instability mode with crystallographic slip planes makes the prediction of the actual activated slip planes difficult.

To show the effect of finite N, we also studied the stability limits in the original discrete setup, see also [213,226]. To this end we computed the smallest eigenvalue of the $2N^2 \times 2N^2$ Hessian matrix K_{ij}^{ab}. Our Figure 10 shows that although the critical value of the loading parameter $\alpha_c^*(N)$ in the discretized problem, chosen by the condition that such eigenvalue is equal to zero, is slightly larger than the ideal shear strength α_c in the continuum problem, the two approach each other quickly as the element size $h = 1/N$ decreases. In the case of square lattices the gap closes up already at $N \sim 100$ as the instability directions are almost perfectly aligned with the deformed crystal, see Figure 10(a). In the case of triangular lattices, the misalignement is much stronger and the finite size effect in the form of a gap between the predictions of discrete and continuum theories remains apparent for much smaller element sizes, see Figure 10(b). Note that the asymptotic behavior of the smallest eigenvalues near zero, shown in Figure 10, is different from the prediction of the theory of amorphous plasticity where the corresponding eigenvectors are quasi-localized [227–229]. The linear response of pristine crystalline solids with zero disorder is global and that is why its elastic instabilities can be largely captured by the classical continuum theory.

The dependence of the instability threshold α_c^* on the system size N is illustrated in Figure 11. The theoretical limit, effectively reached by the samples with $N = 1024$, is shown by the red dashed line. At small N we observe the emergence of a nontrivial asymptotics $\alpha_c^* \sim N^{-1/3}$.

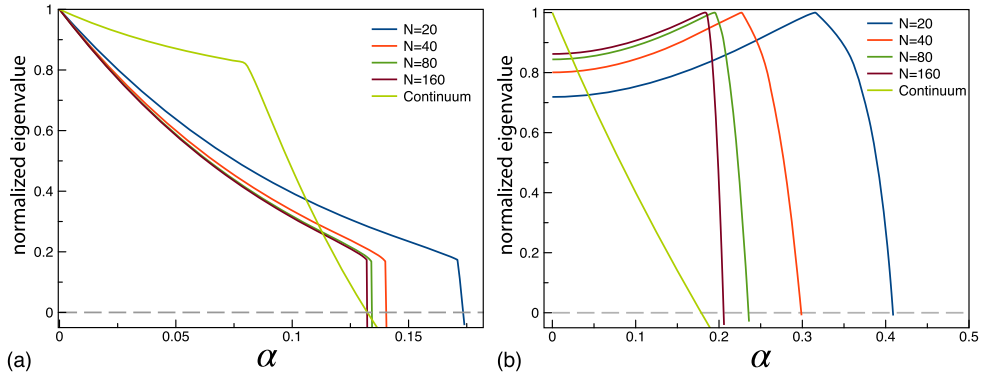

Figure 10. Smallest eigenvalue of the discrete stiffness matrix **K** as a function of the loading parameter α for different values of element size $h = 1/N$: (a) square, (b) triangular lattice. The crystal orientation is always $\phi = 0$. In the continuum case, we show the smallest eigenvalue of the acoustic tensor $\mathbf{Q}(\mathbf{F}, \boldsymbol{n}_c)$.

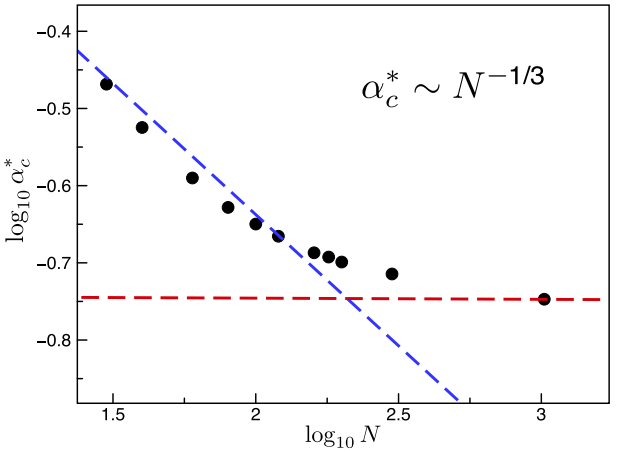

Figure 11. System size dependence of the critical loading parameter $\alpha_c^*(N)$ in numerical experiments with triangular crystals oriented at $\phi = 0$.

It suggest that the spatial scale of the dislocation microstructure is of the order $\sim h^{1/3}L^{2/3}$, which may imply hierarchical "domain splitting" near the external boundaries.

For square and triangular lattices with $N = 40$ we illustrate in Figure 12(a,b), the $2N^2$ dimensional eigenvectors u_i^a of the corresponding Hessian matrices K_{ij}^{ab} when their lowest eigenvalues crosses zero at α_c^*. These eigenvectors are presented as vector fields with the homogeneous component subtracted. In both cases, the modulations have orientations $\boldsymbol{n}_c^*$ that are close to the ones predicted by the continuum theory. However, if the unstable wavenumber remains arbitrary in the scale-free continuum theory, the discrete theory selects a particular length scale. The strong misalignment, in the case of triangular lattices between the orientation of the macro modulations and the lattice vectors, see Figure 12(b), can delay the transition to the ultimate lattice scale instability culminating in the nucleation of dislocation dipoles. In the case of square lattices, shown in Figure 12(a), we observe lattice scale modulations present already in the original unstable mode. They correspond to the wave vectors at the boundary of the Brillouin zone, see some elementary examples of such multiscale instabilities in [230, 231].

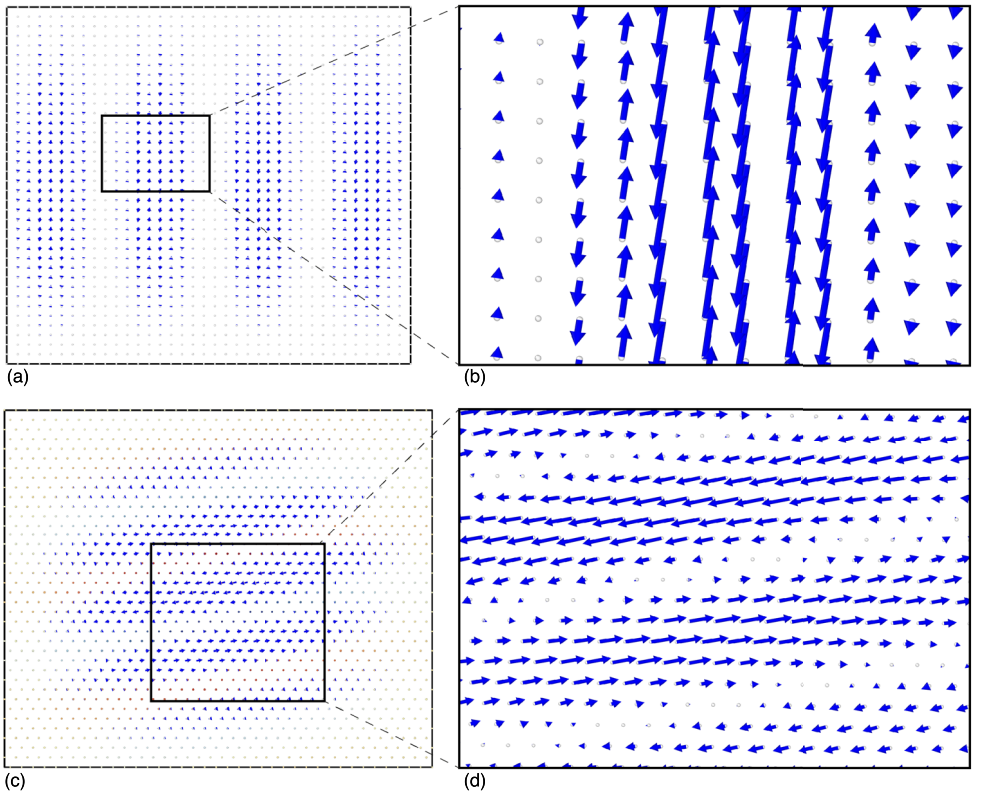

Figure 12. Unstable modes at the instability point for square (a) and triangular (b) lattices. Blue arrows show the modes associated with the lowest eigenvalue of the stiffness matrix **K**. Here $N = 40$ and $\phi = 0$.

To summarize, our numerical experiments show that pristine sub-micron crystals exposed to affine deformation yield discontinuously near the thresholds of theoretical strength. In the case of simple shear loading, the obtained thresholds show dependence on the orientation of the sample in the loading device, which is in qualitative agreement with experimental results, e.g. [35,36]. Our study also reveals a strong link between the structure of the apparent yield surface and the lattice symmetry.

5. Discontinuous yielding

In this section, we turn to the study of the fine structure of the microscopic response following the loss of stability of the homogeneous state. The goal is to reveal the detailed unfolding of the catastrophic dislocation nucleation avalanche and trace how the final configuration, containing a large number of defects, emerges in the process of energy minimization. In particular, we show that complementary pictures of the evolving defect configurations emerge in the real and the configurational spaces.

All numerical experiments start with a dislocation-free crystal $\mathbf{u} = 0$, and we drive the system using an athermal quasistatic protocol. We use hard device boundary condition controlling the positions of surface nodes and impose in this way an affine deformation $\bar{\mathbf{F}}$ on the boundary of a square domain and choose the loading step (strain increment) sufficiently small to ensure

continuity of the minima outside the avalanches. The macroscopic stress–strain and energy–strain curves obtained in such numerical experiments are summarized in Figures 4(a) and 4(b) for the square and triangular crystals, respectively.

For $\alpha < \alpha_c^*$ the picture is rather simple. In real space, the deformation is affine $\mathbf{F}(\mathbf{x}) \equiv \bar{\mathbf{F}}$ and in the configurational space of the metric tensors $\mathbf{C}$ we observe the perfect overlap for all elements. As we have already mentioned, there is an excellent agreement between the numerical value of α_c^* and the predicted value of ideal shear strength, see Figure 4. As soon as stability is lost, the homogeneous configuration breaks down. The pristine crystal transforms into a highly defected one, with most of the dislocations eventually escaping from the bulk and forming various pile-ups near the fixed boundaries. The configurational points, corresponding to different elastic elements, spread in the space of metric tensors $\mathbf{C}$, reaching the neighborhoods of distant energy wells. The emerging dislocation patterns, which we discuss in detail below, were obtained from the simulations involving more than a million elements.

5.1. *Square lattices*

Consider first a square crystal loaded in a crystallographically exact simple shear with $\phi = 0$. In Figure 13, we show the snapshots of the distribution of the shear component of the Cauchy stress $\sigma = (\det \mathbf{F})^{-1}\mathbf{F}\mathbf{P}^T$ in the physical space as the crystal evolves (in fast computational time) through the avalanche after the loading parameter has reached the value α_c^*. In the insets, we illustrate the concurrent evolution of the cloud of configurational points in the space of metric tensors which tracks different stages of the implied energy minimization process.

At positive values of the loading parameter α the crystal is driven along the energy valley away from the energy minimum S_0 towards the minima S_1, S_{11}, etc. This could suggest the development of plastic slip along the horizontal plane, however, as we have seen, the first instability is "vertical" which means activation of the slip system represented by the minima S_2, S_{22}, etc., see Figure 6. While the initial states of the avalanche are indeed dominated by the activation of the vertical dislocation dipoles, see Figure 13(a), horizontal dipoles appear later as well because of local stress concentration and consequent involvement of the second slip system which is predicted by the instability analysis to be activated at slightly larger loading levels, see Figure 13(b).

Note that the two low energy valleys merge around the point T_0, which describes a triangular lattice. The structure of the energy landscape around this point is close to a monkey saddle[3] and passing of configurational points through such region creates non-trivial coupling between horizontal and vertical slip systems. As a result, even though most of the units move towards the energy well S_2 some of the configurational points eventually also populate the energy well S_1. As the crystal is driven further, it is pulled towards another (almost) monkey saddle describing the triangular lattices T_1. Around this intersection of the low energy valleys, the configurational points take a turn towards the energy well S_{12} instead of continuing towards apparently more natural well S_{11}. Similarly, around the (almost) monkey saddle T_2 the configurational flow is directed towards the energy well S_{21}, see Figure 13(b–d). All these choices depend sensitively on the boundary conditions and will be rationalized in a separate publication.

To see how the spreading of the configuration points in the space of metric tensors transforms when we move into the physical space, we focused in Figure 14 on three randomly selected fragments of the post-avalanche equilibrium configuration shown in Figure 13(d). The emerging

[3] As discussed in detail in [40], for our choice of the elastic potential it is not exactly a degenerate "monkey saddle" but rather a shallow energy maximum (triangular lattice) surrounded by three closely located non-degenerate (classical) saddles (rhombic lattices).

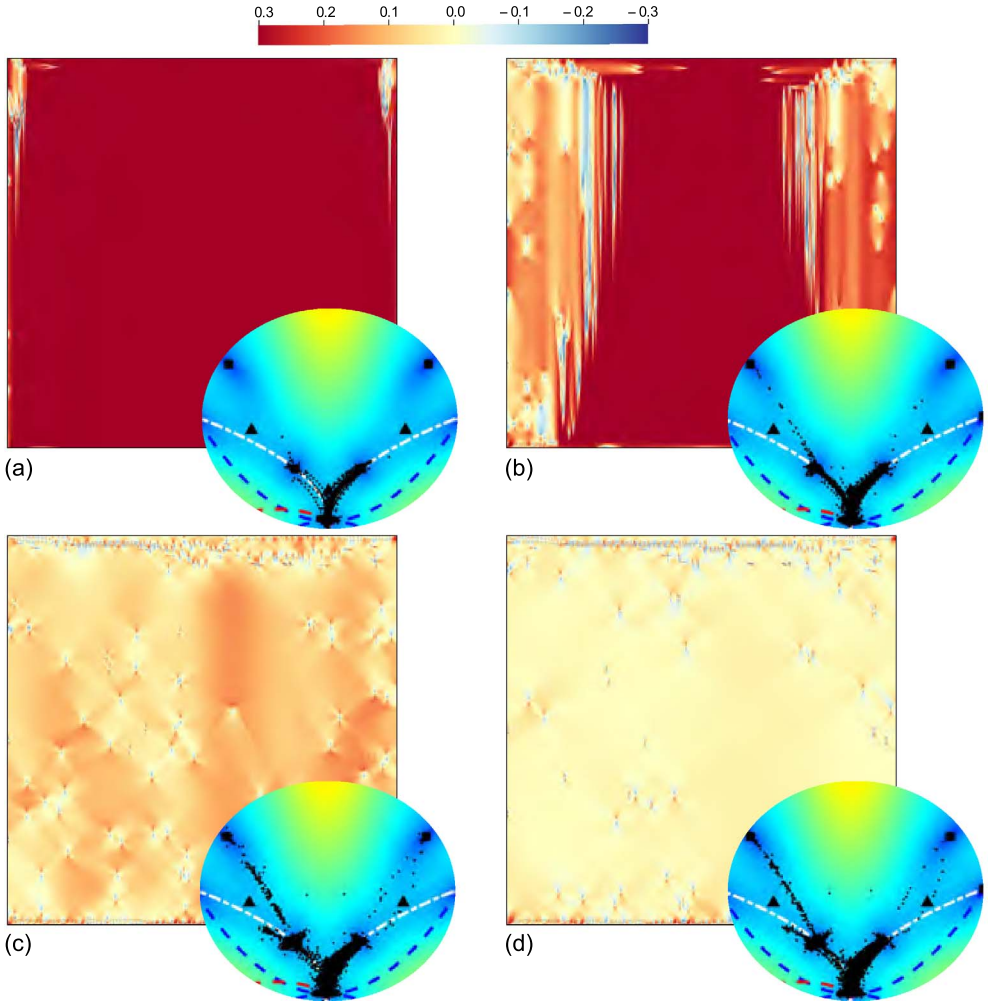

Figure 13. Snapshots of the stress field during discontinuous yield in pristine square crystals. Colors indicate the level of the shear component of the Cauchy stress. Insets show the same images in the configurational space. Black dots indicate the value of the metric tensor in individual finite elements. Here $N = 1024$ and $\phi = 0$.

equilibrium pattern contains dislocational pile ups near the boundaries and few locked up dislocational dipoles in the bulk of the specimen. Note, in particular, the pairs of dislocations on two parallel slip planes blocking each other, see Figure 14(b), and on two perpendicular slip planes forming characteristic locks, see Figure 14(d). The fact that after the system spanning avalanche most of the nucleated defects manage to either annihilate or escape to the boundaries of the crystal, explains why the crystal becomes almost pristine after such a devastating discontinuous yield event.

To check the generality of these conclusions, we also performed numerical simulations of the discontinuous yield at $\alpha \sim \alpha_c^*$ with initially *perturbed* displacement field which was "dirtied" by random Gaussian perturbations with zero mean and small variance (∼0.0001). Such disorder is too small to suppress brittleness [68] and, we show in Figure 15 the equilibrium stress field after the catastrophic avalanche. Since the pre-avalanche state was not "pristine", the energy minimiz-

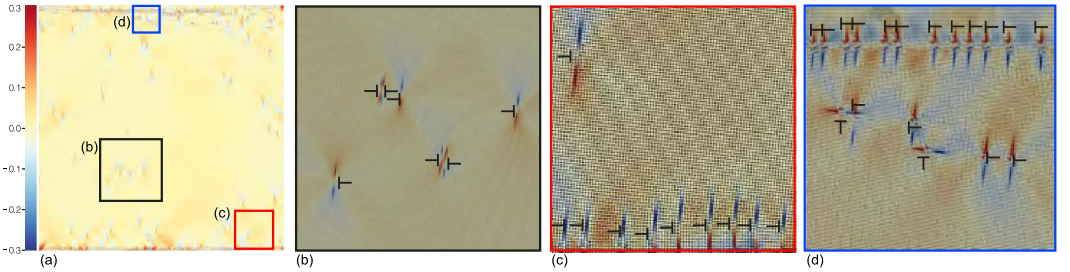

Figure 14. Final stress configuration after the discontinuous yield in pristine square crystals: (b–d) show the enlarged versions of the square indicated by the same letters in (a). Here $N = 1024$ and $\phi = 0$.

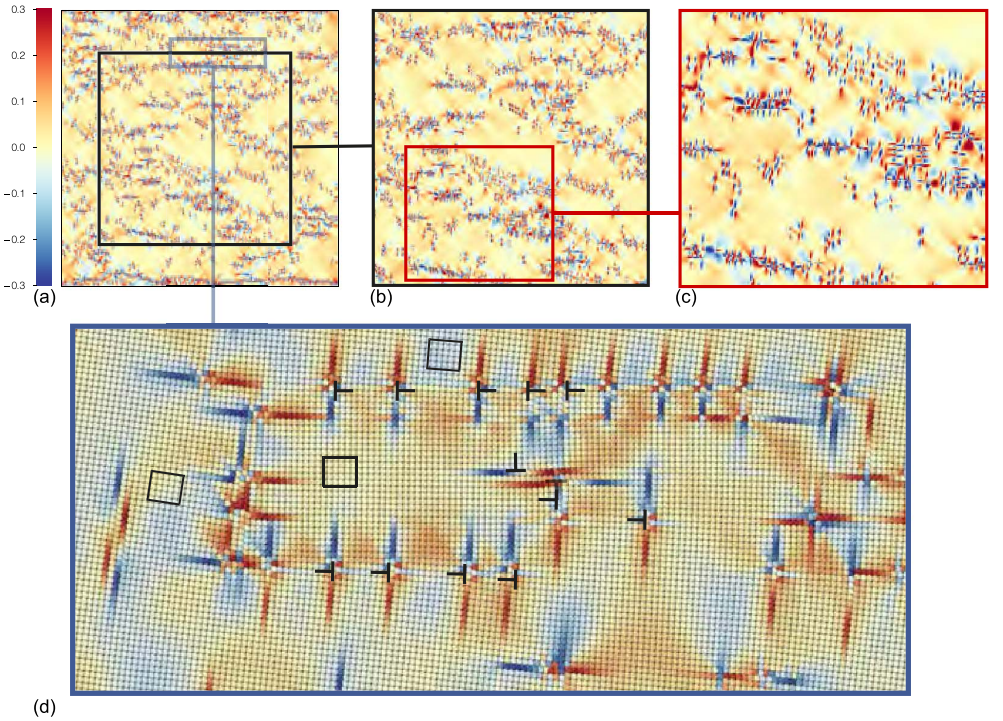

Figure 15. Final stress configuration after the discontinuous yield in a square crystal which was randomly perturbed at the point of instability. Colors indicate the level of the shear component of the Cauchy stress. Squares show the rotated versions of the unstressed lattice. Here $N = 1024$ and $\phi = 0$.

ing self organization of dislocations is compromised by the geometrical frustration imposed by the disorder. The resulting dislocation pattern appears to be structurally similar at several scales, see the successive insets shown in Figure 15(b,c). The two main perpendicular slip planes are now activated at almost the same level. Note the formation of self screening dislocation-rich walls, reminiscent of low-angle grain boundaries, which separate dislocation-poor, low-stress domains where the lattice undergoes simple rotations, see small rotated squares in Figure 15(d); all these structural features have been previously recorded in physical experiments. Note also, that since samples containing imperfections show diminished brittleness [68], the discontinuous yield can disappear in cyclic loading already after few cycles.

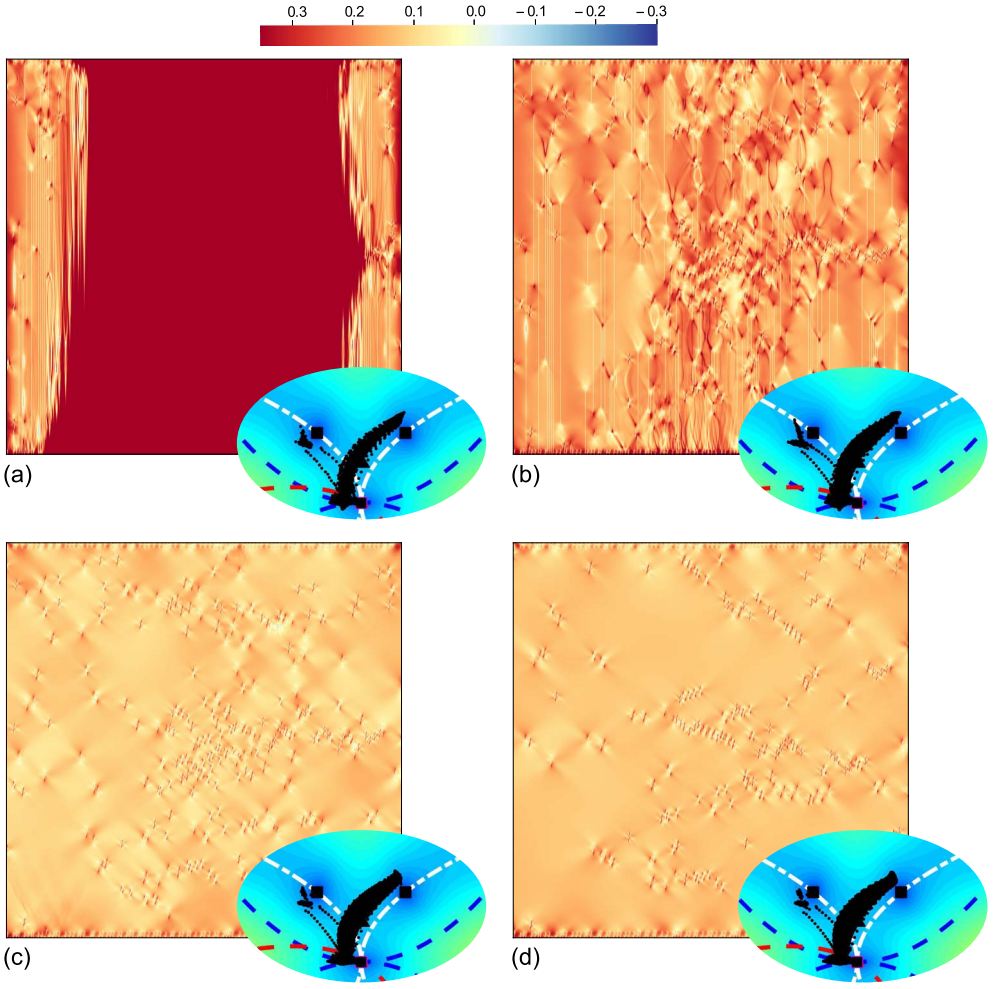

Figure 16. Snapshots of the stress field during discontinuous yield in pristine square crystal. Colors indicate the level of the shear component of the Cauchy stress. Insets show the same images in the configurational space. Black dots indicate the value of the metric tensor in individual finite elements. Here $N = 1024$ and $\phi = \arctan(1/2)$.

Consider next a "harder" shear loading path with $\phi = \arctan(1/2)$ which does not follow the low energy valley. As we have already mentioned, in this case a homogeneously deformed crystal will store a bit more elastic energy before instability than in the case of the symmetric "soft" paths. The breakdown scenario is shown in Figure 16: after reaching the (regularized) ideal strength limit $\bar{\mathbf{F}}(\alpha_c^*, \arctan 1/2)$, dislocations nucleate along the "vertical" slip plane which agrees with the prediction of the stability analysis. In the configurational space of metric tensors the stream of points describing such dislocations is directed from S_0 to S_2, see Figure 16(a). Eventually few "horizontal" dislocations form as well, see Figure 16(b,c), and because of geometrical frustration they are not all expelled to the boundaries of the crystal, see Figure 16(d). Therefore the system is left with considerable residual energy and the stress drop is relatively small.

The most interesting yield scenario is obtained for the non-generic $\phi = \pi/4$ loading path which leads from the reference state S_0 to the second closest energy minimum S_{11} after passing a much higher energy barrier than in the case $\phi = 0$. Here even more elastic energy is stored before

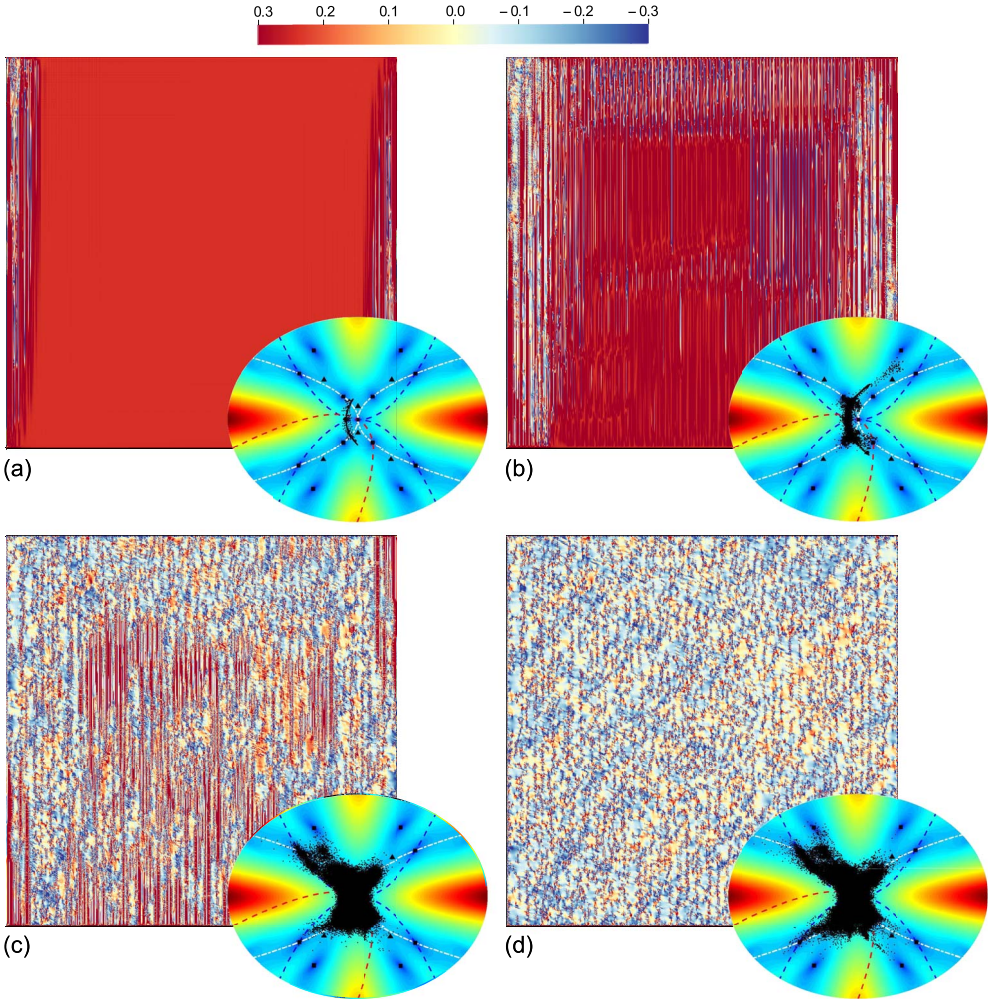

Figure 17. Snapshots of the stress field during discontinuous yield in pristine square crystal. Colors indicate the level of the shear component of the Cauchy stress. Insets show the same images in the configurational space. Black dots indicate the value of the metric tensor in individual finite elements. Here $N = 1024$ and $\phi = \pi/4$.

the instability than in the case $\phi = \arctan(1/2)$. The breakdown takes place at $\bar{\mathbf{F}}(\alpha_c^*, \pi/4)$ with a single instability mode activated, see Figure 17(a). However, the ensuing process of collective dislocation nucleation quickly becomes very complex. Due to the presence of the considerable amount of stored elastic energy and attending geometrical frustration, almost instantaneously, in addition to the original energy well S_0, all four neighboring square wells (S_1, $S_{\bar{1}}$) and (S_2, $S_{\bar{2}}$) become engaged and few elements even reach more distant square wells, see Figure 17(b,c). More specifically, the flow of configurational points in the space of metric tensors is so "intense" that it passes through a series of (almost) monkey saddles corresponding to triangular lattice configurations to accesses not only the nearest but also the next nearest square energy wells S_{11} and $S_{\bar{1}\bar{1}}$ which represent *compositions* of shears from both main slip systems.

The post-avalanche dislocation pattern is then multi-slip with minimal pile up on the boundaries and most of dislocations self-organizing in the bulk of the crystal, see Figure 17(d). A close-

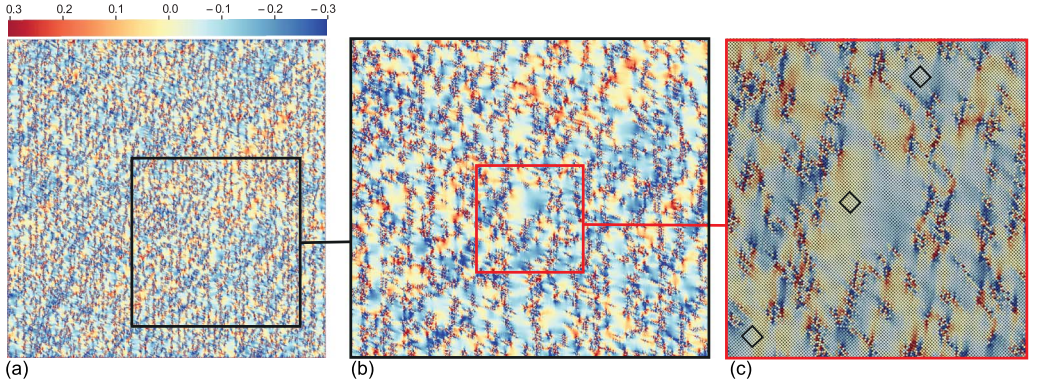

Figure 18. Stress field after the avalanche for a pristine square crystal with orientation $\phi = \pi/4$ (a); zoomed view of the marked area (b); further zoom to the scale of the discrete finite element nodes (c).

up of the highlighted region shown in Figure 18(a,b) down to the scale of finite element nodes puts in evidence the formation of dislocation walls separating almost unstressed *cells* with correlated lattice mis-orientations. In other words, we observe the formation of dislocation-rich bands which self screen long-range elastic fields allowing the strains inside the dislocation-poor regions to relax by reducing the deformation gradient to pure rotation. In Figure 18(c), we show such differently re-oriented crystal (almost) stress free regions in more detail. Interestingly, molecular dynamics simulations also suggest that at almost theoretical strength, dislocations alone can no longer release the elastic energy, and the reorientation of crystal lattices emerges as an important mechanism of plastic response [97]. In other words, a perfect sub-micron crystal appears to be yielding by catastrophic strain-induced reorientation of the crystal lattice with the formation of generalized twin and grain boundaries.

To summarize, our numerical experiments conducted on square lattices suggests that while in *specially oriented* crystals, pristine-to-pristine brittle yield at ideal shear strength threshold is a possibility, the *generically oriented*, dislocation free sub-micron crystals, can be expected to yield discontinuously with massive dislocation nucleation culminating in the formation of complex dislocational patterns. During such instabilities a large amount of stored elastic energy is released and the connection between the initial instability mode and the developing deformation pattern is quickly lost. To minimize elastic energy, dislocations do not only nucleate cooperatively but also self organize hierarchically forming multi-scale cell structures with presumably complex statistical properties, to be studied separately using, for instance, the approach presented in [68].

5.2. *Triangular lattices*

Consider next the case of higher symmetry triangular lattices. As we have already seen, in this case the macroscopic mechanical response is in overall agreement with the analytical yield surface, modulo the fact that, differently from what we have seen in the case of square lattices, discontinuous yield is observed for values α_c^* which were about a 10% higher than the corresponding analytical predictions α_c, see Figure 10(b). This gap, which is a function of the finite element size h, results from the disregistry between the orientation of the unstable modes and the "soft" directions of the energy landscape.

Consider first the loading path corresponding to a simple shear (4) with $\phi = 0$. An application of the idea of plastic "mechanisms" suggests that crystal should evolve from the initial energy well T_0 to the next closest triangular well T_1; the corresponding low energy valley is shown

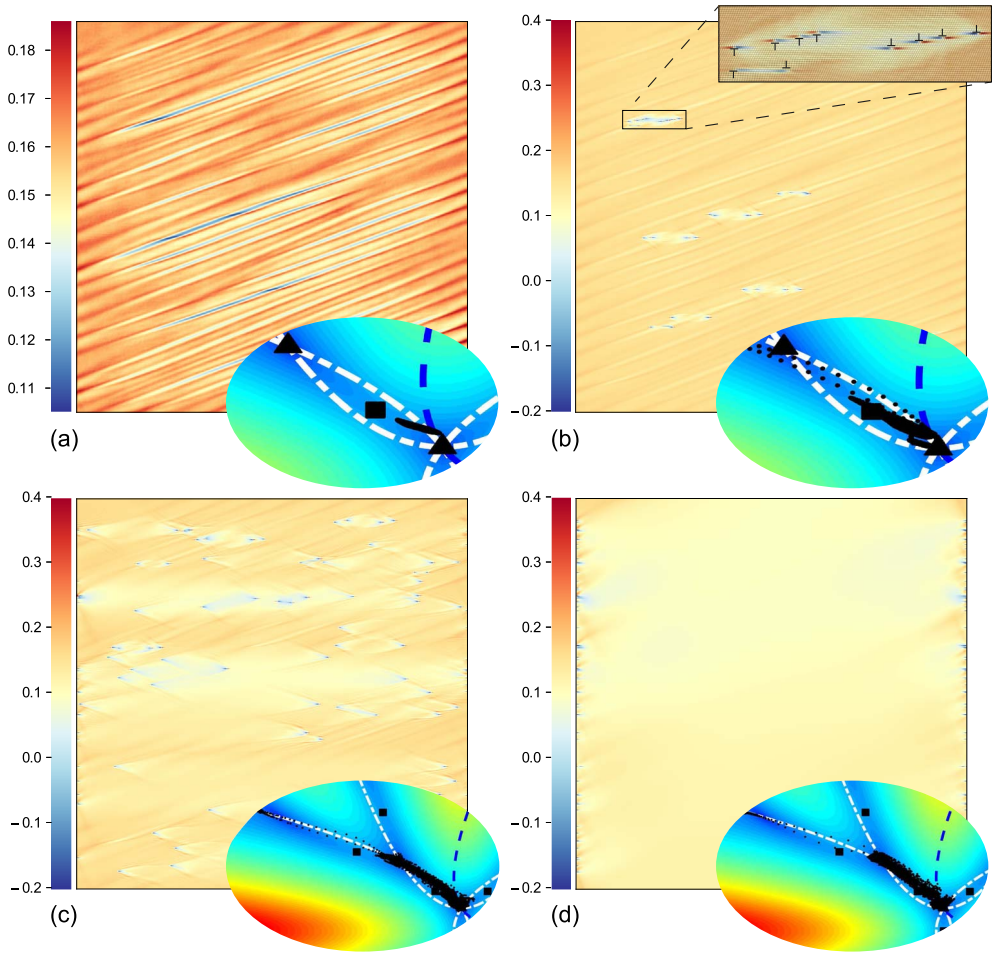

Figure 19. Snapshots of the stress field during discontinuous yield in pristine triangular crystal. Colors indicate the level of the Cauchy shear stress σ_{xy}. Insets show the same images in the configurational space. Black dots indicate the value of the metric tensor in individual finite elements. Here $N = 1024$ and $\phi = 0$.

in Figure 3 as the path 1–1. However, as we have already seen, the actual instability of the homogeneously deformed lattice state T_0 occurs strictly after the determinant of the continuum acoustic tensor has become negative for some orientation $\boldsymbol{n}_c$. To deal with encountered soft directions, the implied dislocation nucleation is postponed. The anticipated low energy valleys in the energy landscape cannot be used because the apparently low barriers leading towards the state T_1 along the path 1–1 are still too high. Instead the softness of the energy landscape drives the system in the direction of the saddle point S_1 which corresponds to the square lattice while still remaining within the fundamental domain. Therefore in our numerical experiments we observed that during the gradient descent type energy minimization at α_c that periodically-spaced modulations develop prior to the dislocation nucleation, see Figure 19(a). The orientation of the modulation bands agrees with the directions $\boldsymbol{n}_c$ obtained using the continuum instability condition.

As the instability develops, the non-equilibrium configurations found by the minimization algorithm show the sharpening of the band boundaries and then the secondary symmetry

breaking through the homogeneous nucleation of dislocation dipoles, see Figure 19(b). Note that the orientation of these dipoles agrees with the lattice (T_0 to T_1 path) but not with the orientation of the bands (T_0 to S_1 path). Note also that the implied pairs of dislocations with opposite signs nucleate at the centers of the modulation bands where the displacement gradients are large which apparently helps the system to overcome the energy barriers leading to T_1 lattice state. The emerging dislocation nucleation scenario is slightly different from the one suggested by the Peierls–Nabarro model where, effectively, the bands are perceived as atomically sharp and lattice oriented.

In Figure 19(b–d) we see that the modulation eventually completely breaks down with only one slip system ending up being activated. Due to the misalignment of the bands with the slip planes and the associated geometrical frustration, the nucleated dislocations interact with each other strongly causing the activation of the double slip represented by the triangular lattice state T_{11}. With dislocations either annihilating or escaping to the boundaries, the resulting picture is in basic agreement with the prediction of a single slip CP theory.

Along the other symmetric loading paths with $\phi = \pi/3$ and $\phi = 2\pi/3$, which also describe shears on dense planes of the triangular lattice, the general scenario of discontinuous yield remains the same. While the degree of misalignment of the initial modulation bands with the lattice does not change, the orientation of these bands relative to the square computational box is slightly different in each of these cases which (mildly) affects the outcome of the instability. The succession of events, constituting the system spanning avalanche in the case of loading orientation $\phi = \pi/3$, is illustrated in Figure 20(a–d). Here again the macroscopic modulations create the nucleation sites responsible for the secondary instability which leads to the formation of almost ideal dislocational dipolar mats [232], see Figure 20(b). Dislocations eventually self organize into bands, see Figure 20(c), but finally all end up on the surface of the crystal, see Figure 20(d).

Here again the primary, purely elastic instability develops in the direction from triangular well T_0 to the square well S_0 as if indicating an incipient phase transition. The secondary instability associated with barrier crossing leads to the flow of configurational points from T_0 to $T_{\bar{1}}$ which therefore creates plastic slip. As dislocations pile up near the boundaries, they activate the secondary slip associated with the well $T_{\bar{1}\bar{1}}$ and even the second slip system represented by the well $T_{\bar{1}\bar{2}}$. Ultimately, all four triangular lattices T_1, T_2, $T_{1\bar{1}}$ and $T_{\bar{1}\bar{2}}$ get involved, however, the ensuing complexity remains localized near the sharp corners of the sample. At the end of the avalanche the bulk of the sample appear to be free of dislocations which explains the dramatic stress drop experienced by the crystal.

In view of the high symmetry of the triangular lattice, the structure of the yielding avalanche for the generic path with $\phi = \pi/2$, which also starts in the original energy well wells T_0, is not very different from what we have already seen in the case of the non-generic path with $\phi = 0$. The influence of the neighboring square well S_0 is again felt in the structure of the initial elastic modulations, see Figure 21(a). The deformation ultimately localizes inside the low energy valley connecting the triangular wells T_0 and $T_{\bar{1}}$. Transient dislocation entanglements eventually get dissociated with dislocations either annihilating or escaping to the boundaries, however, the stored elastic energy is not fully relaxed by such limited plasticity, see Figure 21(b–d). In general, this example suggests that in sub-micron crystals with high symmetry and accordingly "round" surfaces of theoretical strength, the outcome of the discontinuous yield is decided not so much by the orientation of the sample in the loading machine, but rather by the orientation of the sample boundaries vis-a-vis lattice directions.

To summarize, using MTM, we were able to show that, similar to what is observed in experiments, pristine sub-micron crystals undergo discontinuous yielding close to theoretical strength. During the catastrophic avalanche, massive nucleation of dislocations first transforms such crys-

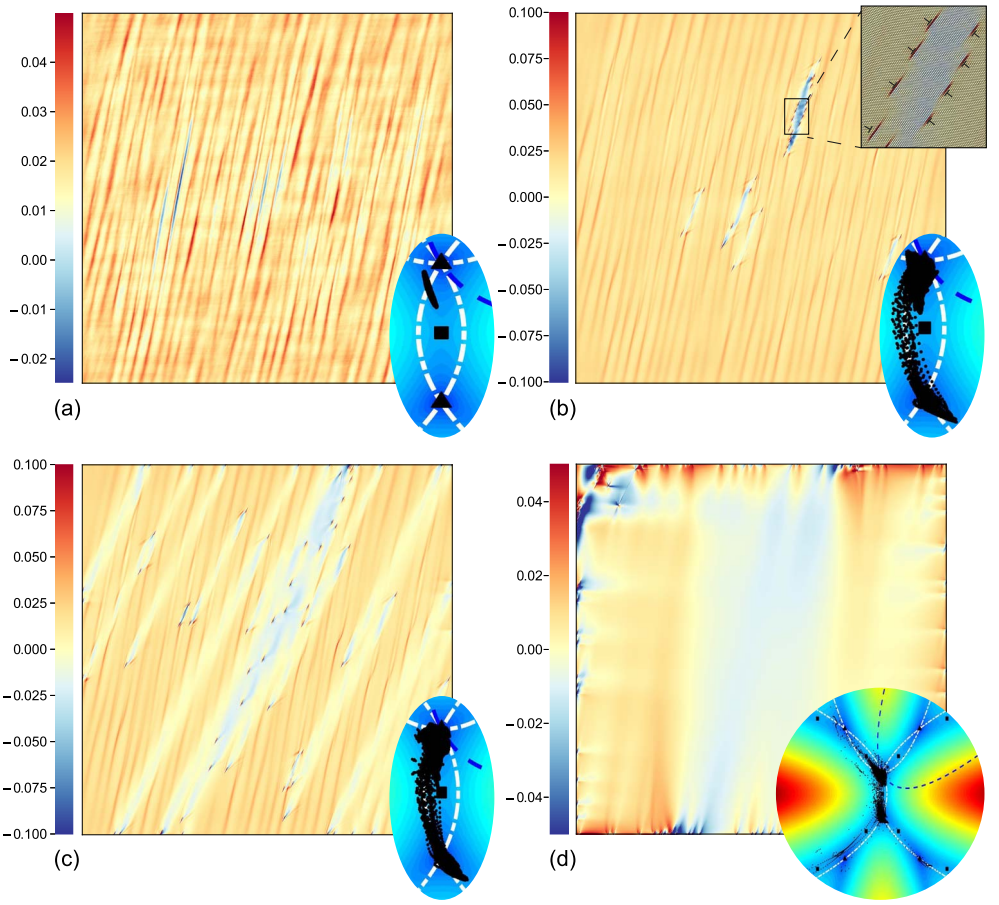

Figure 20. Snapshots of the stress field during discontinuous yield in pristine triangular crystal. Colors indicate the level of the shear component of the Cauchy stress. Insets show the same images in the configurational space. Black dots are placed according to the value of the metric tensor's components in individual finite elements. Here $N = 1024$ and $\phi = \pi/3$.

tals from defect-free to defect-saturated, but then most of the defects either annihilate or escape to the fixed boundaries producing again almost pristine crystals. The access through MTM to *transient nonequilibrium states* allowed us to study for the first time the sensitive dependence of the phenomenon of discontinuous yield on crystal symmetry, crystal orientation in the loading machine, and even crystal shape.

The general feature of the *simulated* discontinuous yield is that the instability starts as a long-wave purely elastic modulation which breaks the affinity of the original homogeneous state. The actual dislocation nucleation emerges as a *secondary* instability, triggered by non-affinity and proceeding collectively. A large number of defects appear almost simultaneously and the "auto-catalytic" nature of such avalanche is due to the fact that already nucleated dislocations trigger new nucleation events. The process terminates only when the elastic repulsion from the walls finally blocks the nucleation in the bulk.

The pristine-to-pristine yield takes place if a non-generic loading allows the system to completely avoid frustration and channel almost all dislocations away from the bulk. Otherwise the avalanche *jams* with dislocations forming *self-locking* patterns. Such patterns can be interpreted

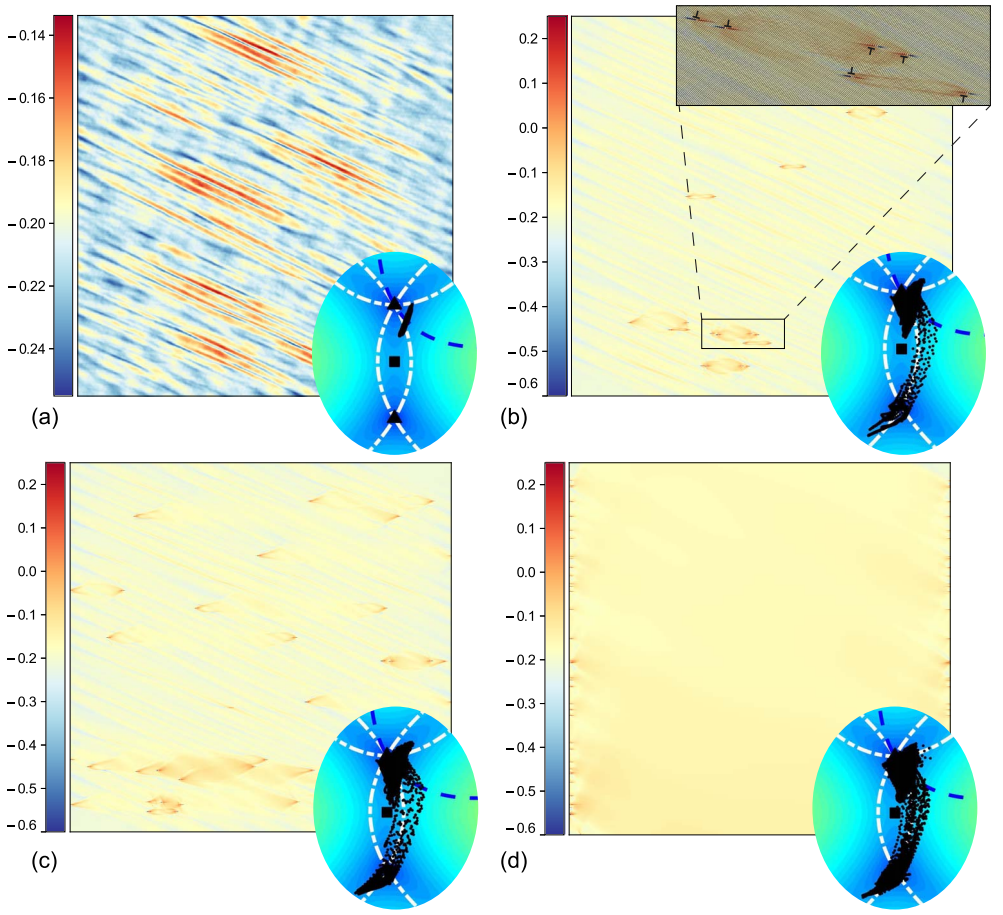

Figure 21. Snapshots of the stress field during discontinuous yield in pristine triangular crystal. Colors indicate the level of the shear component of the Cauchy stress. Insets show the same images in the configurational space. Black dots indicate the value of the metric tensor in individual finite elements. Here $N = 1024$ and $\phi = \pi/2$.

as cell structures because relatively narrow dislocation walls bound extended domains where lattice undergoes simple *rotation*. In the case of open boundaries, the dislocation pile-up, playing an important role in the observed scenario, will be replaced by the global strain *localization*.

6. Beyond the principal avalanche

The analytic and numerical results presented in the previous sections are relevant for conceptualizing the puzzling discontinuous response of nominally ductile crystals. Such brittle-like response is generic for ultra-small and, therefore, dislocation-starved crystals in the sense that it is observed routinely in compression and nano-indentation experiments [16, 29, 34, 233].

As we have shown, to ensure such pseudo-brittle behavior, the crystals should be structurally perfect (dislocation and defect-free). In this case, the main effect is an explosive system spanning avalanche at the end of the elastic regime with massive collective nucleation of dislocations, which results in a catastrophic load drop known as discontinuous yield. In this section, we briefly discuss what happens if the loading resumes after the discontinuous yield and the crystal, whose

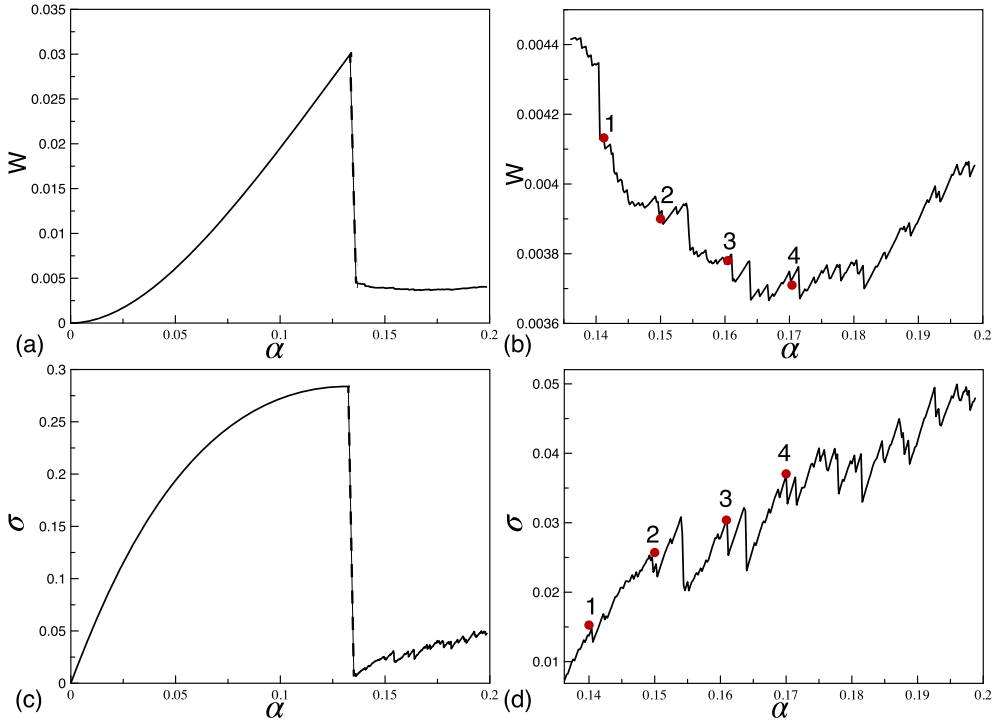

Figure 22. Macroscopic mechanical response of square crystal upon loading beyond the catastrophic system-size avalanche. Here $N = 500$ and $\phi = 0$.

purity is now compromised, continues to yield. We limit the analysis to just a few observations, while the detailed study will be presented elsewhere.

As we have seen, after the termination of the system size avalanche and the re-stabilization of the inhomogeneous state, the generic crystalline sample can be expected to contain a highly correlated configuration of lattice defects. If the quasi-static loading continues, such an imperfect crystal will first undergo another quasi-elastic deformation which will be succeeded by another avalanche, necessarily less dramatic in view of the ubiquity of nucleation sources and the availability of the locking sites. Subsequent monotone loading will be punctuated by an intermittent succession of avalanches, with most of them small, but some reaching again the size of the whole system [8, 48, 68, 104, 234–238]. To illustrate these general observations and show that MTM approach is well suited to study the effects of intermittent discontinuous yield, we now present few illustrations of the mechanical response of square crystals subjected to simple shear with $\phi = 0$ following directly the initial plastic avalanche. Since, naturally, the complexity of the dislocational patterns increases with subsequent loading, we reduce the precision of the description by adopting a smaller value of $N = 512$ and preserve the small *annealed disorder* as in the experiment shown in Figure 15.

The simulated macroscopic response is summarized in Figure 22, where we show the computed energy–strain, see Figure 22(a), and the stress–strain, see Figure 22(c), relations. The corresponding zoom ins are shown in Figures 22(b) and 22(d), respectively.

We first observe that after the major stress/energy drop, the smooth elastic response turns into jerky plastic yield. More specifically, the post-catastrophic response can be decomposed into conservative elastic steps that are interdigitated by dissipative stress/energy drops representing dislocation avalanches broadly distributed in size, see Figure 22(b,d). While the averaged stress

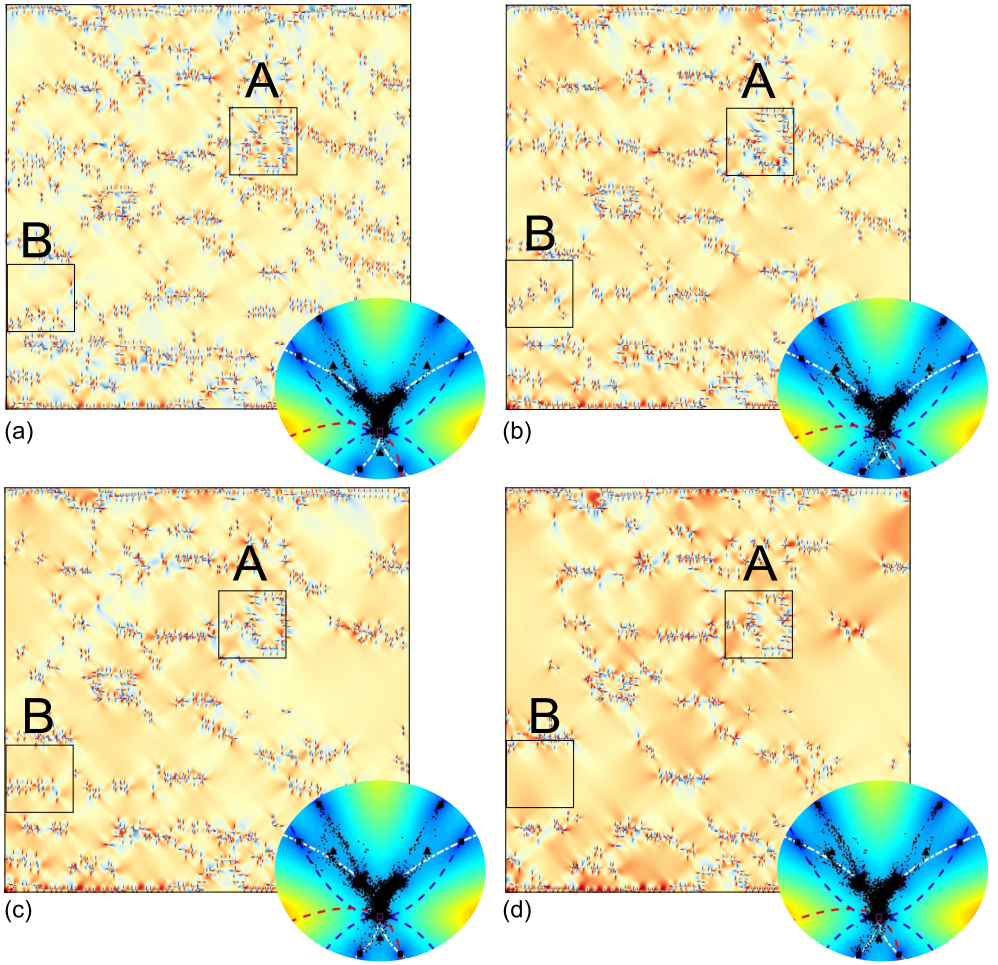

Figure 23. Evolution of the shear component of Cauchy stress in physical space after the catastrophic system-size avalanche. The snapshots correspond to the selected points in Figure 22 marked by numbers 1,2,3,4. The corresponding distributions in the configurational space are shown in the insets. Here $N = 500$ and $\phi = 0$.

response in this range shows monotone hardening, the averaged energy first decreases and then increases. This is due to the fact that the energy losses cannot even be seen on such stress–strain curves, see [189] for more details. The jerkiness of the response originates in transitory elastic deformation of self-locked microstructures which always involves partial or complete unlocking and dynamical restructuring, accompanied by energy dissipation.

To trace such restructuring, we show in Figure 23(a–d) a succession of four snapshots of the stress field in the arbitrary chosen moments of "time" as indicated in by dots marked by numbers 1,2,3,4 in Figure 22(b,d). Afterwards, in Figure 24 we zoom into two spatial regions A and B and follow the "time" evolution of the particular groups of dislocations over several avalanches. The numerical experiment, illustrated by these figures, is similar to the one shown in Figure 14 but with even smaller annealed initial disorder. We observe that continuing loading is accommodated by additional nucleation of dislocations which remain in the bulk due to apparent repulsion from the already saturated boundaries. The configurational points in the space of metric tensors spread more uniformly among the three equivalent square energy wells S_0, S_1 and S_2,

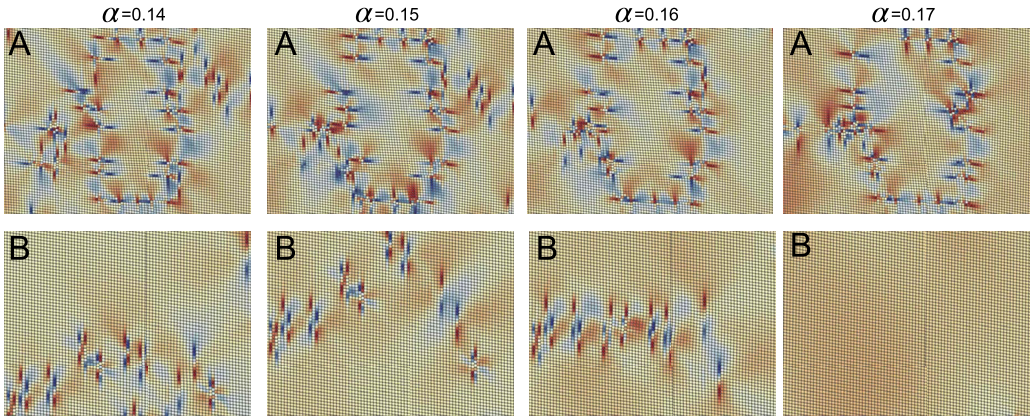

Figure 24. Enlarged view of the dislocation configurations inside the square regions (A) and (B) shown in Figure 23 as they evolve with loading. Colors indicate the shear component of the Cauchy stress tensor.

being distributed almost evenly by the (almost) monkey saddle T_0. The ensuing dislocation pattern includes individual dislocation locks as well as dislocation walls separating domains where the lattice is almost unstressed. This pattern results from dynamic self-organization of dislocations and can be viewed as generic.

Upon further loading, the crystal continues to harden as seen in Figure 22(d). The plastic yield takes the form of an irregular sequence of stress-drops associated with partial restructuring of the dislocation pattern, see Figure 23(b–d). The configurational points continue to spread over the metric space reaching distant wells corresponding to various compositions of simple shears. This means that despite the simple shear strain applied on the boundary, the deformation in the bulk of the sample takes the manifestly multi-slip form. Interestingly, the patterns identified in Figure 23(b–d) are reminiscent of the ones obtained by X-ray diffraction method in [239] where the authors observed the formation of dislocation boundaries separating (nearly) dislocation-free regions with almost perfect lattices. Such subgrains were shown to exhibit intermittent dynamics, appearing and disappearing as well as displaying transient splitting behavior.

We observe that most small-sized avalanches are associated with the transitional motion of depinning dislocations between the dislocation-rich wall-like patterns. During such transitions, dislocations either get locked again or annihilate, however, at least some of the existing large-scale dislocation structures persist during the loading. To illustrate this conclusion, we show in Figure 24 the enlarged view of the time evolution for the two rather arbitrarily selected square sub-domains, which we identify as A and B. In A, we see an almost rectangular dislocation structure based on dipolar walls, which ensure an ideal screening of the long-range elastic fields [235]. With loading, this structure deforms elastically but otherwise remains relatively stable, experiencing only minor rearrangements (addition and subtraction of dislocations from local entanglements). Instead, the incomplete dipolar wall shown in B does not survive the loading, and finally, the participating dislocations disappear entirely due to an abrupt collective annihilation. Usually, such restructuring events give rise to bigger avalanches, and we checked that the largest avalanche between the deformation states (c) and (d) shown in Figure 22(b,d), can be indeed linked to the disappearance of the multi-dislocation structure B, see Figure 24.

Note, however, that the avalanches associated with partial restructuring of the dislocation pattern, are still much smaller in size than the system spanning avalanche responsible for the major restructuring behind the original discontinuous yield of pristine crystal. This is

associated with a "special preparation" of the pristine (homogeneous) crystal whose high degree of degeneracy causes instability to happen simultaneously all over the sample. The dynamic randomization produced by the discontinuous yield generates annealed disorder and reduces the degeneracy, producing more conventional yield represented by mostly small avalanches. However, due to long-range elastic interactions, strong correlations in such apparently random system remain, and they lead to occasional recurrence of the system size avalanches, known as "dragon-king event" [240]. This leads to the supercritical avalanche distribution in sub-micron crystals which was observed in experiment and has been recently successfully simulated in the framework of a scalar version of MTM [68].

7. Conclusions

In this paper, we presented the first systematic demonstration of the *effectiveness* of the mesoscopic tensorial model (MTM) by showing that it can simulate complex plastic phenomena in crystals involving a large number of interacting dislocations. A characteristic feature of the MTM is that it resolves lattice scale dislocation cores while operating with the engineering concept of stress and strain. It can be viewed as a tensorial version of the scalar phase-field model, accounting for large rotations and finite lattice invariant shears in *geometrically precise* way. It is reassuring that the MTM can deal adequately with short-range interactions of dislocations while accounting for full crystallographic symmetry, without direct use of interatomic potentials or other ab-initio methods.

The key feature of the MTM is that it is formulated as a nonlinear *field theory* of Landau-type respecting the discrete $GL(3,\mathbb{Z})$ symmetry. It can also be viewed as a geometrically and physically nonlinear anisotropic elasticity theory. It may first sound paradoxical that *elasticity* framework was chosen to describe *plasticity*. However, this viewpoint is fully consistent with the fact that dislocations are elastic defects whose interaction is largely elastic. Under quasi-static loading, inelastic *dissipation* takes place during fast switching between elastic branches. Such branch switching events are ubiquitous due to the *rugged* nature of the generic MTM energy landscape and the presence of elastic driving.

To generate such energy landscape, the MTM relies on local validity of the *Cauchy–Born* rule even though some features of the nonlocal atomistic description are then inevitably lost. Behind the emergence of the continuum stresses and strains is the *spatial averaging* over a microstructural length scale: the latter characterizes the size of a cluster of atoms (an element) assumed to deform homogeneously. The elastic branches are exchanged when, as a result of elastic instabilities, such *elements* abruptly move between the neighboring wells of the globally periodic Landau energy.

An important feature of the MTM approach to crystal plasticity is that plastic "mechanisms" are not assigned a priori, but take the form of low energy valleys connecting the wells of Landau energy. Plastically deformed state emerges in this representation as a *mixture* of equivalent Landau phases, with dislocations appearing as *incompatible* components of phase boundaries. In such a model slip directions are not rigidly pre-defined and loading along one slip system can, by itself, initiate another slip system. Topological transitions, like the ones involved in the activity of Frank–Read and SA (single arm) sources, are incorporated automatically.

In this paper we used the simplest 2D version of the MTM to simulate numerically a *benchmark* phenomenon: the catastrophic discontinuous yielding in pristine sub-micron crystals due to cooperative nucleation of dislocations. We used Dirichlet type boundary conditions (hard device) to be consistent with our definition of the theoretical strength, but we also checked that switching to periodic boundary conditions changes the results only quantitatively. We showed that in simulations, the development of the collective "brittle-like" dislocation nucleation event

is similar to the one observed in experiments with imperfection-free sub-micron crystals. The use of the MTM allowed us to quantify, for the first time, the dependence of the ensuing dislocation patterning on the crystal *symmetry* and on the *orientation* of the crystal in the loading device. The critical load turned out to be in agreement with analytical predictions. Moreover, the yield criterion based on the Legendre–Hadamard (strong ellipticity) condition was shown to be successful in predicting the overall orientation of the non-affine patterns.

Vastly different dislocation nucleation scenarios were observed during the discontinuous yield in square and triangular lattices. In the case of *square* symmetry, shearing in the "soft" directions causes pristine-to-pristine transitions with stress dropping almost to zero as a result of the catastrophic avalanche. Instead, loading of the same crystals in the "hard" directions leads to the formation of a complex, highly correlated dislocation pattern and results in residual stress. In higher symmetry *hexagonal* crystals, the theoretical strength threshold depends only weakly on the orientation of the crystal. Due to ensuing geometrical frustration, the nucleation of dislocations is preceded by the development of long-wave elastic modulations. While most of the dislocations manage to escape to the boundaries of the crystal, the post avalanche stress remains considerable independently of the sample orientation. In both square and hexagonal cases, lattice configurations with alternative symmetries (hexagonal and square, accordingly) appear as saddle points of the Landau energy and play an important role in fomenting *multi-slip* by re-directing the flow of configurational points between converging energy valleys.

Our study shows the *potential* of the MTM in dealing with plastic flows, involving *strongly interacting* dislocations, while relying only on minimal phenomenological assumptions. It opens new paths in the study of spatial and temporal *complexity* associated with developed plastic flows. Already the first concrete results, obtained in this paper, represent promising steps towards harnessing brittle events in sub-micron crystals compromising forming processes, endangering the load-carrying capacity of micro-machine parts, and jeopardizing reliability in various other micromechanical applications.

Acknowledgments

The first two authors contributed to this paper equally. All authors acknowledge helpful discussions with S. Conti, M. Jędrychowski, N. Greneche, J. Weiss, P. Zhang, S. Queyreau and I. R. Ioanescu. The work was partially supported by the grants ANR-17-CE08-0047 (OUS and LT) and ANR-19-CE08-0010-01 (OUS). The possibility to access computational resources (MAGI) provided by Université Sorbonne Paris Nord is highly appreciated.

References

[1] S.-W. Lee, S. M. Han, W. D. Nix, "Uniaxial compression of fcc Au nanopillars on an MgO substrate: The effects of prestraining and annealing", *Acta Mater.* **57** (2009), no. 15, p. 4404-4415.

[2] R. Li, H. Kang, Z. Chen, G. Fan, C. Zou, W. Wang, S. Zhang, Y. Lu *et al.*, "A promising structure for fabricating high strength and high electrical conductivity copper alloys", *Sci. Rep.* **6** (2016), article no. 20799.

[3] K. Lu, "Stabilizing nanostructures in metals using grain and twin boundary architectures", *Nat. Rev. Mater.* **1** (2016), no. 5, article no. 16019.

[4] T. A. Schaedler, A. J. Jacobsen, A. Torrents, A. E. Sorensen, J. Lian, J. R. Greer, L. Valdevit, W. B. Carter, "Ultralight metallic microlattices", *Science* **334** (2011), no. 6058, p. 962-965.

[5] D. Mordehai, S.-W. Lee, B. Backes, D. J. Srolovitz, W. D. Nix, E. Rabkin, "Size effect in compression of single-crystal gold microparticles", *Acta Mater.* **13** (2011), no. 59, p. 5202-5215.

[6] R. Maaß, L. Meza, B. Gan, S. Tin, J. R. Greer, "Ultrahigh strength of dislocation-free Ni_3Al nanocubes", *Small* **8** (2012), no. 12, p. 1869-1875.

[7] W.-Z. Han, L. Huang, S. Ogata, H. Kimizuka, Z.-C. Yang, C. Weinberger, Q.-J. Li, B.-Y. Liu *et al.*, "From "smaller is stronger" to "size-independent strength plateau": Towards measuring the ideal strength of iron", *Adv. Mater.* **27** (2015), no. 22, p. 3385-3390.

[8] S. Papanikolaou, Y. Cui, N. Ghoniem, "Avalanches and plastic flow in crystal plasticity: An overview", *Model. Simul. Mater. Sci. Eng.* **26** (2017), no. 1, article no. 013001.
[9] R. Maaß, P. M. Derlet, "Micro-plasticity and recent insights from intermittent and small-scale plasticity", *Acta Mater.* **143** (2018), p. 338-363.
[10] W. D. Nix, H. Gao, "Indentation size effects in crystalline materials: A law for strain gradient plasticity", *J. Mech. Phys. Solids* **46** (1998), no. 3, p. 411-425.
[11] M. D. Uchic, D. M. Dimiduk, J. N. Florando, W. D. Nix, "Sample dimensions influence strength and crystal plasticity", *Science* **305** (2004), no. 5686, p. 986-989.
[12] J. R. Greer, W. C. Oliver, W. D. Nix, "Size dependence of mechanical properties of gold at the micron scale in the absence of strain gradients", *Acta Mater.* **53** (2005), no. 6, p. 1821-1830.
[13] D. M. Dimiduk, C. Woodward, R. Lesar, M. D. Uchic, "Scale-free intermittent flow in crystal plasticity", *Science* **312** (2006), no. 5777, p. 1188-1190.
[14] H. Bei, S. Shim, G. M. Pharr, E. P. George, "Effects of pre-strain on the compressive stress–strain response of Mo-alloy single-crystal micropillars", *Acta Mater.* **56** (2008), no. 17, p. 4762-4770.
[15] D. Chrobak, N. Tymiak, A. Beaber, O. Ugurlu, W. W. Gerberich, R. Nowak, "Deconfinement leads to changes in the nanoscale plasticity of silicon", *Nat. Nanotechnol.* **6** (2011), no. 8, p. 480-484.
[16] Z.-J. Wang, Z.-W. Shan, J. Li, J. Sun, E. Ma, "Pristine-to-pristine regime of plastic deformation in submicron-sized single crystal gold particles", *Acta Mater.* **60** (2012), no. 3, p. 1368-1377.
[17] Y. Cui, G. Po, N. Ghoniem, "Influence of loading control on strain bursts and dislocation avalanches at the nanometer and micrometer scale", *Phys. Rev. B* **95** (2017), no. 6, article no. 064103.
[18] F. F. Csikor, C. Motz, D. Weygand, M. Zaiser, S. Zapperi, "Dislocation avalanches, strain bursts, and the problem of plastic forming at the micrometer scale", *Science* **318** (2007), no. 5848, p. 251-254.
[19] A. A. Benzerga, "Micro-pillar plasticity: 2.5D mesoscopic simulations", *J. Mech. Phys. Solids* **57** (2009), no. 9, p. 1459-1469.
[20] M. D. Uchic, P. A. Shade, D. M. Dimiduk, "Plasticity of micrometer-scale single crystals in compression", *Annu. Rev. Mater. Res.* **39** (2009), no. 1, p. 361-386.
[21] A. S. Argon, "Strain avalanches in plasticity", *Philos. Mag.* **93** (2013), no. 28–30, p. 3795-3808.
[22] P. Zhang, O. U. Salman, J.-Y. Zhang, G. Liu, J. Weiss, L. Truskinovsky, J. Sun, "Taming intermittent plasticity at small scales", *Acta Mater.* **128** (2017), p. 351-364.
[23] J. R. Greer, J. T. M. De Hosson, "Plasticity in small-sized metallic systems: Intrinsic versus extrinsic size effect", *Prog. Mater. Sci.* **56** (2011), no. 6, p. 654-724.
[24] S. S. Brenner, "Tensile strength of whiskers", *J. Appl. Phys.* **27** (1956), no. 12, p. 1484-1491.
[25] S. S. Brenner, "Growth and properties of "whiskers"", *Science* **128** (1958), no. 3324, p. 569-575.
[26] A. Sharma, J. Hickman, N. Gazit, E. Rabkin, Y. Mishin, "Nickel nanoparticles set a new record of strength", *Nat. Commun.* **9** (2018), no. 1, article no. 4102.
[27] D. Mordehai, O. David, R. Kositski, "Nucleation-controlled plasticity of metallic nanowires and nanoparticles", *Adv. Mater.* **30** (2018), no. 41, article no. 1706710.
[28] E. T. Lilleodden, W. D. Nix, "Microstructural length-scale effects in the nanoindentation behavior of thin gold films", *Acta Mater.* **54** (2006), no. 6, p. 1583-1593.
[29] S. G. Corcoran, R. J. Colton, E. T. Lilleodden, W. W. Gerberich, "Anomalous plastic deformation at surfaces: Nanoindentation of gold single crystals", *Phys. Rev. B* **55** (1997), no. 24, p. R16057-R16060.
[30] R. Maaß, P. M. Derlet, J. R. Greer, "Small-scale plasticity: Insights into dislocation avalanche velocities", *Scr. Mater.* **69** (2013), no. 8, p. 586-589.
[31] S. Lee, A. Vaid, J. Im, B. Kim, A. Prakash, J. Guénolé, D. Kiener, E. Bitzek, S. H. Oh, "*In-situ* observation of the initiation of plasticity by nucleation of prismatic dislocation loops", *Nat. Commun.* **11** (2020), no. 1, article no. 2367.
[32] Y. He, L. Zhong, F. Fan, C. Wang, T. Zhu, S. X. Mao, "*In situ* observation of shear-driven amorphization in silicon crystals", *Nat. Nanotechnol.* **11** (2016), no. 10, p. 866-871.
[33] A. Merabet, M. Texier, C. Tromas, S. Brochard, L. Pizzagalli, L. Thilly *et al.*, "Low-temperature intrinsic plasticity in silicon at small scales", *Acta Mater.* **161** (2018), p. 54-60.
[34] C. Chisholm, H. Bei, M. B. Lowry, J. Oh, S. A. Syed Asif, O. L. Warren, Z. W. Shan, E. P. George, A. M. Minor, "Dislocation starvation and exhaustion hardening in Mo alloy nanofibers", *Acta Mater.* **60** (2012), no. 5, p. 2258-2264.
[35] G. Ziegenhain, H. M. Urbassek, A. Hartmaier, "Influence of crystal anisotropy on elastic deformation and onset of plasticity in nanoindentation: A simulational study", *J. Appl. Phys.* **107** (2010), no. 6, article no. 061807.
[36] M. Bagheripoor, R. Klassen, "Effect of crystal orientation on the size effects of nano-scale fcc metals", *Mater. Sci. Technol.* **36** (2020), no. 17, p. 1829-1850.
[37] M. Bagheripoor, R. Klassen, "The effect of crystal anisotropy and pre-existing defects on the incipient plasticity of FCC single crystals during nanoindentation", *Mech. Mater.* **143** (2020), article no. 103311.

[38] O. U. Salman, L. Truskinovsky, "Minimal integer automaton behind crystal plasticity", *Phys. Rev. Lett.* **106** (2011), no. 17, article no. 175503.
[39] O. U. Salman, L. Truskinovsky, "On the critical nature of plastic flow: One and two dimensional models", *Int. J. Eng. Sci.* **59** (2012), p. 219-254.
[40] R. Baggio, E. Arbib, P. Biscari, S. Conti, L. Truskinovsky, G. Zanzotto, O. U. Salman, "Landau-type theory of planar crystal plasticity", *Phys. Rev. Lett.* **123** (2019), no. 20, article no. 205501.
[41] W. T. Read Jr, H. Brooks, "Dislocations in crystals", *Phys. Today* **8** (1955), no. 2, p. 17-18.
[42] A. H. Cottrell, "Commentary. A brief view of work hardening", in *Dislocations in Solids* (F. R. N. Nabarro, M. S. Duesbery, eds.), vol. 11, Elsevier, Amsterdam, Netherlands, 2002, p. vii-xvii.
[43] L. Kubin, *Dislocations, Mesoscale Simulations and Plastic Flow*, vol. 5, Oxford University Press, Oxford, UK, 2013.
[44] K. Differt, U. Esmann, H. Mughrabi, "A model of extrusions and intrusions in fatigued metals II. Surface roughening by random irreversible slip", *Philos. Mag. A* **54** (1986), no. 2, p. 237-258.
[45] S. D. Antolovich, R. W. Armstrong, "Plastic strain localization in metals: Origins and consequences", *Prog. Mater. Sci.* **59** (2014), p. 1-160.
[46] J. Weiss, W. Ben Rhouma, S. Deschanel, L. Truskinovsky, "Plastic intermittency during cyclic loading: From dislocation patterning to microcrack initiation", *Phys. Rev. Mater.* **3** (2019), no. 2, article no. 023603.
[47] R. Madec, B. Devincre, L. P. Kubin, "From dislocation junctions to forest hardening", *Phys. Rev. Lett.* **89** (2002), no. 25, article no. 255508.
[48] J. P. Sethna, M. K. Bierbaum, K. A. Dahmen, C. P. Goodrich *et al.*, "Deformation of crystals: Connections with statistical physics", *Annu. Rev. Mater. Res.* **47** (2017), no. 1, p. 217-246.
[49] D. Gómez-García, B. Devincre, L. P. Kubin, "Dislocation patterns and the similitude principle: 2.5D mesoscale simulations", *Phys. Rev. Lett.* **96** (2006), no. 12, article no. 125503.
[50] Y. S. Chen, W. Choi, S. Papanikolaou, J. P. Sethna, "Bending crystals: Emergence of fractal dislocation structures", *Phys. Rev. Lett.* **105** (2010), no. 10, article no. 105501.
[51] P. Li, S. X. Li, Z. G. Wang, Z. F. Zhang, "Fundamental factors on formation mechanism of dislocation arrangements in cyclically deformed fcc single crystals", *Prog. Mater. Sci.* **56** (2011), no. 3, p. 328-377.
[52] T. Takeuchi, "Work hardening of copper single crystals with multiple glide orientations", *Trans. Jpn. Inst. Met.* **16** (1975), no. 10, p. 629-640.
[53] C. S. Han, H. Gao, Y. Huang, W. D. Nix, "Mechanism-based strain gradient crystal plasticity—I. Theory", *J. Mech. Phys. Solids* **53** (2005), no. 5, p. 1188-1203.
[54] M. E. Gurtin, L. Anand, "Thermodynamics applied to gradient theories involving the accumulated plastic strain: The theories of Aifantis and Fleck and Hutchinson and their generalization", *J. Mech. Phys. Solids* **57** (2009), no. 3, p. 405-421.
[55] F. Roters, P. Eisenlohr, L. Hantcherli, D. D. Tjahjanto, T. R. Bieler, D. Raabe, "Overview of constitutive laws, kinematics, homogenization and multiscale methods in crystal plasticity finite-element modeling: Theory, experiments, applications", *Acta Mater.* **58** (2010), no. 4, p. 1152-1211.
[56] C. Miehe, J. Schotte, "Crystal plasticity and evolution of polycrystalline microstructure", in *Encyclopedia of Computational Mechanics* (E. Stein, R. de Borst, T. J. R. Hughes, eds.), John Wiley & Sons, Chichester, UK, 2nd ed., 2018, p. 1-23.
[57] S. Forest, J. R. Mayeur, D. L. McDowell, *Micromorphic Crystal Plasticity*, Springer International Publishing, Cham, 2019, 643-686 pages.
[58] O. U. Salman, I. R. Ionescu, "Tempering the mechanical response of FCC micro-pillars: An Eulerian plasticity approach", *Mech. Res. Commun.* (2021), article no. 103665.
[59] J. Weiss, W. B. Rhouma, T. Richeton, S. Dechanel, F. Louchet, L. Truskinovsky, "From mild to wild fluctuations in crystal plasticity", *Phys. Rev. Lett.* **114** (2015), no. 10, article no. 105504.
[60] M. Zaiser, P. Moretti, H. Chu, "Stochastic crystal plasticity models with internal variables: Application to slip channel formation in irradiated metals", *Adv. Eng. Mater.* **22** (2019), no. 9, article no. 1901208.
[61] P. Franciosi, "The concepts of latent hardening and strain hardening in metallic single crystals", *Acta Metall.* **33** (1985), no. 9, p. 1601-1612.
[62] M. Zhang, J. Zhang, D. L. McDowell, "Microstructure-based crystal plasticity modeling of cyclic deformation of Ti–6Al–4V", *Int. J. Plast.* **23** (2007), no. 8, p. 1328-1348.
[63] S. Forest, K. Ammar, B. Appolaire, V. d. Rancourt, S. Wulfinghoff, "Generalized continua and phase-field models: Application to crystal plasticity", in *Mesoscale Models: From Micro-Physics to Macro-Interpretation* (S. Mesarovic, S. Forest, H. Zbib, eds.), Springer International Publishing, Cham, 2019, p. 299-344.
[64] A. Marano, L. Gélébart, S. Forest, "Intragranular localization induced by softening crystal plasticity: Analysis of slip and kink bands localization modes from high resolution FFT-simulations results", *Acta Mater.* **175** (2019), p. 262-275.
[65] Y. Lu, J. Song, J. Y. Huang, J. Lou, "Surface dislocation nucleation mediated deformation and ultrahigh strength in sub-10-nm gold nanowires", *Nano Res.* **4** (2011), no. 12, p. 1261-1267.

[66] I. Issa, J. Amodeo, J. Réthoré, L. Joly-Pottuz, C. Esnouf, J. Morthomas, M. Perez, J. Chevalier, K. Masenelli-Varlot, "*In situ* investigation of MgO nanocube deformation at room temperature", *Acta Mater.* **86** (2015), p. 295-304.
[67] Y. Hu, L. Shu, Q. Yang, W. Guo, P. K. Liaw, K. A. Dahmen, J.-M. Zuo, "Dislocation avalanche mechanism in slowly compressed high entropy alloy nanopillars", *Commun. Phys.* **1** (2018), no. 1, p. 1-8.
[68] P. Zhang, O. U. Salman, J. Weiss, L. Truskinovsky, "Variety of scaling behaviors in nanocrystalline plasticity", *Phys. Rev. E* **102** (2020), article no. 023006.
[69] E. Bittencourt, "Interpretation of the size effects in micropillar compression by a strain gradient crystal plasticity theory", *Int. J. Plast.* **116** (2019), p. 280-296.
[70] Z. W. Shan, R. K. Mishra, S. A. Syed Asif, O. L. Warren, A. M. Minor, "Mechanical annealing and source-limited deformation in submicrometre-diameter Ni crystals", *Nat. Mater.* **7** (2008), no. 2, p. 115-119.
[71] S. I. Rao, D. M. Dimiduk, T. A. Parthasarathy, M. D. Uchic, M. Tang, C. Woodward, "Athermal mechanisms of size-dependent crystal flow gleaned from three-dimensional discrete dislocation simulations", *Acta Mater.* **56** (2008), no. 13, p. 3245-3259.
[72] C. R. Weinberger, W. Cai, "Surface-controlled dislocation multiplication in metal micropillars", *Proc. Natl Acad. Sci. USA* **105** (2008), no. 38, p. 14304-14307.
[73] M. Bagheripoor, R. Klassen, "Length scale plasticity: A review from the perspective of dislocation nucleation", *Rev. Adv. Mater. Sci.* **56** (2018), no. 1, p. 21-61.
[74] D. Mordehai, M. Kazakevich, D. J. Srolovitz, E. Rabkin, "Nanoindentation size effect in single-crystal nanoparticles and thin films: A comparative experimental and simulation study", *Acta Mater.* **59** (2011), no. 6, p. 2309-2321.
[75] I. Plans, A. Carpio, L. L. Bonilla, "Homogeneous nucleation of dislocations as bifurcations in a periodized discrete elasticity model", *Europhys. Lett.* **81** (2007), no. 3, article no. 36001.
[76] R. E. Miller, D. Rodney, "On the nonlocal nature of dislocation nucleation during nanoindentation", *J. Mech. Phys. Solids* **56** (2008), no. 4, p. 1203-1223.
[77] A. Garg, C. E. Maloney, "Universal scaling laws for homogeneous dislocation nucleation during nano-indentation", *J. Mech. Phys. Solids* **95** (2016), p. 742-754.
[78] D. Kiener, A. M. Minor, "Source-controlled yield and hardening of Cu(100) studied by *in situ* transmission electron microscopy", *Acta Mater.* **59** (2011), no. 4, p. 1328-1337.
[79] S. H. Oh, M. Legros, D. Kiener, G. Dehm, "*In situ* observation of dislocation nucleation and escape in a submicrometre aluminium single crystal", *Nat. Mater.* **8** (2009), no. 2, p. 95-100.
[80] S.-W. Lee, S. Aubry, W. D. Nix, W. Cai, "Dislocation junctions and jogs in a free-standing FCC thin film", *Model. Simul. Mater. Sci. Eng.* **19** (2011), no. 2, article no. 025002.
[81] K. S. Ng, A. H. W. Ngan, "Effects of trapping dislocations within small crystals on their deformation behavior", *Acta Mater.* **57** (2009), no. 16, p. 4902-4910.
[82] M. C. Miguel, A. Vespignani, S. Zapperi, J. Weiss, J. R. Grasso, "Intermittent dislocation flow in viscoplastic deformation", *Nature* **410** (2001), no. 6829, p. 667-671.
[83] M. Koslowski, R. Lesar, R. Thomson, "Avalanches and scaling in plastic deformation", *Phys. Rev. Lett.* **93** (2004), no. 12, article no. 125502.
[84] M. D. Uchic, P. A. Shade, D. M. Dimiduk, "Micro-compression testing of FCC metals: A selected overview of experiments and simulations", *J. Miner.* **61** (2009), no. 3, p. 36-41.
[85] L. X. Li, Y. Lou, L. B. Yang, D. S. Peng, K. P. Rao, "Flow stress behavior and deformation characteristics of Ti-3Al-5V-5Mo compressed at elevated temperatures", *Mater. Des.* **23** (2002), no. 5, p. 451-457.
[86] Q. Ruan, M. Yang, W. Liu, A. Godfrey, "Plastic yielding and tensile strength of near-micrometer grain size pure iron", *Mater. Sci. Eng. A* **744** (2019), p. 764-772.
[87] L. Truskinovsky, A. Vainchtein, "The origin of nucleation peak in transformational plasticity", *J. Mech. Phys. Solids* **52** (2004), no. 6, p. 1421-1446.
[88] H. Zheng, A. Cao, C. R. Weinberger, J. Y. Huang, K. Du, J. Wang, Y. Ma, Y. Xia, S. X. Mao, "Discrete plasticity in sub-10-nm-sized gold crystals", *Nat. Commun.* **1** (2010), no. 1, article no. 144.
[89] J. Wang, Y. Wang, W. Cai, J. Li, Z. Zhang, S. X. Mao, "Discrete shear band plasticity through dislocation activities in body-centered cubic tungsten nanowires", *Sci. Rep.* **8** (2018), no. 1, p. 4574.
[90] A. Parakh, S. Lee, K. A. Harkins, M. T. Kiani, D. Doan, M. Kunz, A. Doran *et al.*, "Nucleation of dislocations in 3.9 nm nanocrystals at high pressure", *Phys. Rev. Lett.* **124** (2020), no. 10, article no. 106104.
[91] S. Xia, A. El-Azab, "Computational modelling of mesoscale dislocation patterning and plastic deformation of single crystals", *Model. Simul. Mater. Sci. Eng.* **23** (2015), no. 5, article no. 055009.
[92] E. Clouet, D. Caillard, N. Chaari, F. Onimus, D. Rodney, "Dislocation locking versus easy glide in titanium and zirconium", *Nat. Mater.* **14** (2015), no. 9, p. 931-936.
[93] M. Salvalaglio, A. Voigt, K. R. Elder, "Closing the gap between atomic-scale lattice deformations and continuum elasticity", *NPJ Comput. Mater.* **5** (2019), no. 1, article no. 48.
[94] E. van der Giessen, P. A. Schultz, N. Bertin, V. V. Bulatov, W. Cai, G. Csányi, S. M. Foiles, M. G. D. Geers, C. González,

M. Hütter *et al.*, "Roadmap on multiscale materials modeling", *Model. Simul. Mater. Sci. Eng.* **28** (2020), no. 4, article no. 043001.
[95] N. Bertin, R. B. Sills, W. Cai, "Frontiers in the simulation of dislocations", *Annu. Rev. Mater. Res.* **50** (2020), no. 1, p. 437-464.
[96] T. Niiyama, T. Shimokawa, "Atomistic mechanisms of intermittent plasticity in metals: Dislocation avalanches and defect cluster pinning", *Phys. Rev. E* **91** (2015), no. 2, article no. 022401.
[97] L. A. Zepeda-Ruiz, A. Stukowski, T. Oppelstrup, V. V. Bulatov, "Probing the limits of metal plasticity with molecular dynamics simulations", *Nature* **550** (2017), no. 7677, p. 492-495.
[98] M. Salvalaglio, L. Angheluta, Z.-F. Huang, A. Voigt, K. R. Elder, J. Viñals, "A coarse-grained phase-field crystal model of plastic motion", *J. Mech. Phys. Solids* **137** (2020), article no. 103856.
[99] P. Y. Chan, G. Tsekenis, J. Dantzig, K. A. Dahmen, N. Goldenfeld, "Plasticity and dislocation dynamics in a phase field crystal model", *Phys. Rev. Lett.* **105** (2010), no. 1, article no. 015502.
[100] A. Finel, D. Rodney, "Phase field methods and dislocations", in *Influences of Interface and Dislocation Behavior on Microstructure Evolution, MRS Proceedings* (M. Aindow, M. Asta, M. Glazov, D. Medlin, A. Rollet, M. Zaiser, eds.), vol. 652, Cambridge University Press, Cambridge, UK, 2000.
[101] M. Koslowski, A. M. Cuitiño, M. Ortiz, "A phase-field theory of dislocation dynamics, strain hardening and hysteresis in ductile single crystals", *J. Mech. Phys. Solids* **50** (2002), no. 12, p. 2597-2635.
[102] A. Hunter, I. J. Beyerlein, T. C. Germann, M. Koslowski, "Influence of the stacking fault energy surface on partial dislocations in fcc metals with a three-dimensional phase field dislocations dynamics model", *Phys. Rev. B* **84** (2011), no. 14, article no. 144108.
[103] A. Vattré, B. Devincre, F. Feyel, R. Gatti, S. Groh, O. Jamond, A. Roos, "Modelling crystal plasticity by 3D dislocation dynamics and the finite element method: The discrete-continuous model revisited", *J. Mech. Phys. Solids* **63** (2014), p. 491-505.
[104] P. D. Ispánovity, L. Laurson, M. Zaiser, I. Groma, S. Zapperi, M. J. Alava, "Avalanches in 2D dislocation systems: plastic yielding is not depinning", *Phys. Rev. Lett.* **112** (2014), no. 23, article no. 235501.
[105] J. A. El-Awady, H. Fan, A. M. Hussein, "Advances in discrete dislocation dynamics modeling of size-affected plasticity", in *Multiscale Materials Modeling for Nanomechanics* (C. R. Weinberger, G. J. Tucker, eds.), Springer International Publishing, Cham, 2016, p. 337-371.
[106] N. Bertin, S. Aubry, A. Arsenlis, W. Cai, "GPU-accelerated dislocation dynamics using subcycling time-integration", *Model. Simul. Mater. Sci. Eng.* **27** (2019), no. 7, article no. 075014.
[107] S. N. Varadhan, A. J. Beaudoin, A. Acharya, C. Fressengeas, "Dislocation transport using an explicit Galerkin/least-squares formulation", *Model. Simul. Mater. Sci. Eng.* **14** (2006), no. 7, p. 1245-1270.
[108] T. Hochrainer, S. Sandfeld, M. Zaiser, P. Gumbsch, "Continuum dislocation dynamics: Towards a physical theory of crystal plasticity", *J. Mech. Phys. Solids* **63** (2014), p. 167-178.
[109] A. El-Azab, G. Po, "Continuum dislocation dynamics: Classical theory and contemporary models", in *Handbook of Materials Modeling: Methods: Theory and Modeling* (W. Andreoni, S. Yip, eds.), Springer International Publishing, Cham, 2020, p. 1583-1607.
[110] V. B. Shenoy, R. Miller, E. b. Tadmor, D. Rodney, R. Phillips, M. Ortiz, "An adaptive finite element approach to atomic-scale mechanics—the quasicontinuum method", *J. Mech. Phys. Solids* **47** (1999), no. 3, p. 611-642.
[111] R. E. Miller, E. B. Tadmor, "The quasicontinuum method: Overview, applications and current directions", *J. Comput.-Aided Mater. Design* **9** (2002), no. 3, p. 203-239.
[112] W. Cia, J. Li, S. Yip, "1.09 Molecular Dynamics", in *Comprehensive Nuclear Materials* (R. J. M. Konings, ed.), Elsevier, Waltham, MA, USA, 2012, p. 249-265.
[113] J. A. Zimmerman, C. L. Kelchner, P. A. Klein, J. C. Hamilton, S. M. Foiles, "Surface step effects on nanoindentation", *Phys. Rev. Lett.* **87** (2001), no. 16, article no. 165507.
[114] J. A. Zimmerman, D. J. Bammann, H. Gao, "Deformation gradients for continuum mechanical analysis of atomistic simulations", *Int. J. Solids Struct.* **46** (2009), no. 2, p. 238-253.
[115] L. A. Zepeda-Ruiz, A. Stukowski, T. Oppelstrup, N. Bertin, N. R. Barton, R. Freitas, V. V. Bulatov, "Atomistic insights into metal hardening", *Nat. Mater.* **20** (2021), no. 3, p. 315-320.
[116] H. Lim, C. C. Battaile, C. R. Weinberger, "Simulating dislocation plasticity in bcc metals by integrating fundamental concepts with macroscale models", in *Integrated Computational Materials Engineering (ICME) for Metals: Concepts and Case Studies*, John Wiley & Sons, New Jersey, USA, 2018, p. 71-106.
[117] K. R. Elder, M. Katakowski, M. Haataja, M. Grant, "Modeling elasticity in crystal growth", *Phys. Rev. Lett.* **88** (2002), no. 24, article no. 245701.
[118] A. Skaugen, L. Angheluta, J. Viñals, "Separation of elastic and plastic timescales in a phase field crystal model", *Phys. Rev. Lett.* **121** (2018), no. 25, article no. 255501.
[119] L. P. Kubin, G. Canova, "The modelling of dislocation patterns", *Scr. Met. Mater.* **27** (1992), no. 8, p. 957-962.
[120] B. Devincre, V. Pontikis, Y. Brechet, G. Canova, M. Condat, L. Kubin, "Three-dimensional simulations of plastic flow

in crystals", in *Microscopic Simulations of Complex Hydrodynamic Phenomena* (M. Mareschal, B. L. Holian, eds.), Springer US, Boston, MA, 1992, p. 413-423.
[121] O. Cazacu, *Multiscale Modeling of Heterogenous Materials: From Microstructure to Macro-Scale Properties*, John Wiley & Sons, London, UK, 2013.
[122] G. Po, M. Lazar, D. Seif, N. Ghoniem, "Singularity-free dislocation dynamics with strain gradient elasticity", *J. Mech. Phys. Solids* **68** (2014), p. 161-178.
[123] J. Wang, I. J. Beyerlein, C. N. Tomé, "Reactions of lattice dislocations with grain boundaries in Mg: Implications on the micro scale from atomic-scale calculations", *Int. J. Plast.* **56** (2014), p. 156-172.
[124] P.-A. Geslin, R. Gatti, B. Devincre, D. Rodney, "Implementation of the nudged elastic band method in a dislocation dynamics formalism: Application to dislocation nucleation", *J. Mech. Phys. Solids* **108** (2017), p. 49-67.
[125] A. A. Kohnert, L. Capolungo, "Spectral discrete dislocation dynamics with anisotropic short range interactions", *Comput. Mater. Sci.* **189** (2021), article no. 110243.
[126] W. Cai, A. Arsenlis, C. R. Weinberger, V. V. Bulatov, "A non-singular continuum theory of dislocations", *J. Mech. Phys. Solids* **54** (2006), no. 3, p. 561-587.
[127] O. Dmitrieva, J. V. Svirina, E. Demir, D. Raabe, "Investigation of the internal substructure of microbands in a deformed copper single crystal: Experiments and dislocation dynamics simulation", *Model. Simul. Mater. Sci. Eng.* **18** (2010), no. 8, article no. 085011.
[128] K. Starkey, G. Winther, A. El-Azab, "Theoretical development of continuum dislocation dynamics for finite-deformation crystal plasticity at the mesoscale", *J. Mech. Phys. Solids* **139** (2020), article no. 103926.
[129] A. Acharya, A. Roy, "Size effects and idealized dislocation microstructure at small scales: Predictions of a phenomenological model of mesoscopic field dislocation mechanics: Part I", *J. Mech. Phys. Solids* **54** (2006), p. 1687-1710.
[130] S. Sandfeld, M. Zaiser, "Pattern formation in a minimal model of continuum dislocation plasticity", *Model. Simul. Mater. Sci. Eng.* **23** (2015), no. 6, article no. 065005.
[131] P.-L. Valdenaire, Y. Le Bouar, B. Appolaire, A. Finel, "Density-based crystal plasticity: From the discrete to the continuum", *Phys. Rev. B* **93** (2016), no. 21, article no. 214111.
[132] E. B. Tadmor, M. Ortiz, R. Phillips, "Quasicontinuum analysis of defects in solids", *Philos. Mag. A* **73** (1996), no. 6, p. 1529-1563.
[133] M. Dobson, R. S. Elliott, M. Luskin, E. B. Tadmor, "A multilattice quasicontinuum for phase transforming materials: Cascading Cauchy–Born kinematics", *J. Comput.-Aided Mater. Design* **14** (2007), no. 1, p. 219-237.
[134] V. Sorkin, R. S. Elliott, E. B. Tadmor, "A local quasicontinuum method for 3D multilattice crystalline materials: Application to shape-memory alloys", *Model. Simul. Mater. Sci. Eng.* **22** (2014), no. 5, article no. 055001.
[135] D. M. Kochmann, J. S. Amelang, "The quasicontinuum method: Theory and applications", in *Multiscale Materials Modeling for Nanomechanics* (C. R. Weinberger, G. J. Tucker, eds.), Springer International Publishing, Cham, 2016, p. 159-193.
[136] E. B. Tadmor, R. E. Miller, *Modeling Materials: Continuum, Atomistic and Multiscale Techniques*, Cambridge University Press, Cambridge, UK, 2011.
[137] D. Rodney, R. Phillips, "Structure and strength of dislocation junctions: An atomic level analysis", *Phys. Rev. Lett.* **82** (1999), no. 8, p. 1704-1707.
[138] J. Knap, M. Ortiz, "Effect of indenter-radius size on Au(001) nanoindentation", *Phys. Rev. Lett.* **90** (2003), no. 22, article no. 226102.
[139] W. Yu, Z. Wang, S. Shen, "Edge dislocations interacting with a Σ11 symmetrical grain boundary in copper upon mixed loading: A quasicontinuum method study", *Comput. Mater. Sci.* **137** (2017), p. 162-170.
[140] J. Jin, P. Yang, J. Cao, S. Li, Q. Peng, "Quasicontinuum simulation of the effect of lotus-type nanocavity on the onset plasticity of single crystal Al during nanoindentation", *Nanomaterials (Basel)* **8** (2018), no. 10, article no. 778.
[141] K. J. Van Vliet, J. Li, T. Zhu, S. Yip, S. Suresh, "Quantifying the early stages of plasticity through nanoscale experiments and simulations", *Phys. Rev. B* **67** (2003), no. 10, article no. 104105.
[142] T. Zhu, J. Li, K. J. Van Vliet, S. Ogata, S. Yip, S. Suresh, "Predictive modeling of nanoindentation-induced homogeneous dislocation nucleation in copper", *J. Mech. Phys. Solids* **52** (2004), no. 3, p. 691-724.
[143] J. L. Ericksen, "On the Cauchy–Born rule", *Math. Mech. Solids* **13** (2008), no. 3–4, p. 199-220.
[144] P. M. Weinan, "Cauchy–Born rule and the stability of crystalline solids: Static problems", *Arch. Rat. Mech. Anal.* **183** (2007), no. 2, p. 241-297.
[145] P. Steinmann, A. Elizondo, R. Sunyk, "Studies of validity of the Cauchy–Born rule by direct comparison of continuum and atomistic modelling", *Model. Simul. Mater. Sci. Eng.* **15** (2006), no. 1, p. S271-S281.
[146] P. Podio-Guidugli, "On (Andersen–) Parrinello–Rahman molecular dynamics, the related metadynamics, and the use of the Cauchy–Born rule", *J. Elast.* **100** (2010), no. 1–2, p. 145-153.
[147] D. Rodney, Y. Le Bouar, A. Finel, "Phase field methods and dislocations", *Acta Mater.* **51** (2003), no. 1, p. 17-30.
[148] I. J. Beyerlein, A. Hunter, "Understanding dislocation mechanics at the mesoscale using phase field dislocation dynamics", *Philos. Trans. A Math. Phys. Eng. Sci.* **374** (2016), no. 2066, article no. 20150166.

[149] A. Ruffini, Y. Le Bouar, A. Finel, "Three-dimensional phase-field model of dislocations for a heterogeneous face-centered cubic crystal", *J. Mech. Phys. Solids* **105** (2017), p. 95-115.
[150] L.-Q. Chen, "Phase-field models for microstructure evolution", *Annu. Rev. Mater. Res.* **32** (2002), no. 1, p. 113-140.
[151] O. U. Salman, "Modeling of spatio-temporal dynamics and patterning mechanisms of martensites by phase-field and Lagrangian methods", PhD Thesis, Université Pierre et Marie Curie, 2009.
[152] A. Finel, Y. Le Bouar, A. Gaubert, U. Salman, "Phase field methods: Microstructures, mechanical properties and complexity", *C. R. Phys.* **11** (2010), no. 3, p. 245-256.
[153] O. U. Salman, A. Finel, R. Delville, D. Schryvers, "The role of phase compatibility in martensite", *J. Appl. Phys.* **111** (2012), no. 10, article no. 103517.
[154] O. Shchyglo, U. Salman, A. Finel, "Martensitic phase transformations in Ni–Ti-based shape memory alloys: The Landau theory", *Acta Mater.* **60** (2012), no. 19, p. 6784-6792.
[155] O. U. Salman, B. Muite, A. Finel, "Origin of stabilization of macrotwin boundaries in martensites", *Eur. Phys. J. B* **92** (2019), no. 1, p. 20.
[156] Y. M. Jin, A. G. Khachaturyan, "Phase field microelasticity theory of dislocation dynamics in a polycrystal: Model and three-dimensional simulations", *Philos. Mag. Lett.* **81** (2001), no. 9, p. 607-616.
[157] S. Zheng, D. Zheng, Y. Ni, L. He, "Improved phase field model of dislocation intersections", *NPJ Comput. Mater.* **4** (2018), no. 1, article no. 20.
[158] S. Y. Hu, L. Q. Chen, "Solute segregation and coherent nucleation and growth near a dislocation—a phase-field model integrating defect and phase microstructures", *Acta Mater.* **49** (2001), no. 3, p. 463-472.
[159] M.-A. Louchez, L. Thuinet, R. Besson, A. Legris, "Microscopic phase-field modeling of hcp|fcc interfaces", *Comput. Mater. Sci.* **132** (2017), p. 62-73.
[160] D. Qiu, P. Zhao, C. Shen, W. Lu, D. Zhang, M. Mrovec, Y. Wang, "Predicting grain boundary structure and energy in BCC metals by integrated atomistic and phase-field modeling", *Acta Mater.* **164** (2019), p. 799-809.
[161] P. Biscari, M. F. Urbano, A. Zanzottera, G. Zanzotto, "Intermittency in crystal plasticity informed by lattice symmetry", *J. Elast.* **123** (2016), no. 1, p. 85-96.
[162] M. Javanbakht, V. I. Levitas, "Phase field approach to dislocation evolution at large strains: Computational aspects", *Int. J. Solids Struct.* **82** (2016), p. 95-110.
[163] S. Xu, J. R. Mianroodi, A. Hunter, I. J. Beyerlein, B. Svendsen, "Phase-field-based calculations of the disregistry fields of static extended dislocations in FCC metals", *Phil. Mag.* **99** (2019), no. 11, p. 1400-1428.
[164] Y. Li, S. Hu, X. Sun, M. Stan, "A review: Applications of the phase field method in predicting microstructure and property evolution of irradiated nuclear materials", *NPJ Comput. Mater.* **3** (2017), no. 1, article no. 16.
[165] A. I. Landau, "Application of a model of interacting atomic chains for the description of edge dislocations", *Phys. Stat. Sol. (b)* **183** (1994), no. 2, p. 407-417.
[166] A. Carpio, L. L. Bonilla, "Edge dislocations in crystal structures considered as traveling waves in discrete models", *Phys. Rev. Lett.* **90** (2003), no. 13, article no. 135502.
[167] J. Frenkel, T. Kontorova, "On the theory of plastic deformation and twinning", *Izv. Akad. Nauk Ser. Fiz.* **1** (1939), p. 137-149.
[168] R. Peierls, "The size of a dislocation", *Proc. Phys. Soc. Lond.* **52** (1940), no. 1, p. 34-37.
[169] F. R. N. Nabarro, "Dislocations in a simple cubic lattice", *Proc. Phys. Soc. Lond.* **59** (2002), no. 2, p. 256-272.
[170] A. S. Kovalev, A. D. Kondratyuk, A. M. Kosevich, A. I. Landau, "Theoretical description of the crowdion in an anisotropic crystal based on the Frenkel–Kontorova model including and elastic three-dimensional medium", *Phys. Stat. Sol. (b)* **177** (1993), no. 1, p. 117-127.
[171] P. S. Lomdahl, D. J. Srolovitz, "Dislocation generation in the two-dimensional Frenkel–Kontorova model at high stresses", *Phys. Rev. Lett.* **57** (1986), no. 21, p. 2702-2705.
[172] D. Srolovitz, P. Lomdahl, "Dislocation dynamics in the 2-d Frenkel–Kontorova model", *Physica D* **23** (1986), no. 1–3, p. 402-412.
[173] L. L. Bonilla, A. Carpio, I. Plans, "Dislocations in cubic crystals described by discrete models", *Physica A* **376** (2007), p. 361-377.
[174] P.-A. Geslin, B. Appolaire, A. Finel, "Investigation of coherency loss by prismatic punching with a nonlinear elastic model", *Acta Mater.* **71** (2014), p. 80-88.
[175] V. V. Bulatov, A. S. Argon, "A stochastic model for continuum elasto-plastic behavior. I. Numerical approach and strain localization", *Model. Simul. Mater. Sci. Eng.* **2** (1994), no. 2, p. 167-184.
[176] A. Minami, A. Onuki, "Nonlinear elasticity theory of dislocation formation and composition change in binary alloys in three dimensions", *Acta Mater.* **55** (2007), no. 7, p. 2375-2384.
[177] A. Onuki, "Plastic flow in two-dimensional solids", *Phys. Rev. E* **68** (2003), no. 6 Pt 1, article no. 061502.
[178] A. Carpio, L. L. Bonilla, "Discrete models of dislocations and their motion in cubic crystals", *Phys. Rev. B* **71** (2005), no. 13, article no. 134105.
[179] E. Kaxiras, L. L. Boyer, "Energetics of large lattice strains: Application to silicon", *Phys. Rev. B* **50** (1994), no. 3, p. 1535-1540.

[180] S. Conti, G. Zanzotto, "A variational model for reconstructive phase transformations in crystals, and their relation to dislocations and plasticity", *Arch. Ration. Mech. Anal.* **173** (2004), no. 1, p. 69-88.
[181] J. L. Ericksen, "Nonlinear elasticity of diatomic crystals", *Int. J. Solids Struct.* **6** (1970), no. 7, p. 951-957.
[182] J. L. Ericksen, "Loading devices and stability of equilibrium", in *Nonlinear Elasticity* (R. W. Dickey, ed.), Academic Press, New York, USA, 1973, p. 161-173.
[183] J. L. Ericksen, "Special topics in elastostatics", in *Advances in Applied Mechanics* (C.-S. Yih, ed.), vol. 17, Elsevier, 1977, p. 189-244.
[184] J. L. Ericksen, "Some phase transitions in crystals", *Arch. Ration. Mech. Anal.* **73** (1980), no. 2, p. 99-124.
[185] G. P. Parry, "On the elasticity of monatomic crystals", *Math. Proc. Camb. Philos. Soc.* **80** (1976), no. 1, p. 189-211.
[186] I. Folkins, "Functions of two-dimensional Bravais lattices", *J. Math. Phys.* **32** (1991), no. 7, p. 1965-1969.
[187] G. P. Parry, "Low-dimensional lattice groups for the continuum mechanics of phase transitions in crystals", *Arch. Rat. Mech. Anal.* **145** (1998), no. 1, p. 1-22.
[188] M. Pitteri, G. Zanzotto, *Continuum Models for Phase Transitions and Twinning in Crystals*, Chapman and Hall/CRC, London, UK, 2002.
[189] G. Puglisi, L. Truskinovsky, "Thermodynamics of rate-independent plasticity", *J. Mech. Phys. Solids* **53** (2005), no. 3, p. 655-679.
[190] A. Mielke, L. Truskinovsky, "From discrete visco-elasticity to continuum rate-independent plasticity: Rigorous results", *Arch. Rat. Mech. Anal.* **203** (2011), no. 2, p. 577-619.
[191] I. Fonseca, "Variational methods for elastic crystals", *Arch. Ration. Mech. Anal.* **97** (1987), no. 3, p. 189-220.
[192] G. R. Bhimanapati, Z. Lin, V. Meunier, Y. Jung, J. Cha, S. Das, D. Xiao *et al.*, "Recent advances in two-dimensional materials beyond graphene", *ACS Nano* **9** (2015), no. 12, p. 11509-11539.
[193] J. Chen, G. Schusteritsch, C. J. Pickard, C. G. Salzmann, A. Michaelides, "Two dimensional ice from first principles: Structures and phase transitions", *Phys. Rev. Lett.* **116** (2016), no. 2, article no. 025501.
[194] V. V. Hoang, N. T. Hieu, "Formation of two-dimensional crystals with square lattice structure from the liquid state", *J. Phys. Chem. C* **120** (2016), no. 32, p. 18340-18347.
[195] K. Zhang, Y. Feng, F. Wang, Z. Yang, J. Wang, "Two dimensional hexagonal boron nitride (2D-hBN): Synthesis, properties and applications", *J. Mater. Chem.* **5** (2017), no. 46, p. 11992-12022.
[196] D. Akinwande, C. J. Brennan, J. S. Bunch, P. Egberts, J. R. Felts, H. Gao, R. Huang *et al.*, "A review on mechanics and mechanical properties of 2D materials—Graphene and beyond", *Extreme Mech. Lett.* **13** (2017), p. 42-77.
[197] Y. Chen, Z. Fan, Z. Zhang, W. Niu, C. Li, N. Yang, B. Chen, H. Zhang, "Two-dimensional metal nanomaterials: Synthesis, properties, and applications", *Chem. Rev.* **118** (2018), no. 13, p. 6409-6455.
[198] N. P. Kryuchkov, S. O. Yurchenko, Y. D. Fomin, E. N. Tsiok, V. N. Ryzhov, "Complex crystalline structures in a two-dimensional core-softened system", *Soft Matt.* **14** (2018), no. 11, p. 2152-2162.
[199] V. Van Hoang, N. H. Giang, "Compression-induced square-triangle solid–solid phase transition in 2D simple monatomic system", *Phys. E* **113** (2019), p. 35-42.
[200] R. Ma, D. Cao, C. Zhu, Y. Tian, J. Peng, J. Guo, J. Chen *et al.*, "Atomic imaging of the edge structure and growth of a two-dimensional hexagonal ice", *Nature* **577** (2020), no. 7788, p. 60-63.
[201] C. Cayron, "The transformation matrices (distortion, orientation, correspondence), their continuous forms and their variants", *Acta Crystallogr. A Found. Adv.* **75** (2019), no. Pt 3, p. 411-437.
[202] Y. Gao, "A Cayley graph description of the symmetry breaking associated with deformation and structural phase transitions in metallic materials", *Materialia* **9** (2020), article no. 100588.
[203] Y. Gao, Y. Zhang, Y. Wang, "Determination of twinning path from broken symmetry: A revisit to deformation twinning in bcc metals", *Acta Mater.* **196** (2020), p. 280-294.
[204] Y. Gao, T. Yu, Y. Wang, "Phase transformation graph and transformation pathway engineering for shape memory alloys", *Shape Mem. Superelast.* **6** (2020), no. 1, p. 115-130.
[205] V. I. Marconi, E. A. Jagla, "Diffuse interface approach to brittle fracture", *Phys. Rev. E* **71** (2005), no. 3 Pt 2A, article no. 036110.
[206] P. Engel, *Geometric Crystallography: An Axiomatic Introduction to Crystallography*, Springer, Netherlands, 1986.
[207] T. Friesecke, "Validity and failure of the Cauchy–Born hypothesis in a two-dimensional mass-spring lattice", *J. Nonlinear Sci.* **12** (2002), no. 5, p. 445-478.
[208] M. Ortiz, E. a. Repetto, "Nonconvex energy minimization and dislocation structures in ductile single crystals", *J. Mech. Phys. Solids* **47** (1999), no. 2, p. 397-462.
[209] R. Baggio, "Théorie de la Plasticité Cristalline Tenant Compte de la Symétrie $GL(2,Z)$", PhD Thesis, Université Sorbonne, Paris Nord, France, 2019.
[210] R. W. Grosse-Kunstleve, N. K. Sauter, P. D. Adams, "Numerically stable algorithms for the computation of reduced unit cells", *Acta Crystallogr. A* **60** (2004), no. 1, p. 1-6.
[211] L. C. Andrews, H. J. Bernstein, N. K. Sauter, "A space for lattice representation and clustering", *Acta Crystallogr. A Found. Adv.* **75** (2019), no. Pt 3, p. 593-599.
[212] S. Bochkanov, V. Bystritsky, "Alglib", 2013, available from: https://www.alglib.net/.

[213] C. Sanderson, R. Curtin, "Armadillo: A template-based C++ library for linear algebra", *J. Open Source Softw.* **1** (2016), no. 2, article no. 26.
[214] M. Fishman, S. R. White, E. M. Stoudenmire, "The ITensor software library for tensor network calculations", https://arxiv.org/abs/2007.14822, 2020.
[215] R. Ogden, *Non-Linear Elastic Deformations*, John Wiley and Sons, New York, USA, 1984.
[216] Y. Grabovsky, L. Truskinovsky, "Normality condition in elasticity", *J. Nonlinear Sci.* **24** (2014), no. 6, p. 1125-1146.
[217] J. Merodio, R. W. Ogden, "Material instabilities in fiber-reinforced nonlinearly elasti solids under plane deformation", *Arch. Mech.* **54** (2002), no. 5–6, p. 525-552.
[218] S. Kumar, D. M. Parks, "On the hyperelastic softening and elastic instabilities in graphene", *Proc. R. Soc. A* **471** (2015), no. 2173, article no. 20140567.
[219] R. Hill, "Acceleration waves in solids", *J. Mech. Phys. Solids* **10** (1962), no. 1, p. 1-16.
[220] J. R. Rice, "Localization of plastic deformation", Tech. report, Division of Engineering, Brown University, Providence, RI, USA, 1976.
[221] R. Ogden, *Non-Linear Elastic Deformations*, Ellis Horwood, Chichester, 1984.
[222] P. M. Anderson, J. P. Hirth, J. Lothe, *Theory of Dislocations*, Cambridge University Press, Cambridge, UK, 2017.
[223] Y. Zhong, T. Zhu, "Simulating nanoindentation and predicting dislocation nucleation using interatomic potential finite element method", *Comput. Methods Appl. Mech. Eng.* **197** (2008), no. 41, p. 3174-3181.
[224] D. Bigoni, *Nonlinear Solid Mechanics: Bifurcation Theory and Material Instability*, Cambridge University Press, Cambridge, UK, 2012.
[225] A. Onuki, A. Furukawa, A. Minami, "Sheared solid materials", *Pramana* **64** (2005), no. 5, p. 661-677.
[226] C. Sanderson, R. Curtin, "A user-friendly hybrid sparse matrix class in C++", in *Mathematical Software — ICMS 2018*, Springer International Publishing, South Bend, IN, USA, 2018, p. 422-430.
[227] R. Dasgupta, S. Karmakar, I. Procaccia, "Universality of the plastic instability in strained amorphous solids", *Phys. Rev. Lett.* **108** (2012), no. 7, article no. 075701.
[228] S. Bonfanti, R. Guerra, C. Mondal, I. Procaccia, S. Zapperi, "Elementary plastic events in amorphous silica", *Phys. Rev. E* **100** (2019), no. 6-1, article no. 060602.
[229] D. Richard, M. Ozawa, S. Patinet, E. Stanifer, B. Shang *et al.*, "Predicting plasticity in disordered solids from structural indicators", *Phys. Rev. Mater.* **4** (2020), article no. 113609.
[230] L. Truskinovsky, A. Vainchtein, "Quasicontinuum modelling of short-wave instabilities in crystal lattices", *Philos. Mag.* **85** (2005), no. 33–35, p. 4055-4065.
[231] K. Bertoldi, M. C. Boyce, "Wave propagation and instabilities in monolithic and periodically structured elastomeric materials undergoing large deformations", *Phys. Rev. B* **78** (2008), no. 18, article no. 184107.
[232] N. Hansen, D. Kuhlmann-Wilsdorf, "Low energy dislocation structures due to unidirectional deformation at low temperatures", *Int. J. Green Nanotech. Mater. Sci. Eng.* **81** (1986), p. 141-161.
[233] H. Bei, S. Shim, M. K. Miller, G. M. Pharr, E. P. George, "Effects of focused ion beam milling on the nanomechanical behavior of a molybdenum-alloy single crystal", *Appl. Phys. Lett.* **91** (2007), no. 11, article no. 111915.
[234] N. Friedman, A. T. Jennings, G. Tsekenis, J.-Y. Kim, M. Tao, J. T. Uhl, J. R. Greer, K. A. Dahmen, "Statistics of dislocation slip avalanches in nanosized single crystals show tuned critical behavior predicted by a simple mean field model", *Phys. Rev. Lett.* **109** (2012), no. 9, article no. 095507.
[235] M. Zaiser, "Statistical aspects of microplasticity: Experiments, discrete dislocation simulations and stochastic continuum models", *J. Mech. Behav. Mater.* **22** (2013), no. 3–4, p. 89-100.
[236] P. M. Derlet, R. Maaß, "The stress statistics of the first pop-in or discrete plastic event in crystal plasticity", *J. Appl. Phys.* **120** (2016), no. 22, article no. 225101.
[237] Y. Cui, N. Ghoniem, "Spatio-temporal plastic instabilities at the nano/micro scale", *J. Micromech. Mol. Phys.* **03** (2018), no. 03n04, article no. 1840006.
[238] G. Sparks, Y. Cui, G. Po, Q. Rizzardi, J. Marian, R. Maaß, "Avalanche statistics and the intermittent-to-smooth transition in microplasticity", *Phys. Rev. Mater.* **3** (2019), no. 8, article no. 080601.
[239] B. Jakobsen, H. F. Poulsen, U. Lienert, J. Almer, S. D. Shastri, H. O. Sørensen, C. Gundlach, W. Pantleon, "Formation and subdivision of deformation structures during plastic deformation", *Science* **312** (2006), no. 5775, p. 889-892.
[240] D. Sornette, G. Ouillon, "Dragon-kings: Mechanisms, statistical methods and empirical evidence", *Eur. Phys. J. Spec. Top.* **205** (2012), no. 1, p. 1-26.